

Zeitschrift: IABSE reports = Rapports AIPC = IVBH Berichte
Band: 37 (1982)

Rubrik: Theme 5: Structural concrete elements

Nutzungsbedingungen

Die ETH-Bibliothek ist die Anbieterin der digitalisierten Zeitschriften auf E-Periodica. Sie besitzt keine Urheberrechte an den Zeitschriften und ist nicht verantwortlich für deren Inhalte. Die Rechte liegen in der Regel bei den Herausgebern beziehungsweise den externen Rechteinhabern. Das Veröffentlichen von Bildern in Print- und Online-Publikationen sowie auf Social Media-Kanälen oder Webseiten ist nur mit vorheriger Genehmigung der Rechteinhaber erlaubt. [Mehr erfahren](#)

Conditions d'utilisation

L'ETH Library est le fournisseur des revues numérisées. Elle ne détient aucun droit d'auteur sur les revues et n'est pas responsable de leur contenu. En règle générale, les droits sont détenus par les éditeurs ou les détenteurs de droits externes. La reproduction d'images dans des publications imprimées ou en ligne ainsi que sur des canaux de médias sociaux ou des sites web n'est autorisée qu'avec l'accord préalable des détenteurs des droits. [En savoir plus](#)

Terms of use

The ETH Library is the provider of the digitised journals. It does not own any copyrights to the journals and is not responsible for their content. The rights usually lie with the publishers or the external rights holders. Publishing images in print and online publications, as well as on social media channels or websites, is only permitted with the prior consent of the rights holders. [Find out more](#)

Download PDF: 01.04.2026

ETH-Bibliothek Zürich, E-Periodica, <https://www.e-periodica.ch>



THEME 5

Structural Concrete Elements

Éléments de construction en béton

Bauteile aus Beton

Leere Seite
Blank page
Page vide

Fatigue Design Concept Considering the Indefinite State of Stress in the Reinforcement of RC-Beams

Concept de dimensionnement à la fatigue en considérant l'état de tensions indéfini dans l'armature des poutres en béton armé

Bemessungskonzept für Ermüdung unter Berücksichtigung der unbestimmten Spannungen in der Bewehrung von Betonbalken

R.P. FREY

Research Associate
Swiss Federal Institute of Technology
Zürich, Switzerland

SUMMARY

In order to analyse the fatigue behaviour of reinforced concrete structures a knowledge of the state of stress is essential. With the emphasis on the shear behaviour a series of six reinforced concrete beams under cyclic loading was tested. From the measured strains it becomes evident that the stresses vary within a considerable range. However, the stress amplitude can be determined more accurately. It follows that a fatigue design concept should be based on the stress range.

RESUME

La connaissance de l'état de tensions est importante pour la compréhension du comportement à la fatigue des membres en béton armé. Pour étudier spécialement celui de la résistance à l'effort tranchant, on a exécuté six essais sur des poutres en béton armé. Les résultats des mesures montrent que les tensions varient considérablement tandis que leurs différences peuvent être déterminées avec plus de précision. Il s'en suit qu'un concept de dimensionnement à la fatigue devrait donc être basé sur les différences de tensions.

ZUSAMMENFASSUNG

Für die Erfassung des Ermüdungsverhaltens von Betonbauteilen ist die Kenntnis des Spannungszustandes Voraussetzung. Mit Schwerpunkt auf dem Schubverhalten wurden sechs Ermüdungsversuche an Stahlbetonbalken durchgeführt. Die Messungen zeigen, dass die Spannungen über einen grossen Bereich variieren, die Spannungsdifferenzen jedoch besser erfasst werden können. Daraus wird gefolgert, dass ein Bemessungskonzept für Ermüdung auf den Spannungsdifferenzen basieren sollte.



1. INTRODUCTION

Recent studies on the shear strength of reinforced concrete beams under static loading led to new design rules and codes (CEB Model Code, 1978; SIA 162-RL 34, 1976; [1], [2]) which permit less web reinforcement. In order to study the fatigue behaviour of beams designed according to the new static rules, a knowledge of the stresses under service load conditions is essential. With emphasis on the shear behaviour a series of six reinforced concrete beams under cyclic loading were tested.

2. TEST PROGRAM, MAIN PARAMETERS

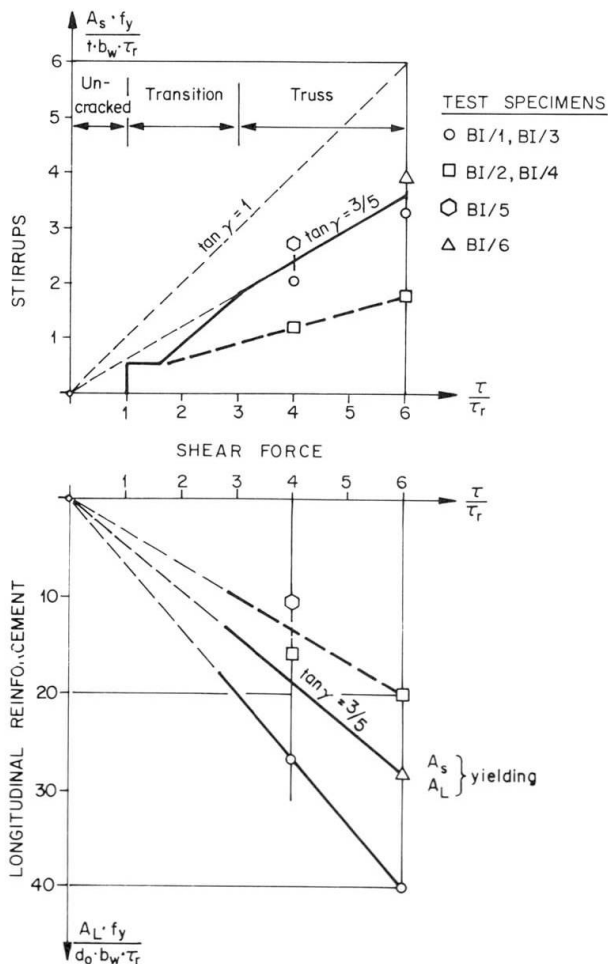


Fig. 1: Design Parameters

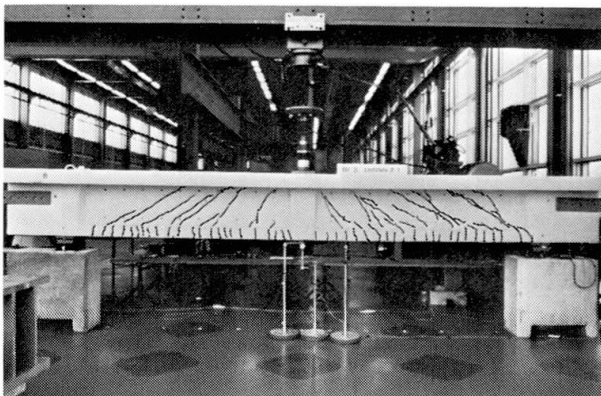


Fig. 2: Test Set-up, Beam BI/3

The layout of the tests was based on the ultimate load design approach given in the Swiss Code SIA 162-RL 34, which assumes a truss model with variable inclination of the diagonal concrete compression field (Fig. 1). The minimum angle, $\tan \gamma = 0.6$, was chosen. This led to the minimum shear reinforcement for the beams BI/1,3,5,6. The longitudinal reinforcement was varied from values below the level at which the stirrups and longitudinal reinforcement yield to values corresponding to an over-reinforced beam (specimens BI/1 and 3) and including the case where both reinforcements yield (specimen BI/6). Two beams were tested with only 50% of the reinforcements of beams BI/1 and 3.

The second main parameter was the nominal shear stress (web thickness). This led to four beams unsymmetric with respect to the web thickness (specimens BI/1,2,3,4) and two symmetric beams (specimens BI/5 and 6).

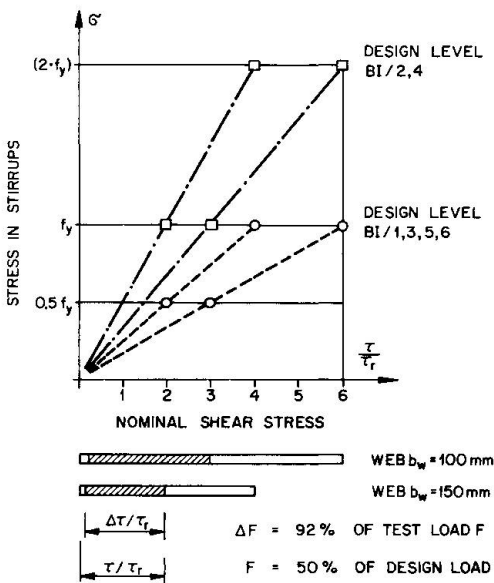
The test set-up consisted of simply supported beams with a concentrated load at midspan (Fig. 2) producing a constant shear force but different nominal shear stresses for the unsymmetric beams. All specimens had the same span and depth. Table 1 gives the essential dimensions of all six beams.

The upper level of the cyclic loading was chosen to fall in the region of service loads and fixed at 50% of the ultimate design load. The maximal possible load range, fixed by the limitations of the testing arrangement, was chosen (Fig. 3). All beams were loaded statically up to the maximum load $F_{\max} = 370$ kN and then subjected to a constant cyclic loading with a load range of 30 to 370 kN with the exception of beam BI/1. A statical test to failure was done at the end of the test program for each beam. Beam BI/1 was tested under cyclic loading with increasing maximum load levels.

SPECIMEN	BI/1	BI/2	BI/3	BI/4	BI/5	BI/6
LOAD EQUIPMENT	CLOSED LOOP SYSTEM		PULSATOR			
DIMENSIONS						
SECTION	T	T	T	T	T	T
SPAN L [mm]	5000	5000	5000	5000	5000	5000
DEPTH D	680	680	680	680	680	680
UPPER FLANGE b_{sup}	800	800	800	800	1400	1400
LOWER FLANGE b_{inf}	350	350	350	350	—	200
WEB THICKNES b_w	100/150	100/150	100/150	100/150	150	100
REINFORCEMENT						
LONG REINFORCEMENT A_L [mm ²]	5650	2830	5650	2830	2830	3890
STIRRUPS A_S [mm ² /m]	786	402	786	402	786	786
LONG REINFORCEMENT ρ_L [%]	1.13	0.52	1.13	0.52	0.33	0.45
STIRRUPS ρ_S [%]	0.79/0.52	0.40/0.27	0.79/0.52	0.40/0.27	0.52	0.79
MATERIAL PROPERTIES						
CONCRETE:			$f_{cwk} \geq 30 \text{ N/mm}^2$		REINFORCEMENT: $f_{yk} \geq 460 \text{ N/mm}^2$	
			$\tau_R = 1 \text{ N/mm}^2$			

The first two specimens were tested with a closed loop system. The main interest in beams BI/1 and 2 was in the strain history during the first few cycles as well as the influence (in beam BI/1) of previous load cycles on the development of strains at higher load levels. The beams BI/3 to 6 were tested using a Amsler pulsator.

Table 1: Beams BI/1-6, Dimensions and Properties



All measurements were taken from measuring marks glued on the concrete, with exception of those used to measure the strains in the longitudinal reinforcement and the stirrups which were glued directly on the reinforcing bars. The gauge length varied from 100 mm (local stirrup strains) to 300 mm (average stirrup strains over the web depth). 100 mm gauge length for the stirrups was employed on one side of the web. On the other side, only the average stirrup strain over 300 mm was measured. Strain gauges were used to determine local concrete deformations. The measurements were taken under static load corresponding to lower and upper load levels. Deflections during cyclic loading were observed to check for any dynamic effects.

Fig. 3: Load and Design Level

3. BEAM BI/3, RESULTS

Because the results collected during the whole test series are quite extensive, only those of a typical test beam, BI/3 (Fig. 4), are presented. Fig. 5 shows

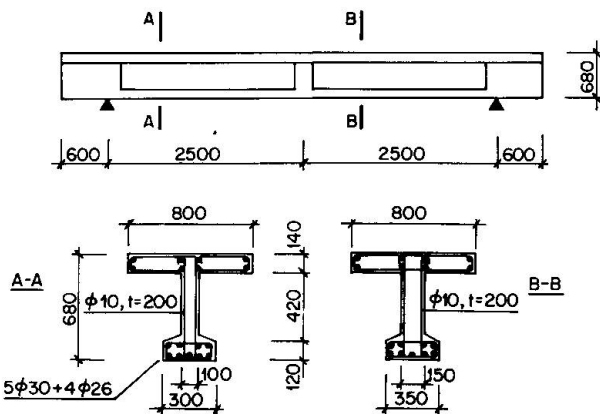


Fig. 4: Beam BI/3

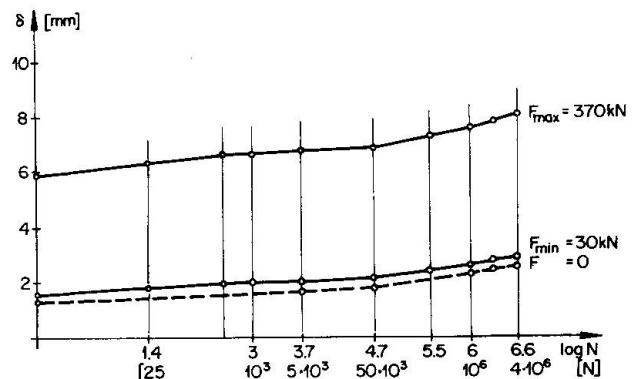


Fig. 5: Beam BI/3, Deflection History

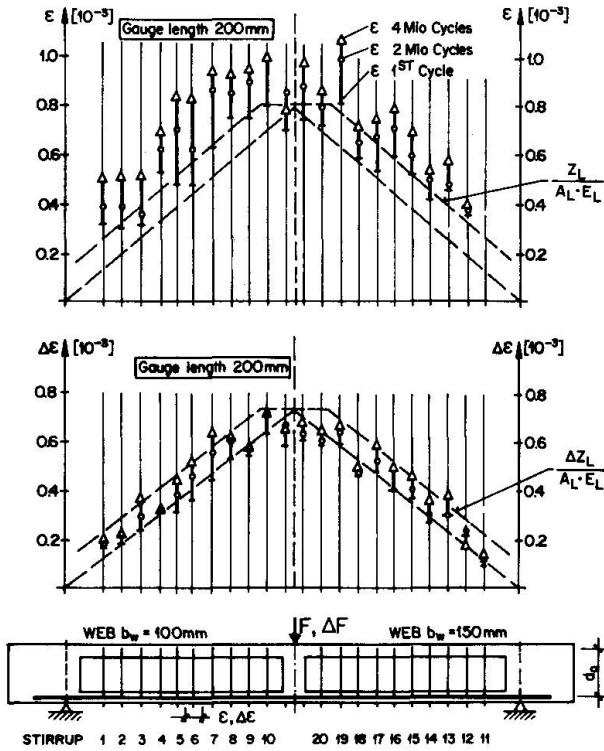


Fig. 6: Beam BI/3: Variation of Strains in Longitudinal Reinforcement under max. Load $F = 370$ kN and under Load Range $\Delta F = 340$ kN

the deflection history at midspan. It is representative of the strain history in the stirrups and the longitudinal reinforcement. The increase of strains with the number of cycles is very high at the start and becomes smaller once the crack pattern is fully formed. It also becomes evident from the figure that the increase in the deflection range is smaller than the increase in deflection under maximum or minimum loads.

Figure 6 shows the measured strains and the measured strain ranges in the longitudinal reinforcement at the first cycle, at two Mio cycles and at four Mio cycles. The difference in the scatter between the maximum strains ϵ and the strain range $\Delta\epsilon$, as well as different growth rates is apparent.

Analogous conclusions can be drawn with respect to the stirrup strains (Figs. 7 and 8). In addition, it can be seen that stirrups with small initial strains after the first few cycles have a larger increase than stirrups with already high stresses. This is due to the development of the final crack pattern and a rearrangement of the internal forces.

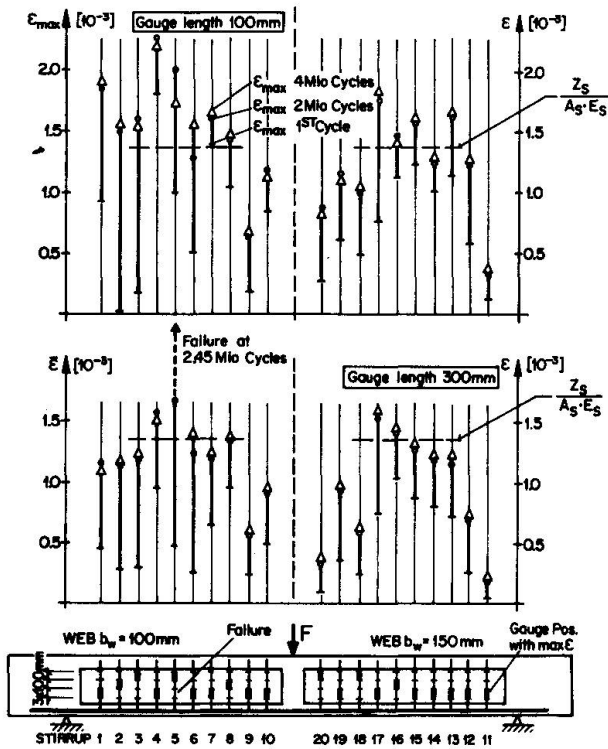


Fig. 7: Beam BI/3: Variation of Stirrup Strains under max. Load $F = 370$ kN

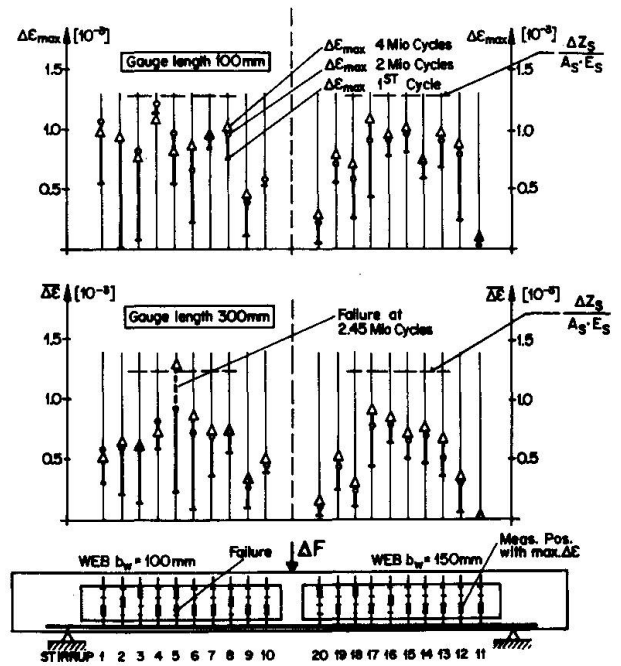
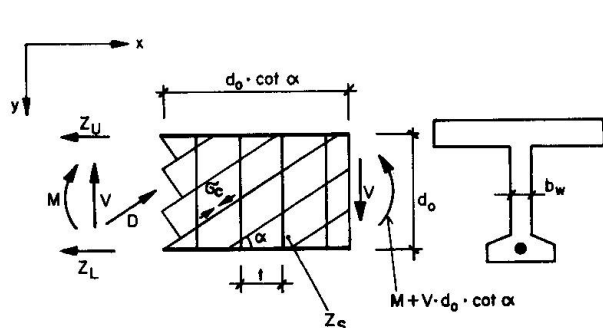


Fig. 8: Beam BI/3: Variation of Stirrup Strains under Load Range $\Delta F = 340$ kN

4. TRUSS MODEL

Beams under high shear forces can be decomposed into their functional elements. For a static analysis under service load conditions a truss model is used with the upper and lower stringers as chords, the stirrups as ties and the concrete as diagonal compression field inclined at angle α (Fig. 9, [3]).



$$D = \frac{V}{\sin \alpha}$$

$$z_L = \frac{M}{d_o} + \frac{1}{2} V \cdot \cot \alpha$$

$$z_U = -\frac{M}{d_o} + \frac{1}{2} V \cdot \cot \alpha$$

$$z_S = \frac{V \cdot t}{d_o} \tan \alpha$$

$$\sigma_c = \frac{-D}{b_w \cdot d_o \cdot \cos \alpha} = \frac{V}{b_w \cdot d_o} \cdot \frac{1}{\sin \alpha \cdot \cos \alpha}$$

Fig. 9: Truss Model for Bending and Shear

5. DISCUSSION OF RESULTS

For the discussion of the test results the following assumptions are made to calculate the stirrup stresses. Using the experimentally observed inclination of the cracks in the undisturbed section, not directly influenced by the load nor the reactions, as angle α (Fig. 2, $\alpha \approx 33^\circ$) for an uniaxial web compression field, the stirrups are determined from equilibrium consideration. They constitute an upper limit because of the assumption of zero tensile strength for the concrete.

The measured strains under maximum load, which are average values over the gauge length, and hence somewhat smaller than the maximum strains in the cracks, increase during cycling, whereas the strain differences under ΔF do not reach the level of the measured maximum $\Delta \epsilon$ over 100 mm gauge length (Figs. 7 and 8). An analogous consideration can be made for the strains and stresses in the longitudinal reinforcement (Fig. 6).

From the measured values it can also be seen that the increase of the strains under maximum load is higher than the increase of the differences of the strains. These observations show that a marked scatter of the maximum and minimum strains in the different stirrups exist. This situation is due to residual stresses caused by blocking of the cracks, local overstresses, etc. The strain variation $\Delta \epsilon$ becomes more regular with increasing number of cycles, in particular, it does not exceed the calculated value $\Delta \epsilon$. This strongly suggests the use of the stress variation $\Delta \sigma$ as a basis for the fatigue design of the reinforcement. Such a $\Delta \sigma$ -concept is proposed for the revision of the Swiss Code SIA 162.

6. STIRRUP FAILURES

In four beams stirrups of diameter 10 mm were used while two beams had stirrups of diameter 8 mm. A total of 76 fatigue failures were observed. Only two stirrups failed at the lower bend. These two failures at the bend occurred in both cases after two or more stirrups, crossed by the same crack, had previously failed. No failure of longitudinal reinforcement occurred.

From the first failure until loss of serviceability occurred, a considerable number of cycles elapsed. The above discussed specimen BI/3 for example was loaded



up to 5.75 Mio cycles with a stirrup failure in one leg occurring at 2.45 Mio cycles.

In Fig. 10 a summary of stirrup failures is given. The observed $\Delta\sigma$ in the stirrups is plotted against the number of cycles to failure. In many cases the failure of one leg of a stirrup induced the failure of the other leg at the same position in the crack after a few more cycles due to a considerable increase of stress.

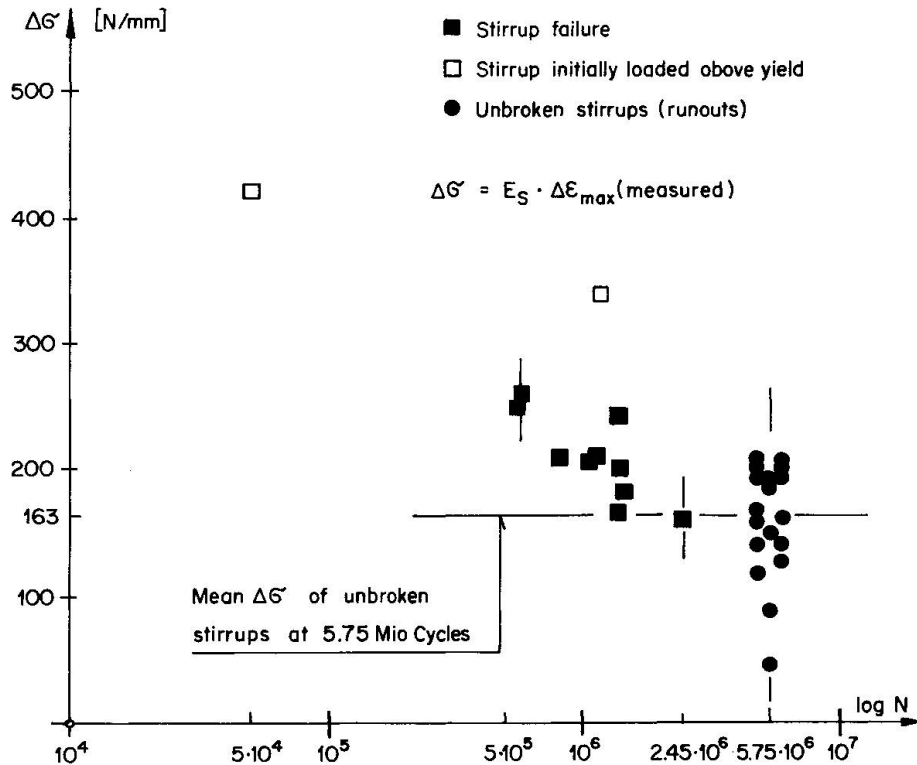


Fig. 10: $\Delta\sigma$ -N Diagram for Stirrups, diameter 10 mm

7. CONCLUSIONS

The results of fatigue tests of six beams under bending and shear showed a big scatter in the stresses of the stirrups and the longitudinal reinforcement. During cycling increases were observed, in a few cases even producing yielding of stirrups. The analysis showed that the stress amplitude can be determined more reliably than the maximum and minimum values. Hence, it follows that a fatigue design concept should be based on the stress range considering a mean $\Delta\sigma$ calculated from a fully developed truss model.

REFERENCES

- 1 Directive RL 34, Supplement to Structural Design Code SIA 162, 1976. Schweiz. Ingenieur- und Architekten-Verein, Zürich, 1976.
- 2 Comité Euro-International du Béton (CEB): "Code modèle pour les structures en béton", Système internat. de réglementation technique unifiée des structures, vol. II, Bulletin d'information, No. 117, Paris, décembre 1976.
- 3 Thürlimann, B.: "Plastic Analysis of Reinforced Concrete Beams", IABSE Colloq. Copenhagen 1979, Reports of the WC, IABSE Vol. 28, 1979.
- 4 Frey, R., Thürlimann, B.: "Ermüdungsversuche an Stahlbetonbalken" (Fatigue Tests on Reinforced Concrete Beams). Institut für Baustatik und Konstruktion, ETH Zürich (in preparation).



Fatigue Behaviour of Reinforced Concrete Beams under Shear Force

Comportement à la fatigue de poutres en béton armé sollicitées par un effort tranchant

Ermüdungsverhalten von Stahlbetonbalken unter Ermüdungsbeanspruchung

HAJIME OKAMURA

Associate Professor
University of Tokyo
Tokyo, Japan

TAMON UEDA

Graduate Student
University of Tokyo
Tokyo, Japan

SUMMARY

This report summarises a series of investigations on the shear behaviour of reinforced concrete beams under static and repeated loading. Procedures are given for calculating the average strain of stirrups in a beam under varied loading with variable maximum and minimum shear levels. The assumptions on which these procedures are based and the fatigue life of beams, with or without stirrups, are also presented.

RESUME

Ce rapport énumère une série de recherches sur le comportement à l'effort tranchant des poutres en béton armé soumises à des charges statiques et répétées. On donne des procédés pour calculer la déformation relative moyenne des étriers dans une poutre soumise à une charge variable oscillant entre les niveaux d'effort tranchant maximum et minimum. Les hypothèses sur lesquelles sont basées ces procédés et la durée de vie des poutres, avec ou sans étriers, sont également présentées.

ZUSAMMENFASSUNG

Der Beitrag beschreibt zusammenfassend eine Reihe Untersuchungen über das Schubverhalten von Stahlbetonbalken unter statischer und wiederholter Belastung. Das Vorgehen für die Berechnung der mittleren Bügeldehnungen in Stahlbetonträgern unter variabler maximaler und minimaler Schubbeanspruchung wird beschrieben. Die Annahmen, auf welche sich die Berechnungsmethoden abstützen, sowie die Lebensdauer von Schubträgern mit und ohne Bügelbewehrung werden besprochen.



1. INTRODUCTION

Recent shear design tends to request less web reinforcement than in the previous codes. This tendency demands the further study on fatigue. Concerning the fatigue behavior of beams with stirrups it was pointed out that (1) stirrup strains increased during fatigue loading [1][2][3], (2) fatigue fracture of stirrup was found [2][4][5] and (3) fatigue strength of stirrup was smaller than that of bar itself [2][5].

However no report, which deals with the phenomena systematically and rationally, is available. In order to get the fundamental knowledge of fatigue behavior, a series of research works have been carried out. This paper presents the summary of these investigations and the details are found in the original papers [6][7][8].

2. BEHAVIOR OF BEAMS WITH STIRRUPS UNDER FATIGUE LOADING

The general shear behavior of beams with stirrups under fatigue loading can be summarized as follows [6][7].

(1) Under the effect of repeated loading the inclined cracks increase gradually in width and extend upward or downward, but new diagonal cracks are seldom formed. With increase of the inclined cracks in width and in length, strains of stirrups intersected by the cracks increase. The rate of increase is not always the same among the stirrups, but the total strain or the average strain in a beam continues to increase at an almost constant rate against the logarithms of loading cycles.

(2) When the applied maximum shear level is lower than the shear capacity of concrete, average strain of stirrups hardly increases during the early stage of loading, and it begins to increase noticeably after some cycles of loading when two or three inclined cracks appear.

(3) Due to repeated loading fracture of stirrup generally occurs. The first fractured stirrup is usually the one that has developed the highest strain in the beam. When fracture of one leg occurs, the strain of another leg or the leg of the adjacent stirrup increases exceedingly, and the next fracture usually occurs in either of the legs after some thousand cycles. The beam will fail if it becomes unable to sustain the applied maximum shear force with the remaining legs.

(4) Fracturing of longitudinal bar is sometimes found. The fracture usually occurs just beside the first fractured stirrup.

3. FATIGUE STRENGTH OF BEAMS WITHOUT WEB REINFORCEMENT

Knowledge of fatigue strength of beams without web reinforcement is significant for investigating how stirrup strains increase under fatigue loading and when stirrup strains begin to increase in the case that the applied maximum shear level is lower than the shear capacity of concrete.

The experimental researches on fatigue strength of beams without web reinforcement had made clear the followings:

(1) Fatigue strength at 10^6 cycles is about 60% of the static strength [9][10][13][14].



- (2) S-N curve of a beam with larger span-depth ratio is different from that with smaller span-depth ratio [14].
 (3) Fatigue fracture of longitudinal bar tends to occur at the crossing point of diagonal crack when the span-depth ratio is small [13][14].
 (4) The beam, which should fail in flexure under static loading, sometimes fails in shear under fatigue loading [10].

However, the influence of loading range on the fatigue strength and the size effect had not yet been cleared. There had not been any S-N curves which include these factors.

Therefore, fatigue tests of beams were carried out under the condition in which the loading range and effective depth were changed. As a result, the influence of the loading range was clarified and an equation of the fatigue strength of beam was introduced for larger span-depth ratio [8].

$$\log(V_{\max}/V_u) = -0.036 (1-r|r|) \log N_f \quad (1)$$

- V_u calculated static shear strength of beam without web reinforcement [15]
 V_{\max} applied maximum shear level
 V_{\min} applied minimum shear level
 r V_{\min}/V_{\max}
 N_f failure life of a beam

The calculated values of Eq.(1) fit well the authors' and the previous tested values [9]-[14] as shown in Fig.1.

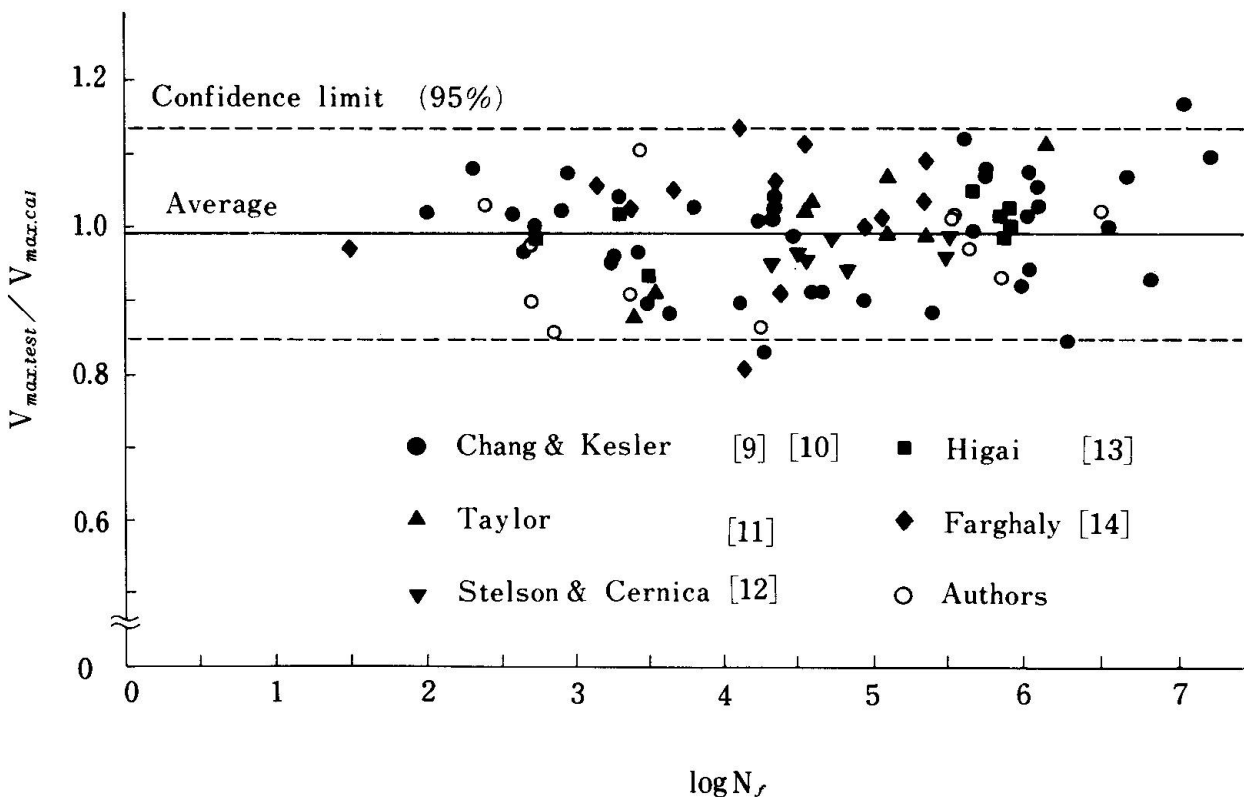


Fig.1 Ratio of Tested Value of (V_{\max}/V_u) to Calculated One by Eq.(1)



4. STRAIN OF STIRRUP UNDER REPEATED LOADING WITH CONSTANT MAXIMUM AND MINIMUM SHEAR LEVELS

4.1 Strain of Stirrup at the Maximum Shear Level

Although behavior of each stirrup under fatigue loading is fairly complicated, average strains apparently increase approximately in proportion to the logarithm of loading cycles as shown in Fig.2. And the rate of increase is not dependent on the strain at the first cycle, but is almost the same in spite of differences in the applied maximum shear level. This seems strange but can be explained by the following idea.

Since it may be reasonably considered from Reference [16] that the total shear force is carried by V_s and V_c , where V_s is shear force carried by assumed truss with 45 degree's diagonals and V_c is shear force carried by other means than the assumed truss, Eq.(2) is obtained under the maximum shear level in the fatigue test. The shear force V_c can be obtained by extending the shear - stirrup stress line toward the shear axis. Under fatigue loading the value of V_c is not considered as constant but should be decreased with the increase in number of loading cycles. When the decrease of V_c is assumed to be the same as that of

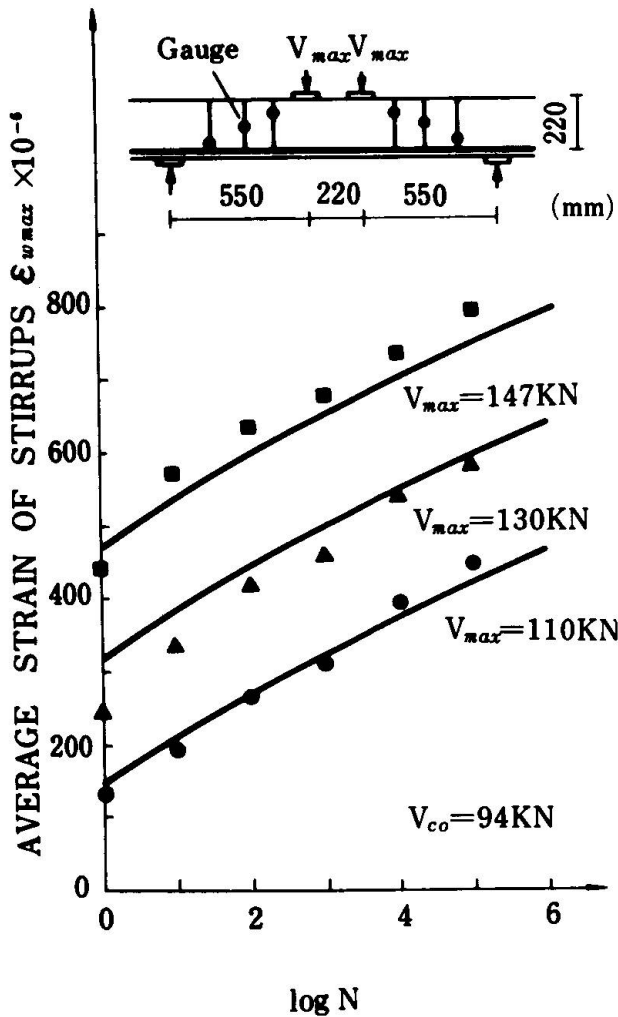


Fig.2 Average Strain of Stirrups ($V_{max} > V_{co}$)

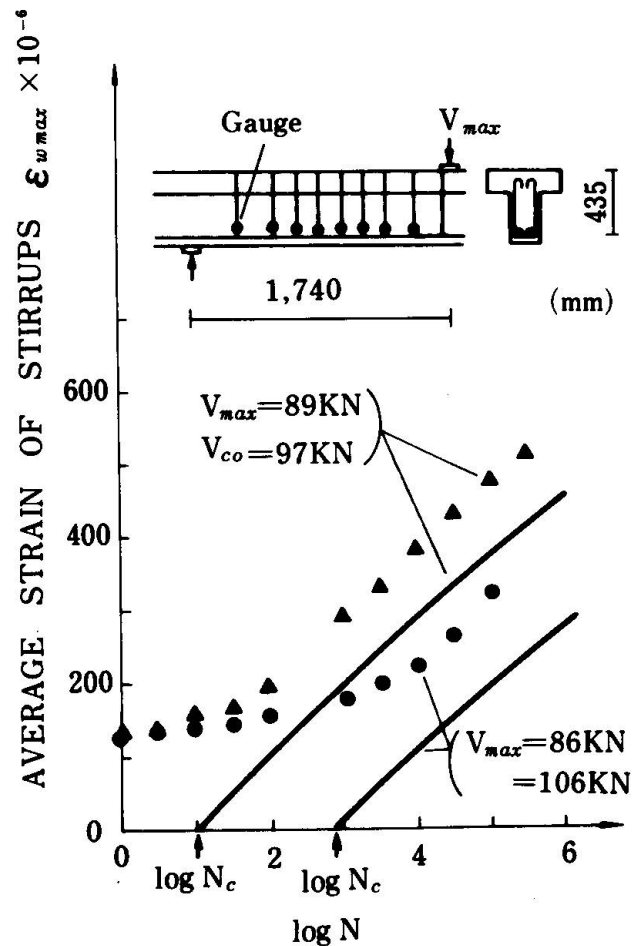


Fig.3 Average Strain of Stirrups ($V_{max} < V_{co}$)

fatigue strength of beam without web reinforcement, Eq.(3) is obtained. When the maximum shear level V_{max} is constant, the value of V_s should increase with decrease in the value of V_c as indicated in Eq.(2). Eq.(2) is, however, for the part of a beam where the influence of the support or loading point is negligibly small. For the part where this influence does exist, the shear force V_s is lightened by multiplying coefficient $\beta_x (< 1)$ [16]. Finally, the strain of the stirrup at the maximum shear level is expressed by Eq.(4). The values calculated by Eq.(4) are also shown in Fig.2.

$$V_s = V_{max} - V_c \quad (2)$$

$$V_c = V_{co} 10^{-0.036(1-r|r|)\log N} \quad (3)$$

$$\epsilon_{wmax} = \beta_x \{ V_{max} - V_{co} 10^{-0.036(1-r|r|)\log N} \} / (A_w E_w z/s) \quad (4)$$

V_{co} V_c at the initial loading
 N cycles of loading
 ϵ_{wmax} strain in stirrup at the applied maximum shear level
 β_x coefficient covering the influence of support or loading point [16]
 A_w cross sectional area of stirrups within distance s
 E_w Young's modulus of stirrup
 z arm length of truss
 s spacing of stirrups

When the applied maximum shear level is lower than the shear capacity of concrete, the increase in strains of stirrups is very small until a certain number of loading cycles. The idea on which Eq.(4) is based can be extended to estimate not only the number of cycles when stirrup strains begin to increase but also the increase of the strains thereafter.

$$\log N_c = - \log(V_{max}/V_{co}) / \{0.036(1-r|r|)\} \quad (5)$$

N_c loading cycles when average strain of stirrups begins to increase

After the loading cycles exceed the value of N_c , the stirrup strain at the applied maximum shear level can be calculated by Eq.(4), substituting for N the total loading cycles from the start of fatigue loading. The calculated values compared with experimental ones are shown in Fig.3.

4.2 Strain of Stirrup at the Applied Minimum Shear Level or Strain Range

Fig.4 shows the relationship between average strain of stirrups and applied shear force. The relation is considered as a straight line, and the inclination becomes larger with increase in number of cycles of fatigue loading, so that the strain range becomes larger. And a significant increase of the residual strain is observed.

The observed relationship can be explained if it is assumed that the curve is on the line between the point representing the strain at the applied maximum shear level and the specific point $(-V_{co}, 0)$ as shown in Fig.4. Then, the strain range is calculated by Eq.(6).

$$\epsilon_{wr} = \{ (V_{max} - V_{min}) / (V_{max} + V_{co}) \} \epsilon_{wmax} \quad (6)$$

ϵ_{wr} strain range in stirrup

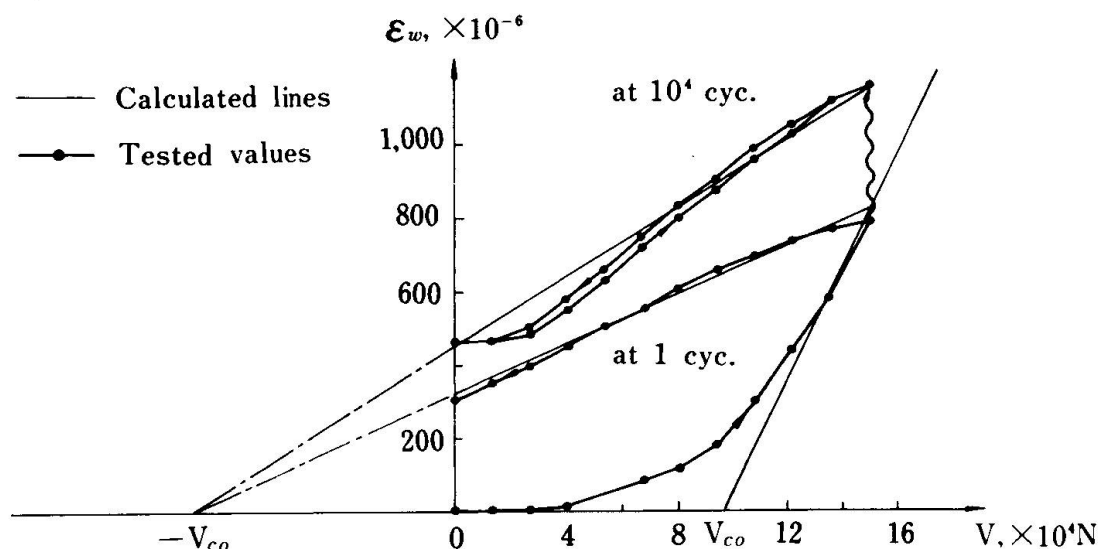


Fig.4 Observed and Assumed Relationships between Average Strain of Stirrups and Applied Shear Force

5. STRAIN OF STIRRUP UNDER FATIGUE LOADING WITH VARIED LOADING RANGE

Since actual structures are not subjected to fatigue loading with constant load range but generally subjected to varied loadings, it is necessary to know the behavior in this case.

General fatigue loading can be divided to some sets of repeated loading with constant maximum and minimum shear levels, and each set is named the first repeated loading, the second and so on according to the sequence of loading. The stirrup strain after subjected to the first repeated loading can be calculated as in Section 4. The strain during the second repeated loading can be calculated if the loading history of the first loading is expressed as equivalent cycles of loading whose maximum and minimum shear levels are equal to those of the second one. All the changes of stirrup strain under loading with varied loading range thus can be calculated by the same way.

In order to calculate the equivalent cycles, the following assumption is made. If stirrup strains produced by the shear force applied are same in beams subjected to different loading history, the changes of the strains during subsequent loading are essentially same in spite of the difference of the previous loading history. In other words, the behavior of a stirrup after subjected to a certain loading, static or fatigue or sustained loading, is only dependent on the strain corresponding to the shear force applied. Consequently any loading history can be substituted by an equivalent fatigue loading with the constant maximum and minimum shear levels as shown in Fig.5, and the stirrup strain can be calculated.

After a stirrup strain is subjected to N_2 cycles of the second repeated loading, stirrup strain at V_{max2} can be calculated by using Eq.(4), substituting $N_{eq}+N_2$ for N (See Fig.5). Therefore the strains hardly increase if the figures of N_2 are smaller than that of N_{eq} (See Fig.6(a)). When the applied maximum shear level of the second repeated loading is above the point A in Fig.5, there is no



influence of the previous fatigue loading and hence Eq.(4) can be used without any modification for calculating the strain of stirrup (See Fig.6(b)).

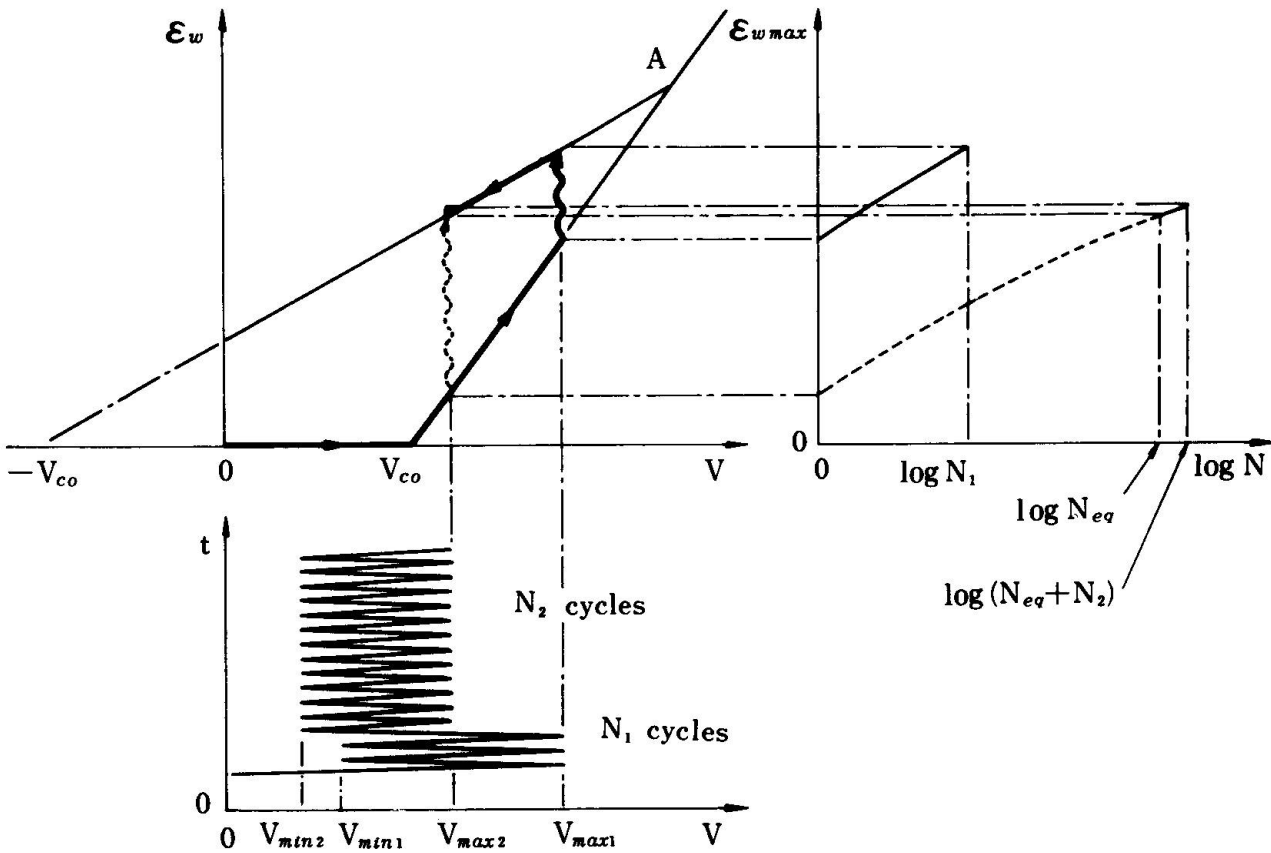


Fig.5 Assumption of an Equivalent Fatigue Loading (N_{eq} is equivalent loading cycles with constant maximum and minimum shear levels.)

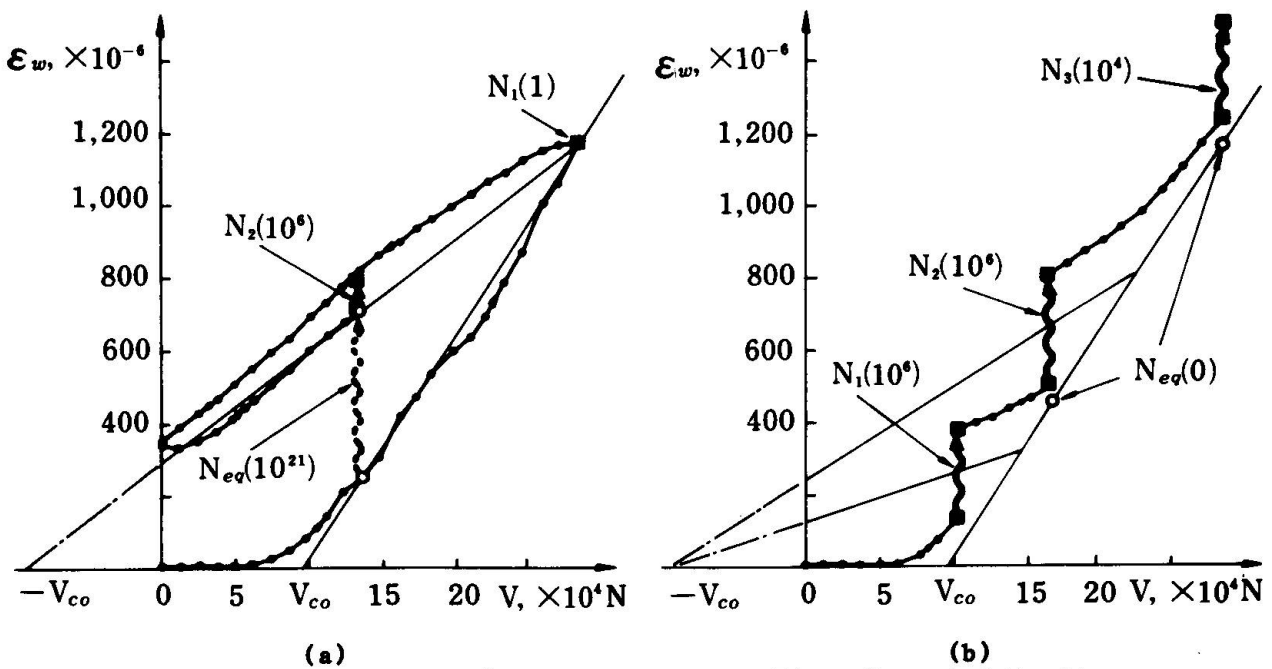


Fig.6 Average Strain of Stirrups after the First Repeated Loading



6. DESIGN CONSIDERATIONS

The fatigue fracture of stirrup occurs not only at lower bent portion where stirrup is bent around longitudinal bars but also at middle straight portion and upper hook portion. The portion of fracture is generally along the main diagonal crack making the beam to fail. The fatigue strength of stirrup is not cleared at present but supposed to lie between the fatigue strength of the straight bar and that of the bent bar, which is about 50% of the fatigue strength of the straight bar [2][14][17]. It is suggested that the fatigue life of a beam failing in shear due to stirrup fracture has the mutual correlation with the fatigue strength of stirrup [7].

ACKNOWLEDGEMENT

The authors heartily express their gratitude to Professor Dr. B. Thurlimann, Swiss Federal Institute of Technology, who discussed the problem on the occasion of our visit to the Institute.

REFERENCES

- [1] Ruhnau, J. : Influence of Repeated Loading on the Stirrup Stress of Reinforced Concrete Beams, ACI Publication SP-42, 1974
- [2] Hawkins, N.M. : Fatigue Characteristics in Bond and Shear of Reinforced Concrete Beams, ACI Publication SP-41, 1974
- [3] Kaar, P.H. and Mattock, A.H. : High Strength Bars as Concrete Reinforcement - Part 4 Control of Cracking, PCA Bulletin D59, 1963
- [4] Price, K.M. and Edwards, A.D. : Fatigue Strength in Shear of Prestressed Concrete I-Beams, ACI Journal, Vol.68, April 1971
- [5] Hanson, J.M., Hulsbos, C.L. and VanHorn, D.A. : Fatigue Tests of Prestressed Concrete I-Beams, Proc. of ASCE, Vol.96, No. ST11, Nov. 1970
- [6] Okamura, H., Farghaly, S.A. and Ueda, T. : Behaviors of Reinforced Concrete Beams with Stirrups Failing in Shear under Fatigue Loading, Proc. of the Japan Society of Civil Engineers (JSCE), No.308, April 1981
- [7] Ueda, T. and Okamura, H. : Behavior of Stirrups under Fatigue Loading, Transactions of the Japan Concrete Institute (JCI), 1981
- [8] Ueda, T. and Okamura, H. : Fatigue Strength of Beams without Web Reinforcement, Transactions of JCI, 1982 (to be published)
- [9] Chang, T.S. and Kesler, C.E. : Static and Fatigue Strength in Shear of Beams with Tensile Reinforcement, ACI Journal, Vol.55, June 1958
- [10] Chang, T.S. and Kesler, C.E. : Fatigue Behavior of Reinforced Concrete Beams, ACI Journal, Vol.55, August 1958
- [11] Taylor, R. : Discussion of a Paper by Chang, T.S. and Kesler, C.E. : Fatigue Behavior of Reinforced Concrete Beams, ACI Journal, Vol.56, March 1959
- [12] Stelson, T.E. and Cernica, J.N. : Fatigue Properties of Concrete Beams, ACI Journal, Vol.55, August 1958
- [13] Higai, T. : Fundamental Study on Shear Failure of Reinforced Concrete Beams, Proc. of JSCE, No.279, Nov. 1978
- [14] Farghaly, S.A. : Shear Design of Reinforced Concrete Beams for Static and Repeated Loads, PhD Dissertation to University of Tokyo, March 1979
- [15] Okamura, H. and Higai, T. : Proposed Design Equation for Shear Strength of Reinforced Concrete Beams without Web Reinforcement, Proc. of JSCE, No.300, August 1980
- [16] Okamura, H. and Farghaly, S.A. : Shear Design of Reinforced Concrete Beams for Static and Moving Loads, Proc. of JSCE, No.287, July 1979
- [17] Burton, K.T. and Hognestad, E. : Fatigue Tests of Reinforcing Bars - Tack Welding of Stirrups, PCA Bulletin D116, 1967

Fatigue Properties of Concrete Members Subjected to Torsion

Propriétés de fatigue des éléments en béton soumis à la torsion

Ermüdungseigenschaften von Betonbauteilen unter Torsionsbeanspruchung

KIYOSHI OKADA

Professor
Kyoto University
Kyoto, Japan

TAKAYUKI KOJIMA

Associate Professor
Ritsumeikan University
Kyoto, Japan

SUMMARY

Experimental investigation was undertaken to study fatigue properties of concrete members under pure torsion. The experiments included 148 tests consisting of plain, reinforced, prestressed and steel fibre reinforced concrete beam specimens. From results of the fatigue tests, S-N lines were obtained by statistical procedures. Fatigue strength at 10 millions cycles of loading was 53 to 56 % of the static ultimate strength of plain and prestressed concrete, while that of reinforced and steel fibre concrete was 38 to 53 %.

RESUME

Des recherches expérimentales ont été entreprises pour étudier les propriétés de fatigue des éléments en béton sous l'effet de la torsion pure. Les expériences comprenaient 148 essais de poutres en béton seul, armé, précontraint et armé de fibres d'acier. Des résultats des essais de fatigue, les droites S-N ont été obtenues à l'aide de procédés statistiques. La résistance à la fatigue après dix millions de cycles de charges valait 53 à 56 % de la résistance ultime statique du béton seul et précontraint, tandis que celle du béton armé et de fibres d'acier valait 38 à 53 %.

ZUSAMMENFASSUNG

Experimentelle Untersuchungen für das Studium der Ermüdungseigenschaften von Betonbauteilen unter reiner Torsionsbeanspruchung wurden durchgeführt, im ganzen 148 Versuche an unbewehrten, bewehrten, vorgespannten und stahlfaserbewehrten Balken. Aus den Ergebnissen wurden mit Hilfe statistischer Auswerteverfahren S-N-Kurven erstellt. Für vorgespannten sowie unbewehrten Beton betrug die Ermüdungsfestigkeit bei 10 Mio Lastwechseln 53 bis 56 % der statischen Bruchfestigkeit, während sie für Stahl- und Stahlfaserbeton bei 38 bis 53 % lag.



1. INTRODUCTION

The first research work on fatigue of plain concrete members was conducted by Van Ornum[1] in 1903, and since then many research works concerning fatigue properties of a wide range of plain concrete, reinforced concrete, reinforcing steel, prestressing tendon and prestressed concrete have been carried out. In recent years, design procedures of concrete structures have been transformed into ultimate strength design or limit state design, resulting in giving more concerns about fatigue properties of concrete members.

Though the case rarely occurs in which repeated torsion should be considered in designing concrete structures, it is a matter of interest for plain concrete as one of the basic properties of concrete under repeated diagonal tension due to torsional shear stress, and for prestressed concrete as fatigue problem under combined shear and prestress, i.e. under combined tensile-compressive state of stress. On the other hand, there have been many reports on deterioration due to cracking of reinforced concrete slab decks of highway bridges in Japan, and the cracks and their development are pointed out to be caused by repetition of moving wheel loads characterised in highway traffic[2]. This type of progressive failure of concrete slab may be considered due to fatigue under repeated torsion and shear.

Main objective of this study is to obtain basic data on fatigue properties of concrete under pure torsion. Torsional fatigue tests were carried out on plain, prestressed and reinforced concrete small specimens.

2. OUTLINE OF EXPERIMENT

The test program consisted of two series; series A on plain and prestressed concrete, and series B on plain, reinforced and steel fibre concrete. The mix proportions of concrete are listed in Table 1. Normal Portland cement, Yasu river sand for fine aggregate and Takatsuki crushed gravel for coarse aggregate were used in these mixes.

Details of test specimens are shown in Fig.1. A square cross section of 15x15cm were used for all beam specimens in this experiment. In the plain and prestressed beam specimens a small amount of longitudinal reinforcement consisting of four corner bars of 6mm in diameter was provided to prevent a sudden and violent failure. Three kind of steel ratio of 1.0, 1.5 and 2.0 percent in volume were used in reinforced concrete beam specimens of series B. In the reinforced concrete beam specimens, closed stirrups of 12x12cm of deformed bar of 6mm in diameter (D6) were arranged within a torsional span, and the arrangement of stirrups and details of longitudinal reinforcement are listed in Table 2 and also shown in Fig.1.

Table 1 mix proportions of concrete

series	max.size of aggregate (mm)	slump (cm)	W/C (%)	S/a (%)	unit content (kg/m ³)					W.R.A.*
					W	C	S	G	fibre	
A normal	20	10.0	41	41	196	478	671	1003	--	--
B normal	20	7.5	50	43	170	340	754	1038	--	used
B fibre	15	7.5	50	60	210	420	943	653	79	used

*W.R.A.: water reducing agent

In all beam specimens, some additional stirrups were provided near the both ends of the specimen to prevent failure at the support of a torsion arm(see Fig.1). Strengths of steel bars used are listed in Table 3. Steel fibre concrete was

used in beams with steel ratio of 1.5 percent. All specimens were stripped one day after casting of concrete and then stored in a curing room of about 20°C and relative humidity of 90±5 percent during about four months in series A and during about one month in series B. And the age when fatigue test was performed was 122 to 181 days for plain concrete in series A, 144 to 151 days for pre-stressed concrete, 112 to 146 days for plain concrete in B series, 112 to 137 days to 157 days for steel fibre concrete.

In the prestressed concrete specimens, effective prestress of 6.91 MPa was introduced one or two weeks before stating fatigue test and re-introduced immediately before testing.

3. TESTING PROCEDURE

Schematical view of the fatigue test arrangement is shown in Fig.2. All the beam specimens were loaded with a hydraulic pulsator. Before fatigue test, static tests were carried out. The maximum loads in the cycle were selected to 87 - 65 percent of the ultimate load for most of beams, but to 85 - 59 percent for plain concrete beams of series A, and to 75 - 55 percent for steel fibre concrete beams of series B. The minimum load in the cycle was kept at 9.81kN which gave the torque of 490Nm.

Table 2 details of reinforcement

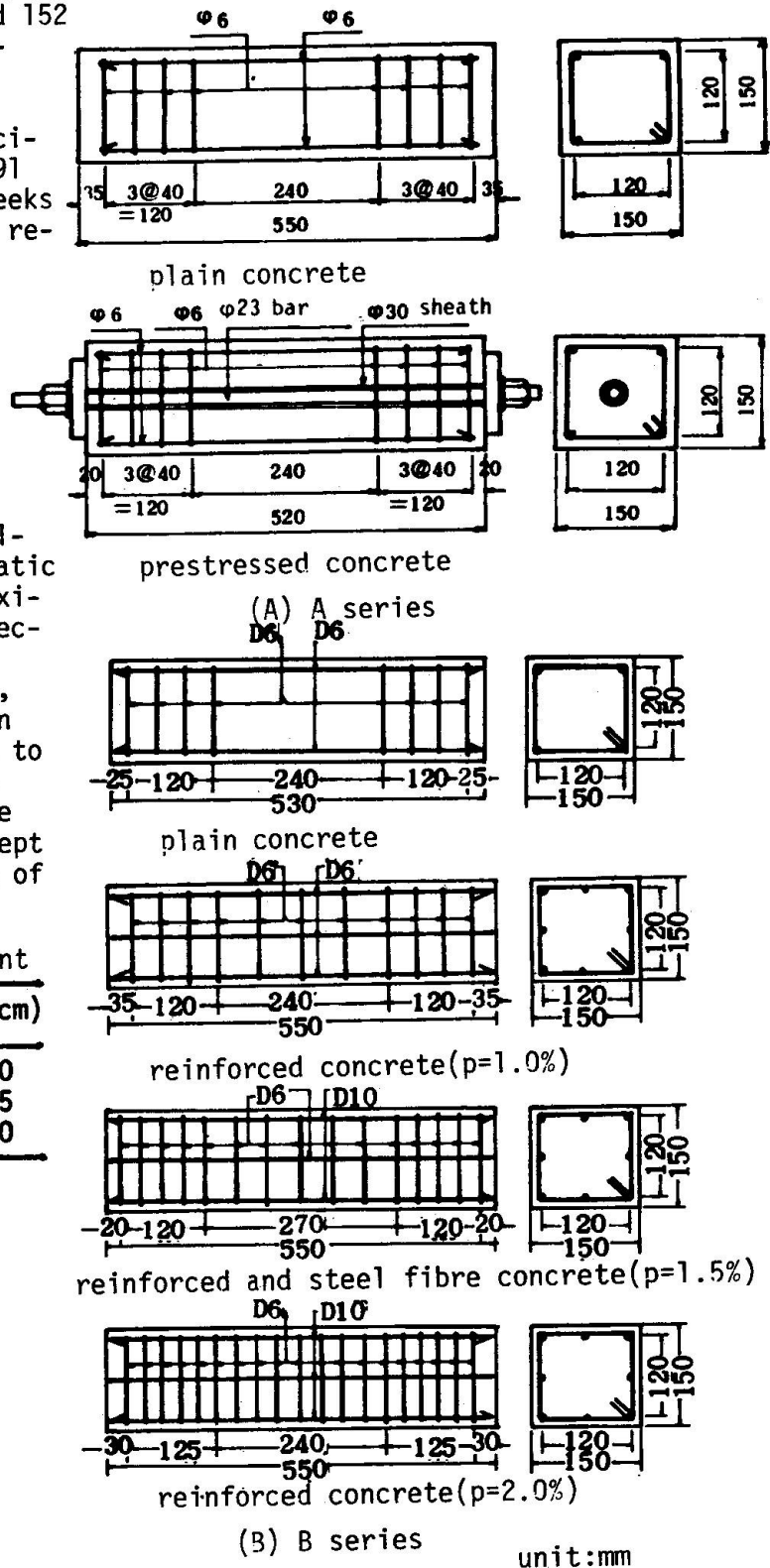
p	P _l (%)	p _v (%)	s(cm)
1.0	1.12(8D6)	1.13	6.0
1.5	1.83(4D10,4D6)	1.50	4.5
2.0	2.54(8D10)	2.25	3.0

P_l, p_v: longitudinal and lateral steel ratio respectively
 s: spacing of stirrup

Table 3 strength of reinforcing bar

	yield strength	ultimate strength
φ6	- -	488
D6	347	534
D10	373	548

unit: MPa



(B) B series unit:mm
 Fig.1 test specimen



The cyclic load was of a constant amplitude sinusoidal wave and its frequency was 7.5Hz for plain and pre-stressed concrete beams and 5.0Hz for reinforced and steel fibre concrete beams. The maximum and minimum loads were controlled and verified periodically by observing the output on a syncroscope of the load cell attached to the test arrangement (see Fig.2).

4. TEST RESULTS AND DISCUSSIONS

4.1 Static Strengths

Strength and elastic moduli of concrete are summarized in Table 4. Results of the static torsional tests are listed in Table 5. In series A the difference in tensile strength between two ages, by which the ultimate torque of the plain concrete was directly affected, was small, but the ultimate torque at the age of 180 days increased by more than ten percent compared with that at the age of 121 days. Such an increase in the ultimate torque may be considered due to difference in moisture contents rather than in ages at testing. The test at the age of 121

days was performed two days after the specimens were taken out from curing room, while the test at the age of 180 days was carried out after the specimens were fully dried in the testing room, and hence the ultimate strength at the age of 121 days seemed to decrease by the effect of drying shrinkage. The maximum

load ratio in the fatigue test of plain concrete in series A, therefore, were determined on the basis of the value at the age of 180 days.

Table 6 shows the theoretical values of the static ultimate torque. The values obtained from Hsu's equation [3], non-linear analysis [4] and Equation (1) gave good estimations for the ultimate strength of plain concrete.

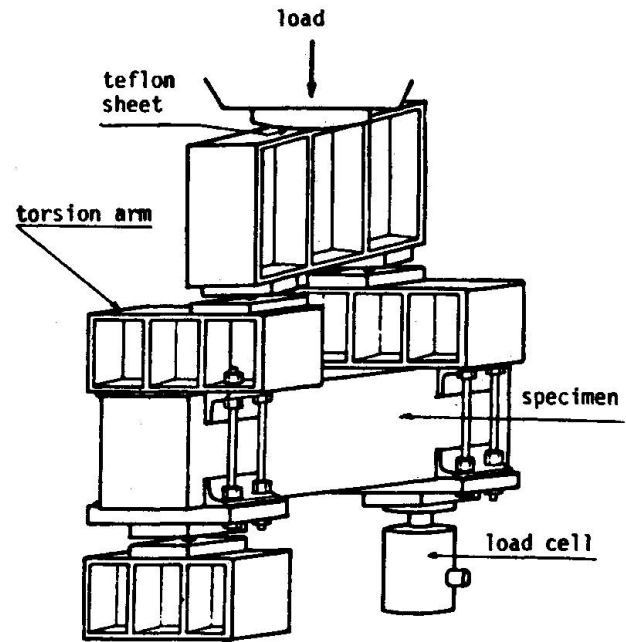


Fig.2 test arrangement

Table 4 strengths and elastic moduli of concrete

series	A series normal		B series normal fibre		
	age (day)	118	182	87	89
compressive strength f_{cu} (MPa)		44.4	48.3	45.7	46.9
tensile strength f_{tu} (MPa)		3.40	3.45	3.45	4.82
modulus of rupture f_{bu} (MPa)		5.34	6.35	5.14	8.65
Young's modulus E_c (GPa)		36.3	36.2	30.3	29.4
Poisson's ratio		0.214	0.204	0.188	0.195
shear modulus G_c (GPa)		14.9	15.0	12.7	12.3

Table 5 torsional strength by static tests

series	ultimate torque	age (day)	series & p(%)	cracking torque	ultimate torque	age (day)
plain concrete			reinforced concrete			
A	3190	121	B,1.0	3600	5720	89
A	3520	180	B,1.5	3840	7000	90
B	2840	87	B,2.0	4090	9340	91
prestressed concrete			steel fibre concrete			
A	6730	155	B,1.5	4170	9910	92

unit:Nm

Table 6 theoretical strengths (unit: Nm)

	Hsu[3]	Kojima[4]	Eq(1)
plain (A series)	3430*	3610*	3390*
concrete (B series)	3370	3320	3050
prestressed concrete	5940	6255	5870
reinforced concrete	cracking Hsu[3]	ultimate Lampart[5] Hsu[3]	
p=1.0%	3670	4510	4420
p=1.5%	3820	6430	5850
p=2.0%	4020	9410	7540

* : the values were calculated from the strength at 182days.

Equation (1) was derived as the approximate equation from the results of the non-linear analysis [4], that is

$$T_{up} = T_e + \frac{1}{4}(f_{bu}/f_{tu}-1)(5-f_{bu}/f_{tu})(T_p-T_e) \quad (1)$$

where $T_e = 1/(3+1.8b/h) \cdot b^2 h f_{tu}$, and $T_p = 1/2 \cdot (1-b/3h) b^2 h f_{tu}$. b and h are shorter and longer sides of rectangular section respectively. f_{tu} and f_{bu} are tensile and modulus of rupture of concrete respectively.

The theoretical values of the ultimate torque of prestressed concrete were obtained as those of plain concrete increased by the factor $\sqrt{1+f_p/f_{tu}}$ due to prestress, where f_p was effective prestress, and they were slightly less than the measurement.

The cracking strengths of reinforced concrete beams increased with steel ratio, and Hsu's equation [3] gave good estimations. As to the ultimate torque of reinforced concrete, the theoretical values by Lampart [5] were agreed with the test results in the range of high steel ratio, but the values by Hsu [3] were about 20 percent lower than the test results. The ultimate strength of steel fibre concrete beam increased by 42 percent compared with that of reinforced concrete beam having the same steel ratio of 1.5 percent.

4.2 Fatigue Properties

In the fatigue tests five specimens for each maximum load ratio were tested for plain concrete in series A, three specimens for prestressed concrete, and six specimens for all beams in series B. Relations between fatigue life and maximum load ratio are shown in Fig.4. An average fatigue life for each maximum load ratio was determined by the statistical procedure as used in analysis of fatigue data of concrete under compression [6]. The relation between probability of survival obtained from fatigue test for the same maximum load and the cycles at fatigue failure indicated an almost linear line when it was plotted on a logarithmic normal probability paper as shown in Fig.3 which is an example of the reinforced concrete with steel ratio of 2.0 percent. And in this study the average fatigue life for each maximum load was determined as the cycles at fifty percent probability of survival given by the regression line obtained from the method of least square. These values are listed in Table 7. In this study S-N curve was assumed to be linear and was determined as a regression line by the method of least square using the value in Table 7. Equations of S-N lines and fatigue strength at two million and ten million cycles of loading obtained by the S-N lines are summarized in Table 8, and S-N lines are also shown in Fig.4.

Fatigue strength of plain concrete at ten million cycles was 56,2 percent in

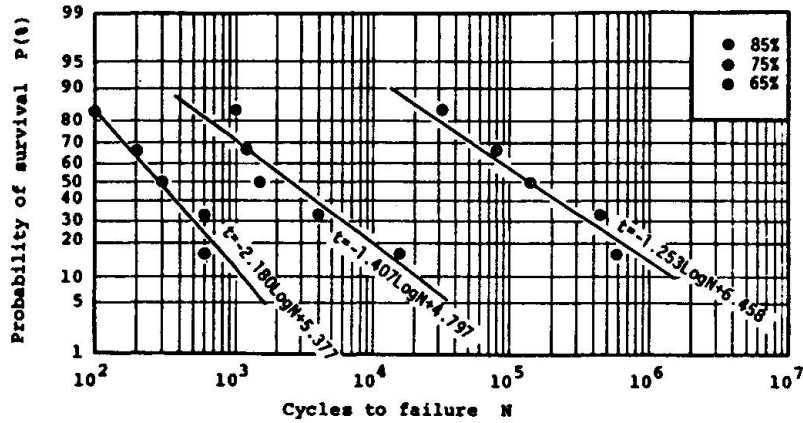


Fig.3 an example of relations between probability of survival and cycles to failure (reinforced concrete:p=2.0%)

Table 7 average fatigue life

	s	\bar{n}	s	\bar{n}	s	\bar{n}	s	\bar{n}
plain (A series)	85%	9200	77%	119100	68%	565700	59%	4627900
concrete (B series)	85	72700	75	- -	65	1944800		
prestressed concrete	85	900	75	34200	65	211000		
reinforced p=1.0%	85	676	75	881	65	25600		
concrete p=1.5%	85	1210	75	1210	65	364000		
concrete p=2.0%	85	293	75	2570	65	142800		
steel fibre concrete			75	2070	65	8180	55	407100

s:maximum load ratio, \bar{n} :average fatigue life(probability of survival:50%)

Table 8 S-N line and fatigue strength

	S-N line	fatigue strength at	
		2×10^6 cycles	10^7 cycles
plain (A series)	$S = -9.81 \log N + 125$	63.0%	56.2%
concrete (B series)	$S = -13.7 \log N + 153$	65.8	56.1
prestressed concrete	$S = -8.07 \log N + 110$	58.8	53.1
reinforced p=1.0%	$S = -10.2 \log N + 110$	45.4	38.2
concrete p=1.5%	$S = -7.78 \log N + 108$	58.5	53.1
concrete p=2.0%	$S = -7.23 \log N + 102$	56.0	51.0
steel fibre concrete	$S = -8.10 \log N + 99.7$	48.6	43.0

series A and 56.1 percent in series B, and it was almost same in spite of difference in mix. That of prestressed concrete was 53.1 percent. It is said that fatigue strength of concrete at ten million cycles is about 55 percent in compression and flexure [7],[8]. It suggests that fatigue strength of concrete under torsional shear stress is not much different from that under compressive or tensile stress.

In reinforced concrete, the static strength under torsion is determined by yielding of reinforcing steel in the range of under-reinforcement. In this experiment, the beams of p=1.0 and 1.5percent were under reinforced and the beam of 2.0 percent was slightly over-reinforced and therefore the fatigue strength of under-reinforced beam under torsion may be affected by fatigue properties of steel bars. By visual observation of the failed specimens, however, steel bars which failed due to fatigue could not be found at all in the beams the maximum load ratio of which was relatively low. It is indicates that the mechanism of fatigue failure of reinforced concrete under torsion should be considered for two cases; one for failure at low cycles by higher maximum load ratio and one for failure at high cycles by lower maximum load ratio. In the former case failure mechanism is similar to that in static failure, but in the latter one the beam usually passes through from uncracked state and gradually to cracked state up to failure. In the

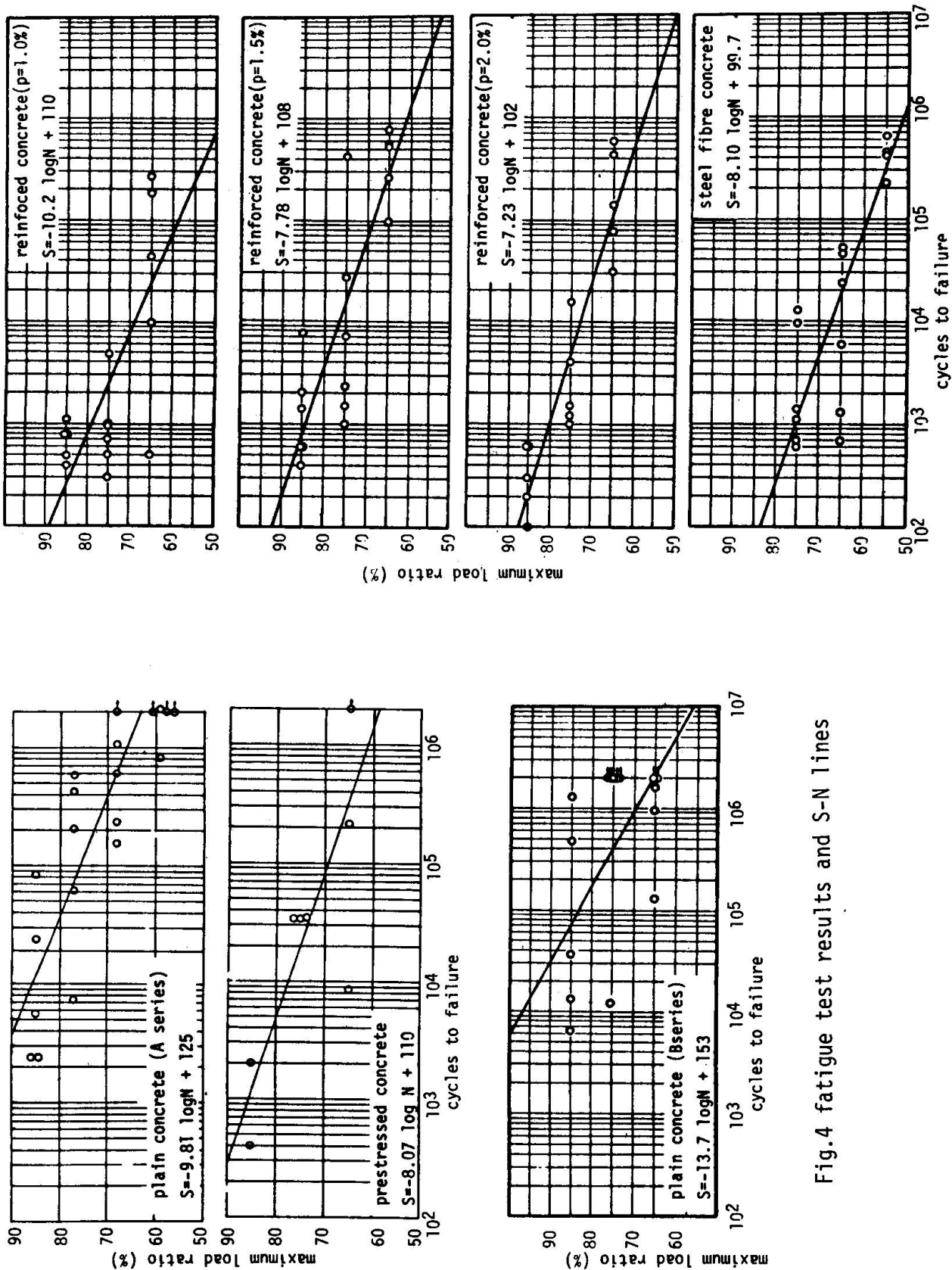


Fig.4 fatigue test results and S-N lines



uncracked state almost no stress occurs in reinforcing steel, while, once cracks occur, torsional shear stress is re-distributed gradually to the bars and torsional stiffness is reduced at the same time. In addition, in concrete near the reinforcing steel across the diagonal cracks, dowel force will act. Therefore failure of reinforced concrete might be caused by fatigue failure of concrete due to dowel force of the reinforcing steel.

Fatigue strength of the reinforced concrete beam of $p=1.0$ percent was somewhat lower than that of the other beams, probably because that its smaller after-cracking-torsional stiffness accelerated failure of concrete due to dowel force.

Fatigue strength of steel fibre concrete was ten percent lower at ten million cycles compared with that of reinforced concrete with the same reinforcement ratio. The effect of steel fibre concrete on fatigue resistance was smaller than that on the static strength, but when the maximum load ratio is calculated on the basis of the static strength of reinforced concrete beam ($p=1.5$ percent), its fatigue strength becomes 60.9 percent at ten million cycles, and as the effect of fibre concrete on fatigue resistance may be noticeable.

5. CONCLUSIONS

From the experimental investigation of fatigue of concrete members under pure torsion, the following conclusions may be drawn.

- (1) Fatigue properties of plain and prestressed concrete under torsion were almost same as those of concrete under compression or flexure, and fatigue strength was 53 to 56 percent of the static strength at ten million cycles of loading.
- (2) Fatigue failure of reinforced concrete did not occur due to failure of reinforcing steel but did due to failure of concrete near diagonal crack, though the static strength was determined by yielding of the bars.
- (3) Fatigue strength of reinforced concrete decreased when steel ratio was low. The effect of torsional stiffness after cracking may be responsible for this fact, but additional research is still needed.
- (4) Fatigue strength of steel fibre concrete was lower than that of reinforced concrete, but when compared with the basis of the static strength of reinforced concrete with the same reinforcement, the effect of fibre concrete was noticeable.

REFERENCES

1. Van Ornum, J.L.: The Fatigue of Cement Product, Trans. ASCE, Vol. 41, 1903.
2. Okada, K. at el.: Fatigue Failure Mechanism of Reinforced Concrete Bridge Deck Slabs, Transportation Research Records 664 and 665, Sept., 1978.
3. Hsu, T.T.C.: Torsion of Structural Concrete-A Summary on Pure Torsion, ACI Special Publication SP-18, 1968.
4. Kojima, T.: Study on Prestressed Concrete Beam of Rectangular Section Subjected to Torsion, Proc. of JSCE, No. 232, Dec., 1975.
5. Lampart, P. at el.: Torsion, Bending and Confusion-An Attempt to Establish the Facts, ACI Journal, No. 69-45, August 1972.
6. Sakata, K. at el.: A Study on the Fatigue Life of Concrete by the Statistic Treatment, Proc. of JSCE, No. 198, Feb. 1972.
7. Antrim, J.C. at el.: Fatigue Study of Air-Entrained Concrete, ACI Journal, No. 11, Vol. 30, 1959.
8. Grey, W.H. at el.: Fatigue Properties of Lightweight Concrete, ACI Journal, August 1961.



Fatigue of Partially Prestressed Concrete Beams

Fatigue de poutres en béton partiellement précontraint

Ermüdung teilweise vorgespannter Betonbalken

R.F. WARNER

Professor
University of Adelaide
Adelaide, Australia

SUMMARY

Constant cycle and cumulative damage fatigue tests were carried out on 5 mm dia crimped prestressing wire and 12.5 mm dia prestressing strand. The fatigue data from both test series, as well as from previous strand tests, correlate well when the stress range, defined as the maximum stress level minus the fatigue limit, is used as the main stress variable. Progressive inelastic changes in concrete beam behaviour under fatigue loading are discussed. It is suggested that fatigue life calculations need to be based on a stress analysis for the mid-life phase of behaviour rather than for the early load cycles.

RESUME

Des essais de fatigue sous cycle constant et de dommage cumulatif furent réalisés sur des fils de précontrainte profilés de 5 mm de diamètre ainsi que sur des torons de 12.5 mm de diamètre. La corrélation des deux séries d'essais ainsi que d'essais antérieurs est bonne lorsque l'on utilise comme variable la différence de contraintes, égale à la contrainte maximum moins la contrainte limite de fatigue. Des remarques sont faites concernant des modifications inélastiques progressives du comportement de poutres en béton soumises à des charges de fatigue. Il est proposé de baser les calculs de durée de vie de fatigue sur une analyse des contraintes correspondant à la demi-période de vie plutôt qu'aux premiers cycles de charge.

ZUSAMMENFASSUNG

An profilierten Vorspanndrähten mit Durchmesser 5 mm und an Vorspannlitzen mit Durchmesser 12.5 mm wurden Einstufen- und Mehrstufen-Versuche mit Schadenakkumulation durchgeführt. Die Ermüdungsergebnisse der beiden Versuchsserien sowie auch früherer Versuche an Litzen stimmen gut überein, wenn als Hauptvariable die Differenz der Maximalspannung zur Ermüdungsgrenzspannung benutzt wird. Progressive, nicht elastische Veränderungen des Verhaltens von Betonbalken unter Ermüdungsbelastung werden diskutiert. Es wird vorgeschlagen, für Lebensdauerberechnungen eher eine Spannungsanalyse nach halb durchlaufener Lebensdauer zu benutzen als nach den ersten Lastwechseln.



1. INTRODUCTION

Previous studies have shown clearly that fatigue in prestressed concrete beams is not a practical design problem provided the prestressing force is large enough to prevent opening and closing of flexural cracks[1]. Fully prestressed concrete is by definition uncracked at full design load and is one of the most suitable materials available for the construction of members subject to fatigue loading. However, partial prestressing is often preferred to full prestressing for reasons of economy and improved deflection control. Partially prestressed concrete members may undergo significant cracking at design load, and fatigue resistance is therefore a relevant design consideration when such members are called on to resist large numbers of repeated loads.

Fatigue failure of a normal, under-reinforced concrete flexural member, with or without prestress, occurs by fatigue in the tensile steel rather than in the compressive concrete[1]. Two distinct forms of information are therefore needed for the evaluation of the fatigue life of a partially prestressed concrete member:

- firstly, data (usually experimental) on the fatigue resistance of the reinforcing steel and prestressing tendon are required;
- secondly, a stress analysis procedure is required which transforms the cyclic load history of the member into cyclic stress histories for the reinforcing steel and prestressing steel in critical sections.

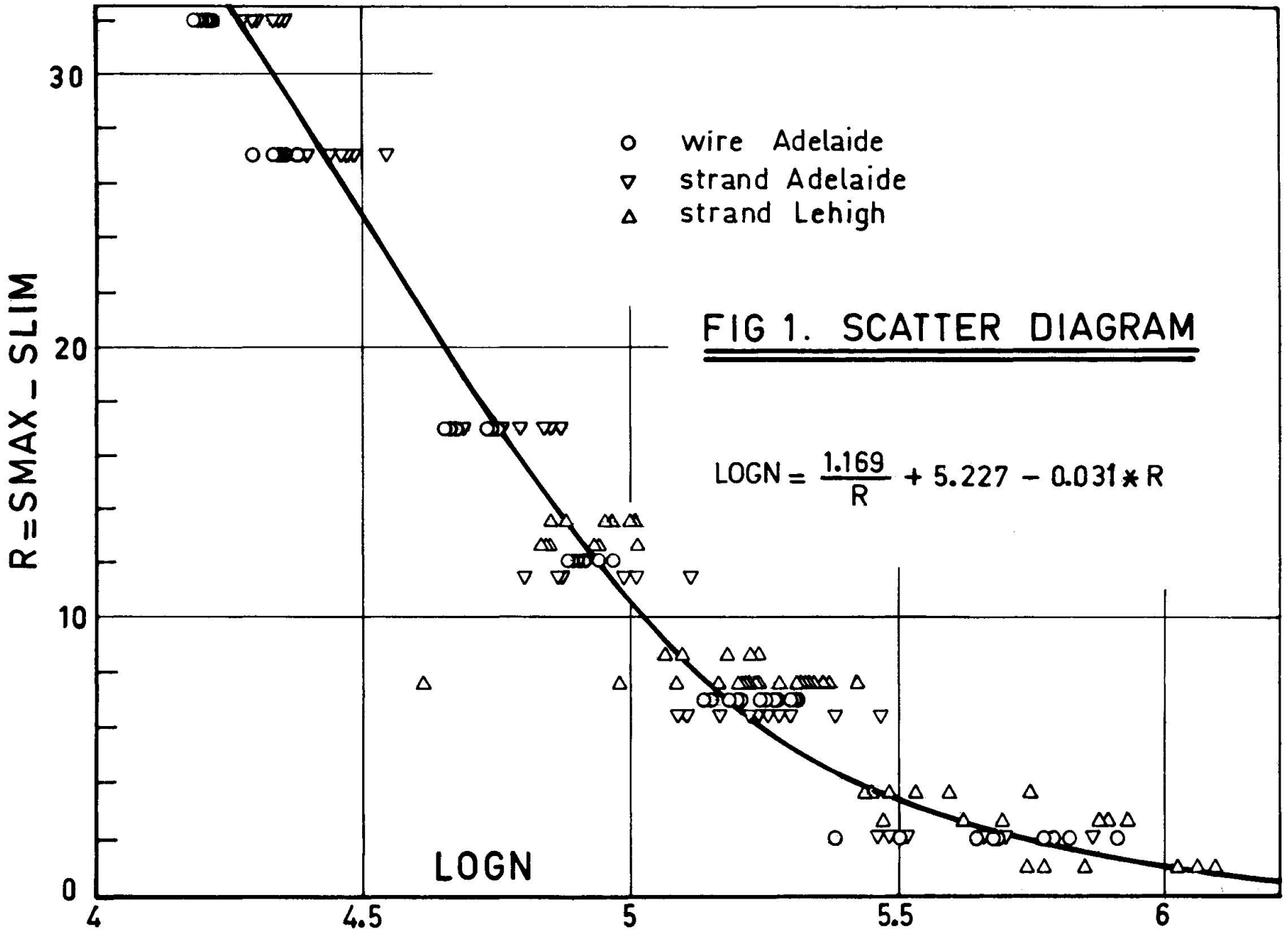
Both the reinforcing steel and the prestressing steel are in a state of near uniform tension in a flexural member, so that the required fatigue properties can be obtained from simple tests of bars and tendons subjected to cycles of uniaxial tensile stress. Results of a program of fatigue tests on two types of prestressing steel are briefly discussed below.

The analysis of stress in a cracked, partially prestressed concrete member under long term and repeated load is complicated by various inelastic and non-linear effects which, even in the case of a section subjected to constant cycles of moment, produce a complex history of progressively changing stress cycles. The main factors contributing to progressive changes in beam response are discussed in Section 3 of this paper.

2. FATIGUE PROPERTIES OF PRESTRESSING STEEL

Constant cycle and cumulative damage tests were carried out on 5 mm dia crimped prestressing wires and 12.5 mm dia 7-wire prestressing strand. All tests were of naked specimens of 900 mm length.

A special end gripping arrangement was used, whereby the ends of the specimen are bound with a fibreglass bandage covered with fresh araldite paste. A snug fitting aluminium tube is slipped over the bandage before the araldite sets. This grip, which deforms considerably when clamped in the jaws of the test machine, provides a simple, cheap and effective means of applying force to the ends of the specimen without causing fatigue failure there.





Constant Cycle Tests

Constant cycle tests were carried out on both wire and strand at minimum stress levels of 40 and 60 per cent of the static ultimate stress. Various maximum stress levels were used to study the relation between stress level and number of cycles to failure. For evaluation of the test results, the stress increment R was defined as follows:

$$R = S_{MAX} - S_{LIM} \quad (1)$$

where S_{MAX} is the maximum stress in the cycle, and S_{LIM} is the fatigue limit corresponding to the minimum stress level S_{MIN} in the cycle. The stress increment was found to be superior to the commonly used stress range, $S_{MAX} - S_{MIN}$, in correlating the constant cycle results.

An unexpected feature of the test results was the good correlation between the wire data and the strand data, when R is related to fatigue life N . The correlation appears to extend to data from other test programs. In the scatter diagram in Fig 1, R is plotted against the logarithm of N . About 100 data points for the current wire and strand tests are shown together with those from an extensive series of tests on 7/16 inch (11mm) dia prestressing strands which were carried out at Lehigh University [2]. The three sets of data display a common trend in this diagram and the relation between R and LOGN is well represented by the curve in Fig 1 which has the following equation:

$$\text{LOGN} = \frac{1.169}{R} + 5.227 - 0.031 \cdot R \quad (2)$$

The scatter around the mean line in Fig 1 is significant, as is to be expected for fatigue behaviour, and suggests that probability should be included in the representation of the test data. Although the scatter in the Lehigh data is somewhat larger than that in the present tests, this may well indicate differences in test procedures rather than inherent differences in material properties.

One reason why the stress increment R provides a better basis for data correlation than the stress range is because it treats the fatigue limit as an open, variable property of the material. Variations in the fatigue notch effect from material to material are thus allowed for indirectly in Eq 2 by possible variations in S_{LIM} . An estimate of the fatigue limit S_{LIM} is required before Eq 1 can be used to calculate mean fatigue life. Values of S_{LIM} for the wire and strand tests and also for the Lehigh tests are summarised in Table 1.

Ambient temperature was found to be a secondary but nevertheless significant factor affecting observed fatigue life in both the wire and the strand tests.

Cumulative Damage Tests

The cumulative damage tests were designed to provide information on the following:

- the applicability of the linear damage hypothesis to mixed stress cycles in which the maximum stress level varies;
 - the applicability of the linear damage hypothesis to progressively varying stress cycles in which the minimum stress level decreases with time; and
 - the effect of mixing small 'non-damaging' cycles with larger damaging cycles.
- The cumulative damage tests are not due for completion until 1982, but the results so far obtained are not seriously in conflict with the linear hypothesis.



Table 1 Fatigue Limit for Test Data

Test	Minimum Stress Level %	Fatigue Limit %
Wire: Adelaide	40	53
Strand: Adelaide	40	53
Strand: Lehigh	40	56.5
Wire: Adelaide	60	73
Strand: Adelaide	60	73
Strand: Lehigh	60	73

3. PROGRESSIVE CHANGES IN BEAM BEHAVIOUR DURING FATIGUE LOADING

The fatigue life of a partially prestressed member can be estimated from the fatigue properties of the component materials if an analytic method is available for determining the stress cycle histories from the known or assumed load cycle history. Such methods are usually based on the assumption of time-independent and cycle-independent structural behaviour[3]. Various inelastic effects are thereby ignored on the grounds that their influence is secondary.

However, laboratory tests have shown that overall deflection, as well as local deformations in high moment regions, may increase substantially in a beam which is subjected to fatigue loading. In Figs 2 and 3, progressive increases in deflection and concrete deformation at the steel level are plotted against number of load cycles. The data, which come from Ref 4, appear to be typical for a beam with a fatigue life in the order of a million cycles. There is a 34 per cent increase in deflection up to fatigue failure and a 44 per cent increase in deformation.

The main inelastic effects which produce progressive changes in the behaviour of a beam section are:

- shrinkage and static creep under minimum moment conditions;
- dynamic creep under cyclic moment;
- permanent deformation caused by repeated cycles of moment.

Shrinkage and static creep both contribute to deferred prestress losses and hence to a gradual decrease in the minimum stress levels in the prestressing steel and reinforcing steel. The stresses occurring in a section during short term moment cycles are also affected by the previous history of sustained moment. However, the magnitude of the minimum moment also has an important effect on the deferred losses. For example, if the minimum moment is large enough to cause decompression of the 'tensile' fibres of the section, then creep losses will be very small.

Dynamic creep occurs in concrete during rapid stress cycling. Balagura[5] has drawn attention to its effect on the fatigue behaviour of partially prestressed members. Dynamic creep is of most significance in cases of high speed fatigue loading, such as occurs in laboratory tests. In many practical situations, peak fatigue loads occur infrequently and dynamic creep may then be much less

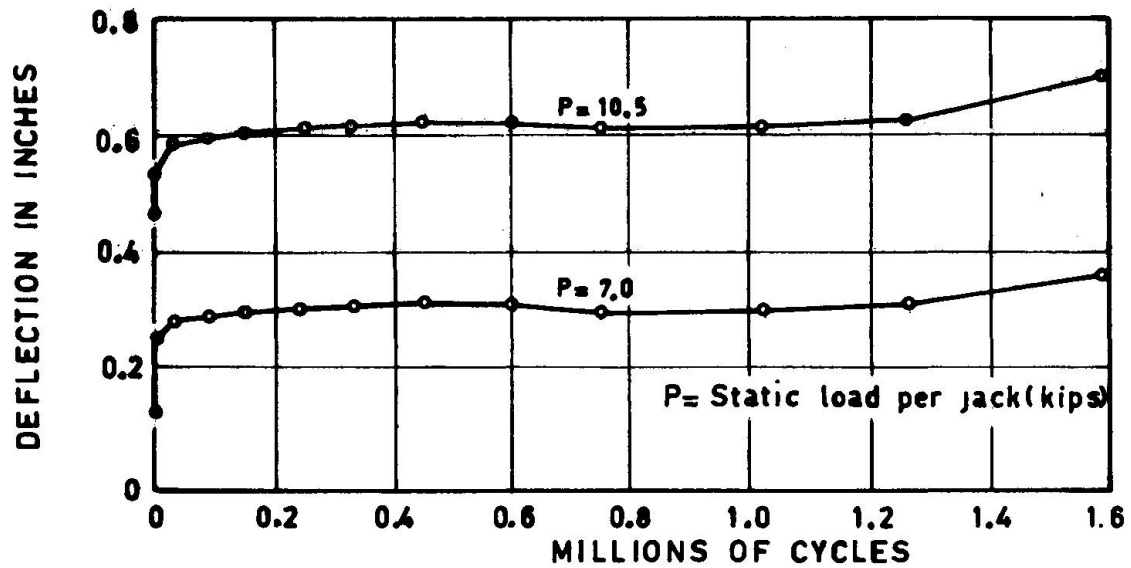


Fig 2. Mid-span deflection, Beam F8 (ref. 4)

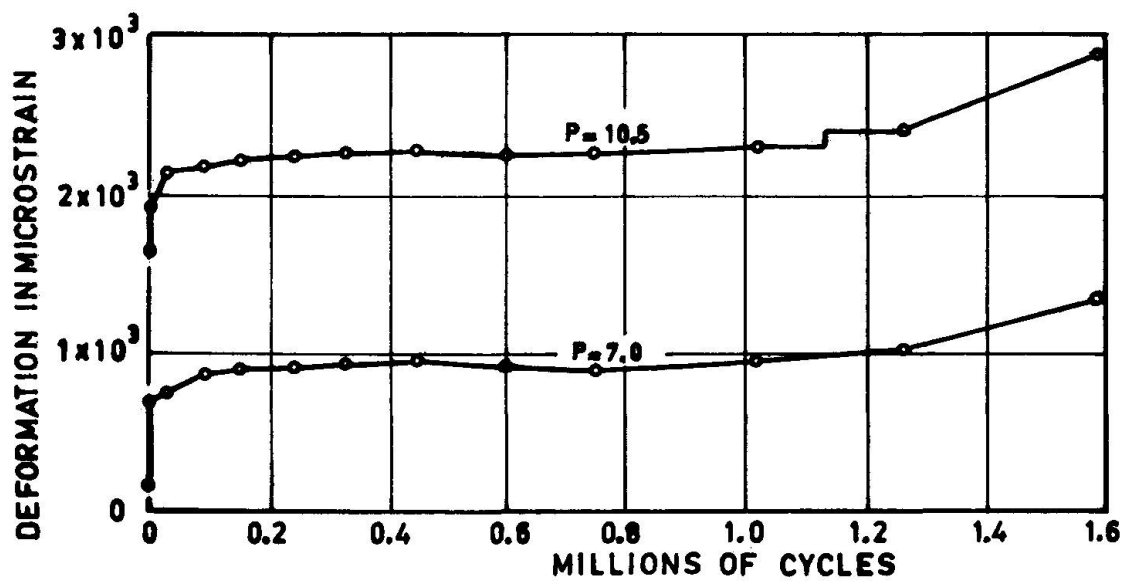


Fig 3. Concrete deformation, Beam F8 (ref. 4)



important than in the laboratory.

Some of the main factors which contribute to permanent deformations during moment cycling include:

- inelastic concrete strains in the compressive zone due to cyclic stressing;
- progressive cracking of the tensile zone and gradual loss of tension stiffening;
- progressive bond breakdown near the main cracks, especially between the concrete and the prestressing tendons.

These factors do not account completely for the permanent deformations which are observed when moment is removed from a section [4,6]. Further possible factors include:

- non-closure of cracks due to mis-match of adjacent crack surfaces and the presence of concrete debris;
- inelastic fatigue softening of the steel [5].

While the combination of such effects obviously has a significant influence on deformations and deflections, their effect on stress levels and fatigue life has not been adequately studied. Their importance lies partly in the fact that the fatigue life of a member in the long life range (eg greater than a million cycles) is sensitive to even very small variations in stress level. On the other hand, long term variations in stress level may not be comparable in magnitude with the observed changes in deformation. For example, loss of tension stiffening and bond breakdown result in an increase in average steel stress throughout the high moment regions, but may not significantly change the peak steel stress at the primary cracks. The end result of bond breakdown and loss of tension stiffening may thus be little significant change in the fatigue life of the section of maximum moment, but an increased probability of fatigue failure in adjacent sections. This conclusion is speculative and awaits the results of a theoretical study of inelastic effects which is at present being undertaken. An analysis of the effect of dynamic creep on fatigue life has recently been published[5].

It is significant that inelastic effects appear to have most influence on beam behaviour in the early load cycles. In Figs 2 and 3, the main increases in deflection and deformation occur in the first 20 per cent of the fatigue life of the beam. Variations in stress level presumably occur at the same time. It therefore seems reasonable to base fatigue life calculations on an assumed constant beam response (constant stress-moment relation). However, the middle life phase of beam behaviour should be considered and not the initial behaviour in the early load cycles.

4. SUMMARY AND CONCLUSIONS

Constant cycle fatigue data obtained from tests on prestressing wire and strand correlate well when the stress increment, $R = S_{MAX} - S_{MIN}$, is plotted against number of cycles to failure. Eq 2 fits the test data for prestressing wire and prestressing strand, as well as data obtained in a previous series of strand tests. The stress increment appears to be more appropriate than the stress range, $S_{MAX} - S_{MIN}$, for the treatment of fatigue data for prestressing steel.

Various inelastic effects cause progressive changes in the deformations and stresses in a partially prestressed concrete member and hence affect the fatigue life of a member. Fatigue life calculations should not therefore be based on an analysis of stresses in the first load cycle, but rather on stress-moment



relations which represent stabilised beam behaviour in the middle life phase after some thousands of load cycles have taken place.

5. ACKNOWLEDGEMENTS

The work described in this paper is being carried out with financial assistance from the Australian Research Grants Commission and the BHP Company. This assistance is gratefully acknowledged. The fatigue tests described in Section 2 were carried out by Dr C Rigon and Mr I Mackereth.

6. REFERENCES

1. WARNER R.F. HULSBOS C.L.: Probable Fatigue Life of Prestressed Concrete Beams. Journal, Prestressed Concrete Institute, Vol 11, No 2, April, 1966.
2. WARNER R.F. HULSBOS C.L.: Fatigue Properties of Prestressing Strand. Journal, Prestressed Concrete Institute, Vol 11, No 1, February, 1966.
3. ACI COMMITTEE 215: Considerations for Design of Concrete Structures Subjected to Fatigue Loading. Journal, American Concrete Institute, Proc Vol 71, No 3, March, 1974.
4. WARNER R.F.: Probable Fatigue Life of Prestressed Concrete Beams. PhD Thesis, Lehigh University, 1961.
5. BALAGURU P.N.: Analysis of Prestressed Concrete Beams for Fatigue Loading. Journal, Prestressed Concrete Institute, Vol 26, No 3, May-June 1981.
6. WARNER R.F.: Serviceability of Cracked Partially Prestressed Concrete Members: Tests and Analysis, FIP Symposium, Bucharest, 1980.



Betriebsfestigkeitsberechnung von Spannbetonquerschnitten

Limit State Design Method for Prestressed Concrete Sections

Méthode de dimensionnement aux états limites pour les sections en béton précontraint

CH. KÖRNER

Dr. -Ing.
Institut für Stahlbeton
Dresden, DDR

ZUSAMMENFASSUNG

Es werden die theoretischen Grundlagen eines Verfahrens zur Betriebsfestigkeitsberechnung dynamisch beanspruchter Spannbetonquerschnitte nach den Prinzipien der Grenzzustände behandelt. Dabei werden die Norm- und Rechenwerte für die Lastgrößen, Schnittgrößen und Baustofffestigkeiten mit Hilfe eines Systems von Normwert-Koeffizienten und Rechenfaktoren bestimmt.

SUMMARY

The paper presents the theoretical basis of the principles of a limit state design method for prestressed concrete sections subjected to dynamic loading. This includes the means of evaluating permissible and calculated values of loads, sectional forces and material strength from statistical coefficients and calculation factors.

RESUME

L'article présente les bases théoriques d'un procédé applicable au calcul de la résistance des sections transversales en béton précontraint sous charges dynamiques selon les principes des états limites. On détermine les valeurs normalisées et de calcul des charges, des efforts intérieurs et des résistances des matériaux à l'aide d'un système de coefficients statistiques et de facteurs de calcul.



1. EINLEITUNG

Die Ablösung der auf die Wöhlerlinie gegründeten Berechnung der Ermüdungstragfähigkeit durch eine Betriebsfestigkeitsberechnung ist eine der wesentlichen Voraussetzungen sowohl für die effektivere Gestaltung dynamisch beanspruchter Stahlbeton- und Spannbetonkonstruktionen als auch für die Nutzung vorhandener Tragreserven /1/. Im folgenden werden die Prinzipien einer Betriebsfestigkeitsberechnung auf der Grundlage von Beanspruchungskollektiven sowie zugeordneter Betriebsdauerlinien vorgestellt.

2. LÖSUNG DES SICHERHEITSPROBLEMS

Dem jeweiligen Stand der bautechnischen Entwicklung entsprechend wurden in der Vergangenheit Berechnungsmethoden entwickelt, in denen der Nachweis ausreichender Sicherheit auf der Basis ganz unterschiedlicher Sicherheitsvorstellungen geführt wird. In Bild 1 ist unter Bezug auf /2/ eine schematische Übersicht über die einzelnen Methoden sowie deren Zuordnung gegeben.

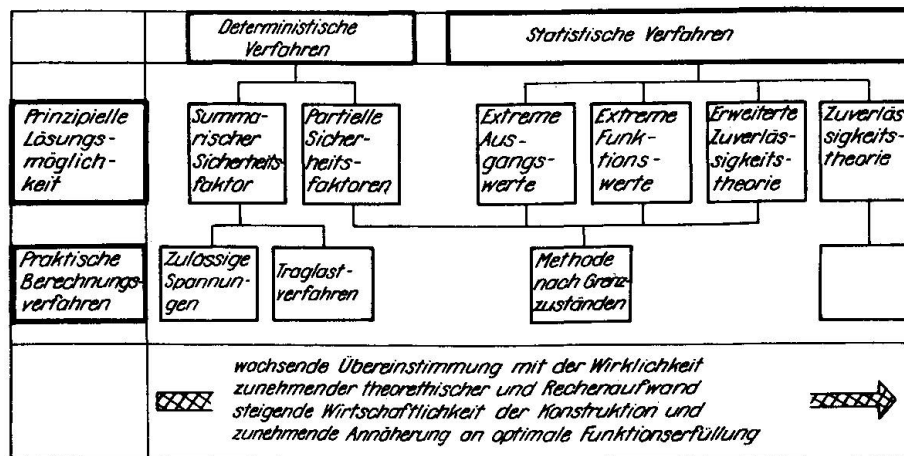


Bild 1 Prinzipielle Lösungsmöglichkeiten und praktische Berechnungsverfahren zur Führung des Sicherheitsnachweises

Die Prinzipien der Methode der extremen Ausgangswerte bilden die theoretische Grundlage für die Berechnungsmethode nach Grenzzuständen, die gegenwärtig als einheitliches und progressives Berechnungsverfahren zur Aufbereitung und Anwendung geeignet ist. Sie ist als eine Stufe zur Einführung der in Zukunft anwendungsfähig

auszuarbeitenden Zuverlässigkeitskonzeption für die Berechnung der Baukonstruktionen anzusehen.

Bei dynamisch beanspruchten Konstruktionen ist die Orientierung auf die Berechnungsmethode nach Grenzzuständen weniger zwingend als bei statisch beanspruchten, weil auch andere Methoden bestimmte Vorzüge aufweisen; doch muß die Entscheidung für das eine oder andere Verfahren vor dem Hintergrund der sich international abzeichnenden Tendenz in der Weiterentwicklung der Berechnungsverfahren gesehen werden. Mit dem RGW-Standard ST RGW 1406-78 "Beton- und Stahlbetonkonstruktionen; Projektierungsgrundlagen" /3/ sowie den "Internationalen Richtlinien des CEB/FIP zur Berechnung und Ausführung von Betonbauwerken" /4/ ist der Weg für die zukünftige Entwicklung abgesteckt.

Aus den dargelegten Gründen ist es zweckmäßig, das Berechnungsverfahren für dynamisch beanspruchte Spannbetonquerschnitte auf die Methode der Grenzzustände zu gründen.

3. GRUNDZÜGE EINES BERECHNUNGSVERFAHRENS /5/

3.1 Form des Sicherheitsnachweises

Im betrachteten Querschnitt steht der Beanspruchung $S(u_i, c_i)$ die Tragfähigkeit $R(v_j, d_j)$ gegenüber. In dieser symbolischen Schreibweise bedeuten u_i die zufallsabhängigen, c_i die nicht zufallsabhängigen Parameter der Beanspruchung S . Analog sind v_j die zufallsabhängigen, d_j die nicht zufallsabhängigen Parameter der Tragfähigkeit R .

Für dynamisch beanspruchte Spannbetonquerschnitte ist nach /1/ der Nachweis ausreichender Sicherheit gegen Eintreten des Grenzzustandes der Tragfähigkeit in zweifacher Hinsicht zu führen:

a) Für statische bzw. quasistatische Lasteinwirkungen darf die Beanspruchung, z. B. das Biegemoment M , die Tragfähigkeit, z. B. das Bruchmoment M_B , nicht überschreiten

$$M(\text{extrem } u_i, c_i) \leq M_B(\text{extrem } v_j, d_j) \quad (1)$$

b) Für dynamische Lasteinwirkungen darf die Beanspruchung M_F nicht größer sein als die Ermüdungstragfähigkeit $M_{B,F}$

$$M_F(\text{extrem } u_i, c_i) \leq M_{B,F}(\text{extrem } v_j, d_j) \quad (2)$$

bzw. die Spannungen σ_F infolge dynamischer Lasteinwirkungen müssen kleiner als die zugeordneten Ermüdungsfestigkeiten R_F sein



$$\sigma_F(\text{extrem } u_i, c_i) \cong R_F(\text{extrem } v_j, d_j) \quad (3)$$

Der Nachweis nach Gl. (1) für statische Lasteinwirkung ist, unabhängig von den Nachweisen für dynamische Lasteinwirkungen, nach den Prinzipien der Berechnung nach Grenzzuständen zu führen.

Beim Nachweis der Ermüdungstragfähigkeit stellt im Hinblick auf den notwendigen Berechnungsvorgang bei der Führung des Sicherheitsnachweises die konventionelle Form nach Gl. (3) die geeignete Grundlage dar. Auf der linken Gleichungsseite steht der Maximalwert σ_F der Beanspruchungsverteilung, die aus den Verteilungen aller zugehörigen Einflußgrößen berechnet werden muß. Erst danach kann durch Einordnung der Beanspruchungsverteilung in ein System der Normbeanspruchungskollektive oder durch direkte Berechnung der zugeordnete Wert der Ermüdungsfestigkeit R_F in Abhängigkeit von der Beanspruchungsverteilung aus dem System der Betriebsdauerlinien festgelegt werden. σ_F stellt somit in Verbindung mit der Kollektivform der Beanspruchung den Schlüsselwert dar, anhand dessen der Vergleich zwischen Beanspruchung und Tragfähigkeit auf der Spannungsebene geführt wird.

3.2 Bildung der Extremwerte für Lastgrößen und Festigkeiten

Gl. (3) zum Nachweis des Grenzzustandes der Tragfähigkeit nimmt für Spannbetonquerschnitt folgende allgemeine Form an

$$\sigma_F(C, Z^{(0)}; F, J, y) \cong R_F(N, K) \quad (4)$$

σ_F ist eine Funktion der Schnittgröße C , der Vorspannkraft $Z^{(0)}$ sowie der Querschnittskenngrößen F, J, y . Im Hinblick auf die Intensität der Streuungen sind die Schnittgrößen C , die Ermüdungsfestigkeit R_F sowie wegen des großen Einflusses auf den Spannungszustand eines Querschnitts auch die Vorspannkraft $Z^{(0)}$ als stochastisch veränderliche Größen mit ihren Verteilungen in die Rechnung einzuführen, während die Querschnittskenngrößen F, J, y , die Lastspielzahl N sowie die Form des Spannungskollektivs K in der Regel als determinierte Größen betrachtet werden können

$$\text{extrem } u_i = \{C, Z^{(0)}\}; \quad c_i = \{F, J, y\} \quad (5)$$

$$\text{extrem } v_j = R_F; \quad d_j = \{N, K\} \quad (6)$$

Diese Festlegungen stehen in Übereinstimmung mit /3/. In der praktischen Berechnung treten die Extremwerte der Ausgangsgrößen

Bild 2 Nachweis der Sicherheit gegen Ermüdungsbruch

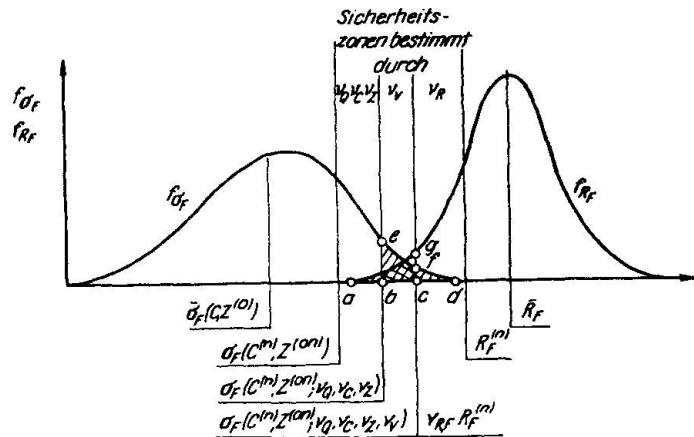


Bild 3 Rechenfaktoren γ_i zur Berücksichtigung von Unsicherheiten in den Einflußgrößen

	Einflußgrößen						
	Zufällige Streuungen unter Berücksichtigung des Prüfverfahrens	Vereinfachte Berechnungsannahmen	Ungünstige Lastkombinationen	Ermüdung unter Berücksichtigung der Spannungsverteilung	Qualität der Bauausführung, Bauüberwachung	Bruchverhalten von Querschnitt und Konstruktion	Folgen eines Versagens
	a	b	c	d	e	f	g
Lastgrößen Q	γ_{Qa}	γ_{Qb}	γ_{Qc}				
Schnittgrößen C (Vorspannkraft Z)		γ_{Cb}	γ_{Cc}	γ_{Cd}			
Festigkeiten R	γ_{Ra}	γ_{Rb}		γ_{Rd}	γ_{Re}	γ_{Rf}	
Verhalten der Konstruktion γ	$\gamma_{\gamma a}$	$\gamma_{\gamma b}$	$\gamma_{\gamma c}$	$\gamma_{\gamma d}$	$\gamma_{\gamma e}$	$\gamma_{\gamma f}$	$\gamma_{\gamma g}$

$C, Z^{(0)}, R_F$ als Rechenwerte (r) auf. Die Sicherheitsbedingung lautet dann (vgl. Bild 2)

$$\sigma_F(C^{(r)}, Z^{(0r)}; F, J, \gamma) \leq R_F^{(r)}(N, K) \quad (7)$$

Zur Festlegung der Extremwerte der Ausgangsgrößen (\approx Rechenwerte) wird mit Hilfe der statistischen Parameter der Häufigkeitsverteilung unter Beschränkung auf den Bereich mittlerer, d. h. statistisch gesicherter Wahrscheinlichkeiten für einen relativ kleinen Normwert-Koeffizienten $k^{(n)}$ zunächst ein statistisch gesicherter Normwert berechnet und hieraus mittels empirischer Rechenfaktoren γ_i der Rechenwert bestimmt.

3.3 Gliederung der Rechenfaktoren

Die unterschiedlichen Unsicherheiten können nach der Art ihres Auftretens und dem Charakter ihrer Auswirkungen in 4 Gruppen zusammengefaßt werden. Sie treten auf in

- den Lastgrößen



- der Ermittlung der Schnittgrößen und Querschnittsbeanspruchungen
- den Materialfestigkeiten
- dem Gesamtverhalten einer Konstruktion.

Für einen dynamisch beanspruchten Spannbetonquerschnitt sind in Anlehnung an /2/ die wichtigsten Einflüsse symbolisch für die genannten Gruppen in Bild 3 zusammengestellt. Es ist gegenwärtig nicht möglich, die einzelnen Einflüsse quantitativ zu belegen. Zur Vereinfachung der praktischen Berechnung sind sie zu wenigen Rechenfaktoren zusammenzufassen und an den entsprechenden Stellen in die Berechnung einzuführen (vgl. Abschn. 3.2).

Die für dynamisch beanspruchte Spannbetonquerschnitte durch Rechenfaktoren γ_i zu berücksichtigenden Einflüsse sind in Bild 3 besonders gekennzeichnet.

Der Inhalt der Sicherheitsbedingung läßt sich symbolisch in der in Bild 2 gezeigten Form darstellen. Die Sicherheit gegen Überschreiten extremer Werte

der Spannung $\sigma_F(C^{(n)}, Z^{(0n)}; \gamma_Q, \gamma_C, \gamma_Z, \gamma_V)$ bzw.

der Ermüdungsfestigkeit $\gamma_{R, F}^{R_F(n)}$

wird durch flexible Wahrscheinlichkeiten charakterisiert, die den Flächen a-c-g bzw. c-d-f zugeordnet sind.

Die zahlenmäßige Belegung der Rechenfaktoren ist zweckmäßig auf dem Wege vergleichender Rechnungen nach dem vorgelegten Entwurf des Berechnungsverfahrens und einem anderen Berechnungsverfahren für dynamisch beanspruchte Spannbetonquerschnitte durchzuführen (calibration method). Dabei werden die disponiblen Rechenfaktoren so festgelegt, daß die Berechnung nach dem Entwurf des Berechnungsverfahrens für einen möglichst großen, verschiedene Beanspruchungsverhältnisse und Querschnittsausbildung umfassenden, Bereich zu den gleichen Ergebnissen führt wie das Vergleichsverfahren.

In Bild 4 ist der Berechnungsgang zum Nachweis der Tragfähigkeit eines dynamisch beanspruchten Spannbetonquerschnitts unter Berücksichtigung der Betriebsbeanspruchung in Form eines Flußdiagramms dargestellt.

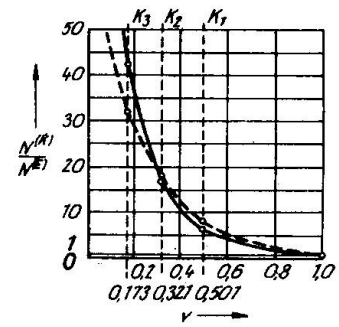
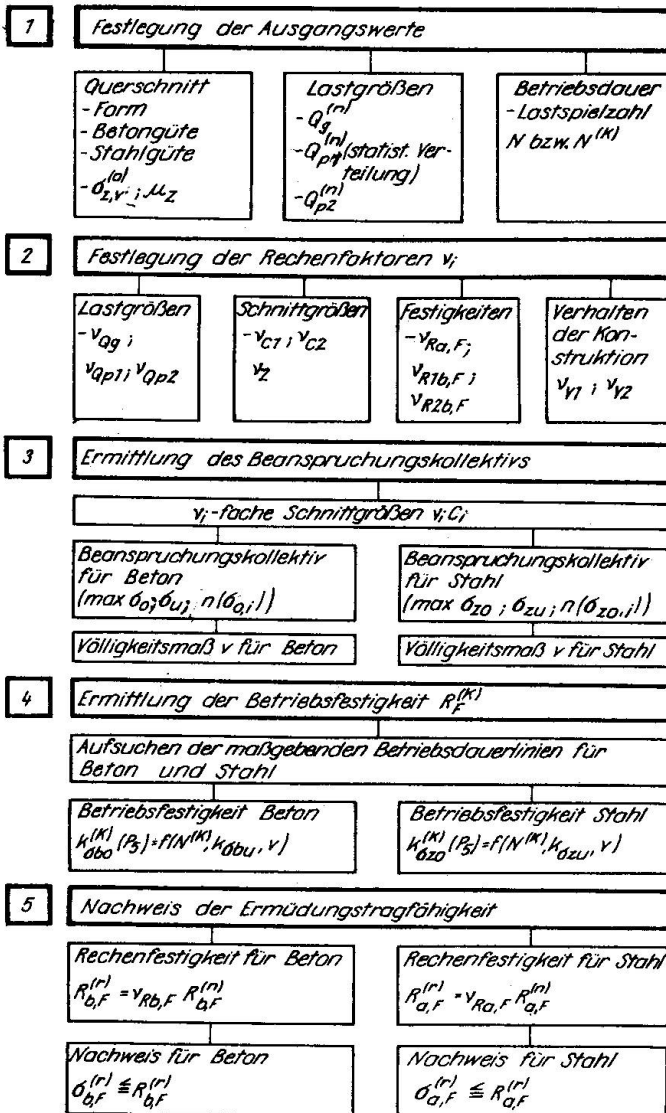


Bild 5 Einfluß der Kollektivform auf die mittlere relative Lebensdauer $\frac{N^{(K)}}{N^{(E)}}$ im Zeitfestigkeitsbereich ($N < 2 \cdot 10^6$)

Bild 4 Rechenvorschrift zum Nachweis der Ermüdungstragfähigkeit eines dynamisch beanspruchten Spannbetonquerschnitts unter Berücksichtigung der Betriebsbeanspruchung

4. PRAKTISCHE ANWENDUNG DER BETRIEBSFESTIGKEITSBERECHNUNG

Die durch eine Betriebsfestigkeitsberechnung aktivierten Tragfähigkeitsreserven eines dynamisch beanspruchten Spannbetonquerschnitts können auf folgende Weise genutzt werden:

- Einsparung an Material durch Reduzierung der Querschnittsabmessungen oder Senkung des Bewehrungsgrads
- Erhöhung der zulässigen Belastung bei Beibehaltung der Querschnittsausbildung
- Verlängerung der Lebensdauer bei Beibehaltung der Querschnittsausbildung und der Belastung.



Der letztgenannte Effekt wird durch Bild 5 verdeutlicht, in dem der Einfluß von Lastkollektiven K unterschiedlicher statistischer Verteilung, gekennzeichnet durch sogenannte Völligkeitsmaße v_1 , v_2 und v_3 , auf die Lebensdauer angegeben ist. Gegenüber einer Bemessung auf der Grundlage der Einstufenbelastung (ertragbare Lastspielzahl $N^{(E)}$) kann bei Ansatz der Betriebsbelastung (ertragbare Lastspielzahl $N^{(K)}$) je nach Kollektivvölligkeit v in vorliegendem Fall die sechs- bis vierzigfache Lebensdauer, d. h. $N^{(K)} = (6 \dots 40) N^{(E)}$, nachgewiesen werden.

LITERATUR

- /1/ Körner, C.: Tragfähigkeit dynamisch beanspruchter Spannbetonquerschnitte. Bauakademie der DDR, Schriftenreihe der Bauforschung, Reihe Stahlbeton, H. 15, Bauinformation, Berlin 1970
- /2/ Dahl, J.; Spaethe, G.: Sicherheit und Zuverlässigkeit von Bauwerken. Bauakademie der DDR, Schriftenreihen der Bauforschung, Reihe Technik und Organisation, H. 36, Bauinformation, Berlin 1970
- /3/ RGW-Standard ST RGW 1406-78 "Beton und Stahlbetonkonstruktionen; Projektierungsgrundlagen"
- /4/ CEB/FIP: Internationale Richtlinie zur Berechnung und Ausführung von Betonbauwerken, 1977
- /5/ Körner, C.: Betriebsfestigkeit dynamisch beanspruchter Spannbetonquerschnitte; Berechnungsgrundlagen. Bauakademie der DDR, Bauforschung-Baupraxis, H. 24, Bauinformation, Berlin 1979

Unexpected Fatigue Failures of Non-prestressed Reinforcements

Rupture inattendue de l'armature passive due à la fatigue

Unerwartete Ermüdungsbrüche in der schlaffen Bewehrung

F.J. SAINZ DE CUETO

Struct. Eng.

Laboratorio Central de Estructuras y Materiales CEEOP

Madrid, Spain

SUMMARY

The calculation models to predict the response of partially prestressed concrete bridge girders, subjected to traffic cyclic loads, usually incorporate many assumptions about the pattern behavior. One of the most widely used is the perfect bond between steel and concrete, neglecting the local bond breakdown surrounding each flexure crack. Laboratory test results given in this paper show that some unexpected fatigue failure, due to cumulative damage in non-prestressed reinforcement, can be found. Fretting secondary stresses, owing to the curvature at deflection, ought to be included in a Class 2 and Class 3 design.

RESUME

Les modèles de calcul pour estimer la réponse d'une poutre d'un pont en béton partiellement précontraint, soumise à des sollicitations dynamiques dues au trafic, contiennent généralement beaucoup de simplifications sur le comportement réel des éléments structuraux de ces ouvrages d'art. Une des hypothèses les plus utilisées est la parfaite adhérence acier-béton, malgré son inexistence à proximité de la fissure. Cet article donne les résultats d'essais montrant quelques ruptures dues à des dommages cumulatifs de l'armature passive. Il faut tenir compte dans le calcul mathématique en Classe 2 et 3, des contraintes secondaires de friction dues à la courbure de l'armature passive.

ZUSAMMENFASSUNG

Die Berechnungsmodelle über das Verhalten teilweise vorgespannter Betonbrückenträger unter zyklischer Verkehrsbelastung enthalten oft viele Vereinfachungen gegenüber dem wirklichen Verhalten. Eine der häufigsten Vereinfachungen betrifft die Vernachlässigung der unvollständigen Haftung zwischen Stahl und Beton in Rissnähe. Die im Beitrag vorgestellten Versuchsergebnisse zeigen unerwartete Ermüdungsbrüche in der schlaffen Bewehrung. Die durch die Biegekrümmung hervorgerufenen Nebenspannungen infolge Reibungseffekten sollten in den Berechnungen für die Brückenklassen 2 und 3 berücksichtigt werden.



1. INTRODUCTION

A research investigation, conducted in the Department of Structures at the Laboratorio Central de Estructuras y Materiales, is being carried out to obtain information on the fatigue life of prestressed concrete bridge beams under traffic cyclic loads. Full size bridge girders have been tested. However, in order to attain an acceptable level of reliability, further beam tests are being made to explain some specific questions. A knotty point was the verification of fatigue behavior of the non-prestressed steel addition (commonly advised against fatigue failure) after cracking. As a matter of fact that situation appears not only in a Class 3 design, but in Class 2 too, for exceptional live loads. This feature was included in the test program of series E2, which the present article deals with. On the other hand, the choice of a good mathematical simulation model, to find out the stresses in those reinforcements, is not an easy task, especially if we incorporate some usual assumptions. With regard to that question, as the present work shows, we might be on the unsafe side.

2. SIMULATION MODEL AT CRACKED SECTION

2.1 Hypothesis for simplification

Technical literature contains many theoretical and experimental works on the behavior of beams bending under repeated overloads. When the external moment exceeds the value at which cracks begin to open and close, their flexural response is non-linear and conditions become more complicated. Nevertheless the computational effort can be reduced if the following assumptions are made:

- Strains vary linearly over the depth of the member throughout the entire load range.
- After cracking, tension in the concrete is neglected.
- Equilibrium of internal forces.
- Linear elastic response of steel instead a more complicated (history dependent) constitutive relation. During the first cycles of loading, this behavior is not true if that material has been stressed up to yield, and some analytical model for steel should be used.
- The perfect bond between steel and concrete seems to be the most doubtful hypothesis in this model. Some authors bear in mind the bond failure introducing a dimensionless compatibility factor. However, the factor evaluation is difficult because of the scatter natures of this phenomenon and values must therefore be determined from beam tests.
- Effects of shear are negligible on sufficiently slender members.

2.2 Striped model

As can be seen from Figure 1, the model is valid for any section shape, with steel (either prestressed or not) reinforcements at several different levels. To compute the integrals appearing in the mathematical equations, the compressive block of section is divided into vertical strips. In every one of them a cubic parabola was approximated from the concrete stress-strain curve (Figure 2) in order to provide the compressive stress distribution. The flow chart in Figure 3 illustrates, step by step, the program for computer which allows the stresses evaluation. [2] [3]

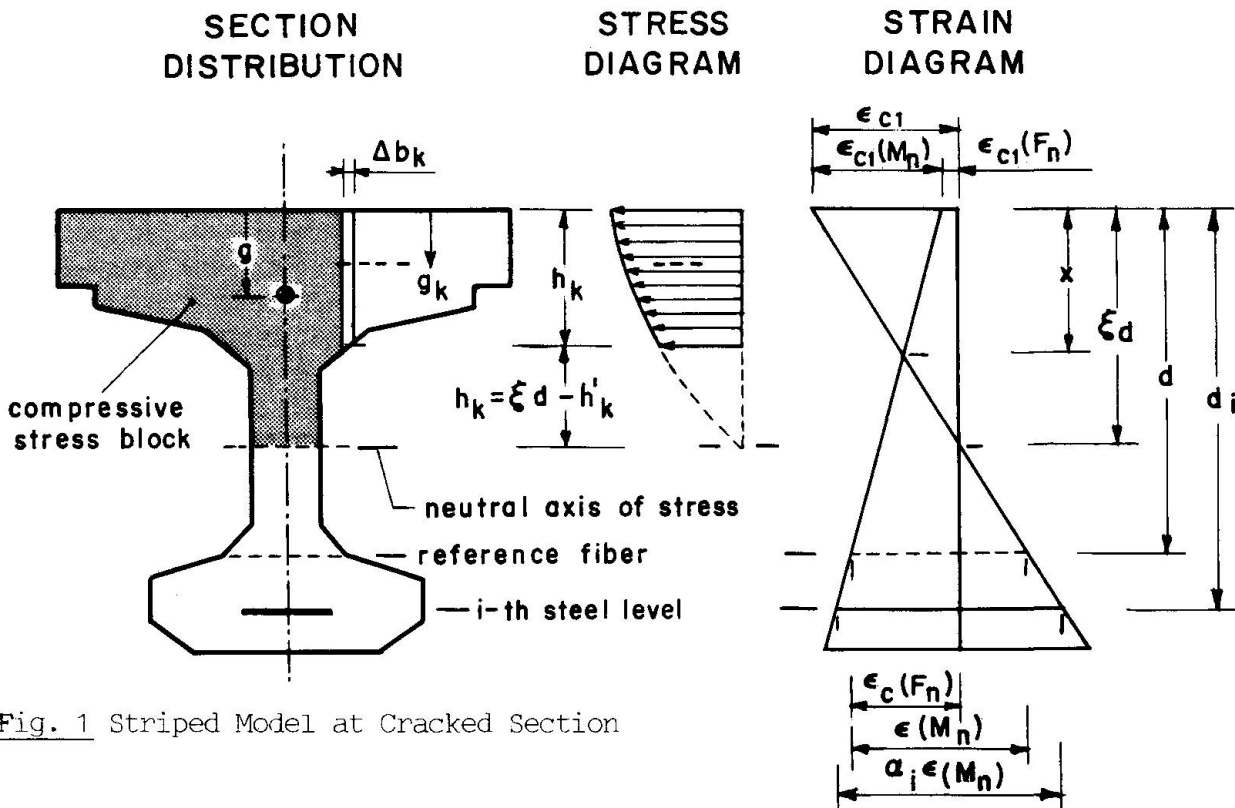


Fig. 1 Striped Model at Cracked Section

2.3 Notations

The following terms have been used in the present model:

- N - number of steel levels (including non-tensioned reinforcements)
- E_s - modulus of elasticity of steel
- A_i - area of longitudinal steel at i -level ($i = 1$ to N)
- d_i - depth of i -level ($i = 1$ to N)
- $f_{si}(F_n)$ - steel stress in the n -th load cycle due to the prestress force at i -level
- F_n - prestressing force in beam during the n -th load cycle
- d - depth of reference fiber
- f_c - concrete cylinder strength
- ϵ_u - concrete strain in cylinder at f_c
- λ - dimensionless parameter defining the shape of the concrete stress-strain relation
- η - dimensionless quantity relating concrete strength in beam and cylinder
- $\epsilon_{c1}(F_n)$ - concrete strain in top fiber of the beam due to the prestress force
- $\epsilon_c(F_n)$ - concrete strain at reference fiber due to the prestress force
- M_n - applied moment in the n -th load cycle
- $\epsilon(M_n)$ - virtual strain at reference fiber due to M_n

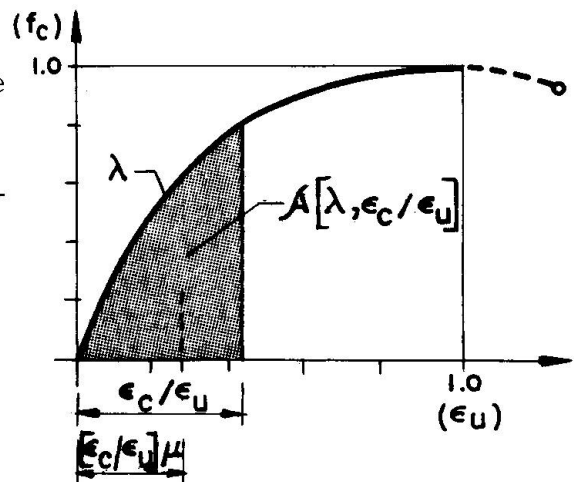
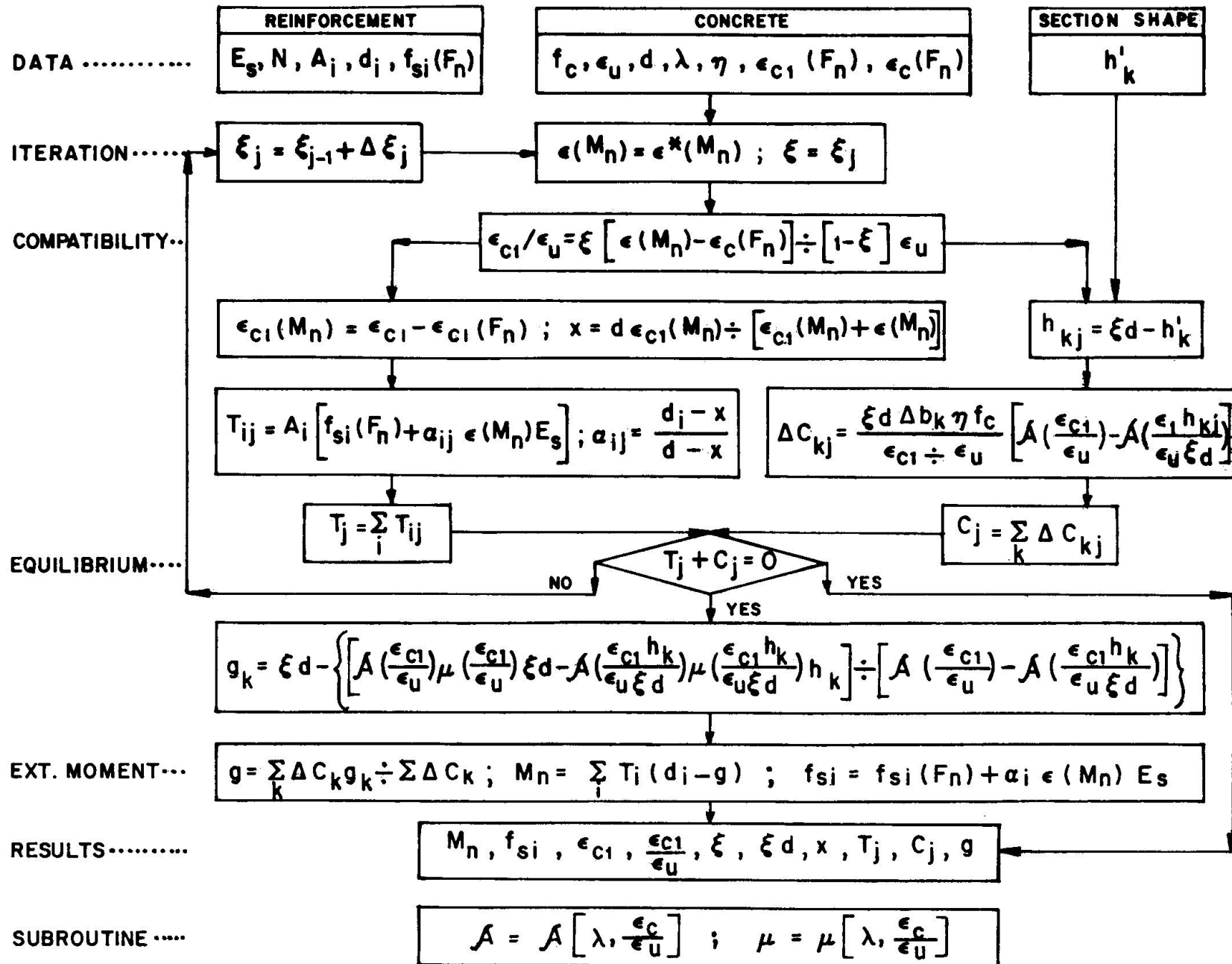


Fig. 2 Concrete Stress-Strain Curve

Fig. 3 Flow Chart for Stress-Moment Curve Evaluation



- $\epsilon_{c1}(M_n)$ - concrete strain in top fiber of the beam due to M_n
- x - depth of neutral axis of bending
- ξ - dimensionless factor defining location of neutral fiber of stress
- ξ_d - depth to neutral fiber of stress
- q_i - strain distribution factor
- f_{si} - steel stress at i -level
- C - total compressive force in concrete

3. SERIES E2 TESTS

3.1 Description of specimens

Each of the 6 m. length T-beams was simply supported. The cross section and the situation of the post-tensioned bonded tendons (level 2) and the non-prestressed reinforcements (level 1 and 3) are shown in Figure 4. The area of concrete section was 0.1252 sq.m. and the moment of inertia of this area about its centroidal axis $243 \times 10^{-5} \text{ m}^4$. Reference fiber was chosen at center of gravity of level 2 plus level 3. The concrete used in the manufacture of specimens was vibrated and twelve standard 150 mm. by 300 mm. test cylinders were cast with each beam.

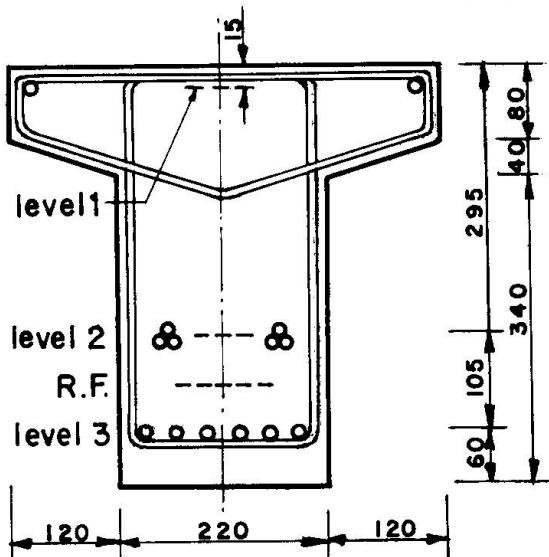


Fig. 4 Beam E2-2 Section

Concrete cylinder strength was about 39 MPa and tensile strength about 2.5 MPa. The stress-strain data for all the beams, without prior loading, follow quite well the $\lambda = 2.6$ curve (below 85% of concrete cylinder strength). This value provides a reasonable fit for the compressive stress block of the beams at all load levels. Only plain cold-drawn wire has been considered in series E2 and the ultimate tensile strength for the 5 mm. diameter wire was 1898 MPa. The amount of web reinforcement, given in Figure 4, was just sufficient to develop the ultimate flexural capacity of the beams. In every one of them, prestressing began 30 days after casting. Previously to grout the tendon ducts at

level 2, losses of stress due to wedge anchorage, elastic shortening, concrete creeping and steel relaxation, were verified during 20 days after prestressing.

3.2 Test procedure

Every one of the beams was tested up to three million cycles of loading. After which, if the beam went beyond this limit, a static test up to failure would be performed in order to compare the ultimate static strength between beams with different load histories. The main difficulty, during the first (about 10^5) cycles of repeated loading, is that prestress force varies due to creep effects and progressive bond failure. Changes in the compressive stress block are less important as a result of low stresses in under-reinforced members. Losses of effective prestress provide increasing stresses at non-tensioned wires. Henceforward, the beam settles down to a fairly steady response. Beams were instrumented with exterior strain gauges at steel levels. The measured values of

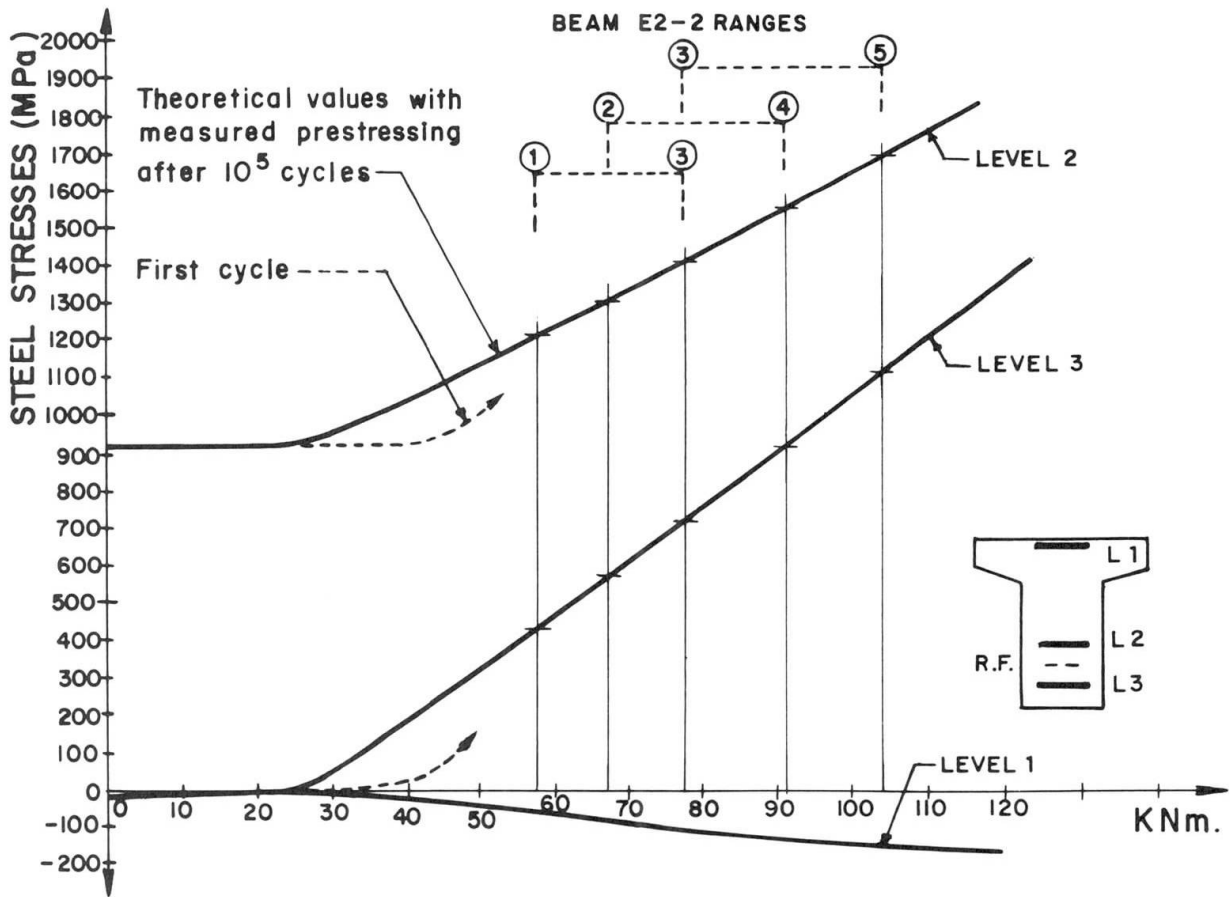


Fig. 5 Reinforcement Stresses vs. Applied Bending Moment

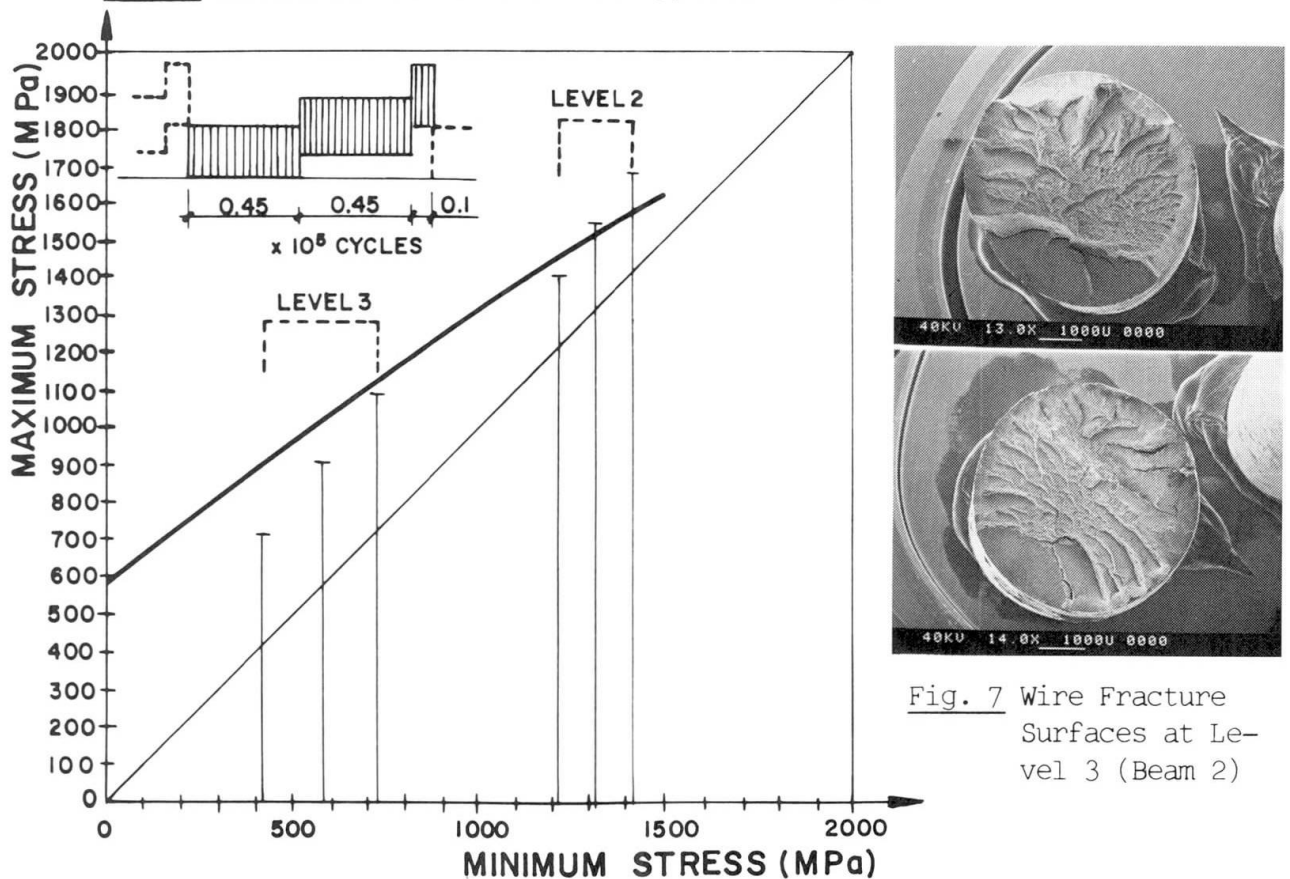


Fig. 7 Wire Fracture Surfaces at Level 3 (Beam 2)

Fig. 6 Goodman Diagram for Steel Reinforcements (Beam E2-2)

reinforcement stresses agreed very well with the calculated ones plotted in Figure 5, which shows the relationship between those stresses and the applied bending moment. The load spectrum has been divided into three steps and varying from each beam to others. Some stress ranges in prestressed reinforcements crossed the Goodman diagram boundary, in all beams, indicating a risk of failure. However, ranges in non-prestressed wires were kept well within that limit. Figure 6 indicates the loading sequences 1-3, 2-4 and 3-5 of the E2-2 beam cumulative test, which is summarised in the following table: (Theoretical values)

Load	Bending Moment (KNm)	Stress at Level 2 (MPa)	% Ultimate Strength of wire	Stress at Level 3 (MPa)	% Ultimate Strength of wire
1	57.52	1215	64	418	22
2	66.78	1310	69	569	30
3	77.38	1405	74	721	38
4	90.61	1537	81	911	48
5	103.90	1670	88	1101	58

3.3 Test results and discussion

Failure was brought about only in E2-2 beam. As Figure 7 illustrates, typical fracture surfaces, due to cumulative damage, appeared in non-prestressed wires at the bottom layer. Failure took place after 1995×10^3 cycles, in spite of theoretical steel stresses, which seem to keep off the modified Goodman diagram boundary. On the other hand, a good agreement between those corresponding strains and the measured ones, proved a fitness of the used model. Therefore it is clear that some kind of supplementary stresses in non-prestressed steel has been neglected. The use of linear elastic fracture mechanics provides an approaching way to estimate the actual maximum stress at failure. Fracture toughness $66.4 \text{ MPa}\sqrt{\text{m}}$ was taken from several plain cold-drawn wire tests. The equalling of this value and the stress intensity factor average, pointed out a real stress up to 1380 MPa, which really cross through the Goodman diagram limit (26% more than expected). These additional stresses might occur due to an oscillatory rubbing action between mating surfaces near each crack. Although the nature of fretting-induced fatigue is not clearly understood, it is well known that fretting stresses can appear with extremely small relative amplitude (10^{-5} mm). Cracks in the present tests opened up to 0.05 mm wide. [5]

4. FINAL REMARKS

To make use of non-prestressed steel is commonly advised in order to safeguard prestressed beams-under traffic loads-against fatigue failure. It seems to be appropriate because the resistance to cracking is considerably improved. However, when cracks have occurred, fretting secondary stresses as consequence of the steel curvature at deflection might take place near each flexure crack. It is early, until series E2 becomes closed, to conclude that some unexpected failure due to non-prestressed steel fatigue could occur if those stresses were overlooked.

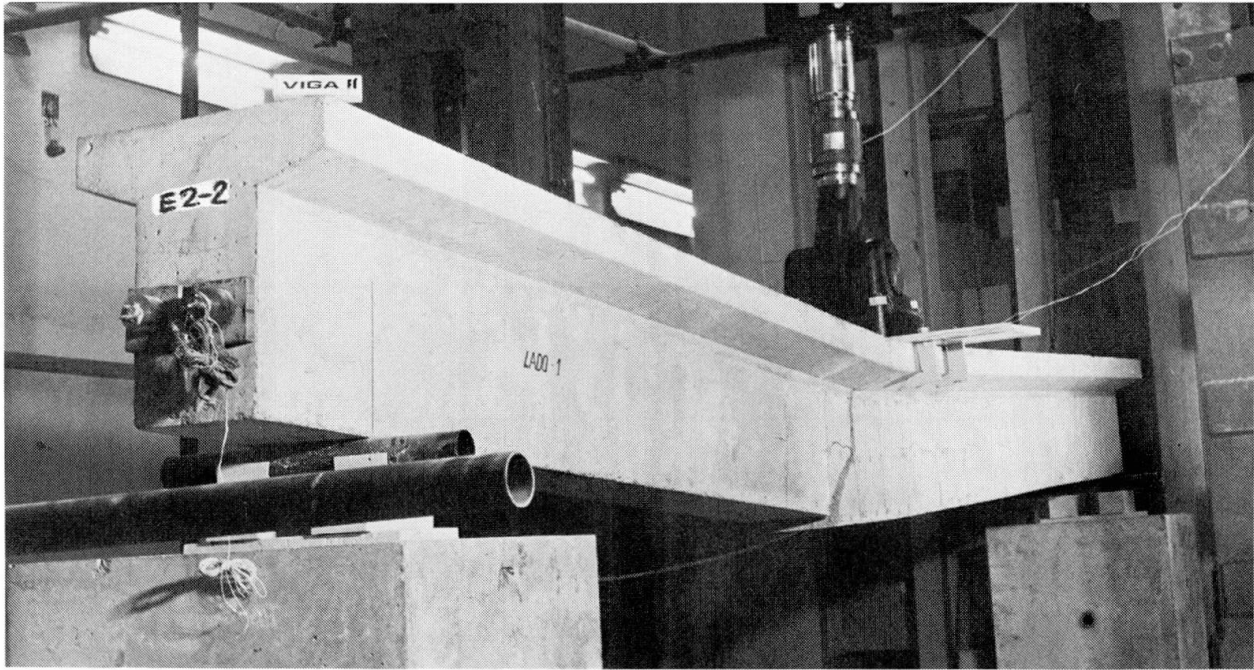


Fig. 8 Photograph of E2-2 Beam After Failure

ACKNOWLEDGEMENTS

The present work has been conducted under the auspices of the Dirección General de Carreteras (Ministerio de Obras Públicas y Urbanismo), as part of a research sponsored by this Corporation. The writer wishes to thank the useful help of the Laboratorio Central staff and technicians.

REFERENCES

- 1 ECKBERG C.E., WALTHER R., SLUTTER R.G.: Fatigue Resistance of Prestressed Concrete Beams in Bending. P-1304, ASCE Proceedings, Vol. 83, 1957
- 2 WARNER R.F., HULSBOS C.L.: Probable Fatigue Life of Prestressed Concrete Beams. PCI Journal Vol. 11 No. 2 April 1966
- 3 BENNET E.W.: Fatigue of Reinforcement in Beams with Limited Prestress. ACI Special Publication SP 41-13. 1974
- 4 ROS M.: Vorgespannter Beton. Bericht No. 155, Eidgenössische Materialprüfungs und Versuchsanstalt für Industrie, Bauwesen und Gewerbe 536, Abb. 55, Zurich 1950
- 5 ASTIZ M.A.: Estudio de la Estabilidad de una Fisura Superficial en un Alambre de Acero de Alta Resistencia. Tesis Doctoral E.T.S.I.C.C.P. Madrid 1976
- 6 ABELES P.W., BROWN E.I.: Expected Fatigue Life of Prestressed Concrete Highway Bridges as Related to the Load Spectrum. ACI Special Publication SP 26-37 1971



Fatigue Strength of Reinforced Concrete Slabs under Moving Loads

Résistance à la fatigue des dalles en béton armé sous des charges mobiles

Ermüdungsfestigkeit von Stahlbetonplatten unter beweglichen Lasten

K. SONODA

Professor
Osaka City University
Osaka, Japan

T. HORIKAWA

Res. Associate
Osaka City University
Osaka, Japan

SUMMARY

Twenty models of a reinforced concrete bridge deck slab were tested under static loading, fixed point pulsating loading and repetitive moving loads. These moving loads were applied along several lines to simulate the passage of truck wheels. Under these loadings, differences in cracking pattern, deflection growth, reinforcement stresses and load carrying capacity are examined.

RESUME

Vingt modèles de dalles en béton armé pour ponts-routes ont été essayés sous charge statique, charge fixe pulsative et charges mobiles répétées. Ces charges mobiles ont été appliquées le long de plusieurs lignes pour simuler le passage de roues de camion. Sous ces charges, des différences dans la fissuration, l'augmentation des flèches, les contraintes des aciers et la capacité portante ont été examinées.

ZUSAMMENFASSUNG

Insgesamt zwanzig Modelle von Stahlbeton-Fahrbahntafeln wurden unter statischer Last, pulsierender Last mit festem Lastpunkt, sowie unter wiederholter beweglicher Last geprüft. Die beweglichen Lasten sollten die Schwerverkehrslasten wirklichkeitsnah simulieren. Die Unterschiede in den Beanspruchungen wie Risszustand, Zunahme der Durchbiegung, Spannung in der Bewehrung sowie das Tragvermögen wurden untersucht.



1. INTRODUCTION

Since bridge deck slabs directly sustain repeated moving wheel loads, they have more the possibility of fatigue failure than other members of the bridge such as beams and girders. In particular, a reinforced concrete deck slab (RC slab) may undergo the influence of fatigue on both sides of inherent strengths of materials and bond strengths between dissimilar materials. However, there has no design code for bridge deck RC slabs in any country, taking into consideration of fatigue effect directly. The reasons for this seem to stem from the understanding that the ultimate load carrying capacities of RC slabs are very large and a conventional design code based on an allowable stress method is too conservative to require consideration of fatigue effect.

In Japan, since about 1965, however, fatigue damage followed by a peeling off of concrete covering bottom reinforcements or a depression of pavement due to punching failure of slab has often occurred, especially in RC deck slabs supported by steel girders. Considering that the resulting damage is so severe as to interfere with the serviceability of bridge deck after the passage of only several years following the opening for service, we must emphasize that the effect of fatigue must be considered in the stage of design, though other factors such as the recent increase of traffic load intensity and the incompleteness of fabrication should perhaps also be included among the cause.

Recently, some fatigue tests of model or prototype RC deck slabs were carried out under central or eccentric pulsating loading through a hydraulic jack [1,2,3]. But such a loading condition is not sufficient to reveal the fatigue characteristics of bridge deck slabs because cracking patterns under the loadings applied at a fixed point were of a radial form spreading from the loading point which differed substantially from a grid-like or tortoiseshell-like form observed in actually damaged deck slabs, and furthermore, the fatigue failure mode in the tests often followed fracture of reinforcements but the failure modes observed in actually damaged slabs were not associated with any fracture of reinforcements.

The purpose of this paper is to clarify the fatigue characteristics of RC deck slabs under repeated moving wheel loads. A total of 20 model slabs of about 1/3 scale to one panel between adjacent main girders of a typical steel-concrete composite girder bridge were tested under static loading, pulsating loading at a fixed point and repeated moving loadings on several different points used to simulate the travelling of wheel loads. In particular, differences in cracking pattern, growth of deflection, stresses of reinforcements and load carrying capacities under these loading conditions are discussed.

2. DESCRIPTION OF SPECIMENS AND TESTS

The details of test slabs are shown in Table 1. The slabs marked " I " have isotropic bottom reinforcements, while the slabs marked " O " have orthotropic bottom reinforcements whose transverse reinforcements, arranged in parallel to the longer side of the slabs, are reduced to half the amount of the longitudinal ones. The reinforcement-ratio in longitude was 1.32% which corresponded to a moderate amount in RC deck slabs designed by the current Japanese code. The sizes of the test slabs were 90 cm long, 260 cm wide, and 6.0 cm thick. The test slabs were simply supported over two way spans, 80 cm and 250 cm, respectively, and their aspect ratio, about 3.0, was chosen so as to approximately reflect the characteristics of one-way slab supported by adjacent steel girders.

Test programs are shown in Table 2. A single concentrated load was applied

through a rubber pad 1.0 cm thick which was stuck to a steel plate 0.5 cm thick, and the contact area of the rubber pad to the top surface of the slab was taken as 17 cm x 7 cm which corresponded to about 1/3 scale of the contact area of a rear wheel tire of the truck specified by the Japanese code. Four types of loading were used in the tests, static, pulsating at a fixed point, repeated moving on a single track along the transversal center line, A-A, shown in Fig. 1 and repeated moving on three tracks, A-A, B-B, and C-C, in the figure. The moving loadings on a single track were carried out in such a way as to move the concentrated load every one cycle of loading at each discrete point in the transverse direction. While the moving loadings on the three tracks were carried out by changing cyclically a loading track after 100 rounds of moving loadings along each track. Load levels, namely the ratio of a repeated load to a static collapse load, were set approximately at 50, 55, 60, 65, 75, 80 and 85%, where the static collapse loads were determined by the results of the slabs IS and OS apriori tested. The rate of loading ranged from 3 Hz to 4 Hz in the pulsating loading and was about 1 Hz per each point in the moving loadings. A electro-hydraulic loading machine was used and the movement of load was carried out by moving the actuator by hand.

3. MATERIAL PROPERTIES

The concrete used in the test slabs consisted of ordinary portland cement with a unit weight 370 kg/m^3 , water-cement ratio 0.5, aggregate-cement ratio 5.0, and maximum size of crushed gravels 1.5 cm, and the slump of fresh concrete was 12 cm and the average compressive strength in cylinder at the age of 28 days was 28.3 MN/m^2 . The reinforcements consisted of round steel bars of diameter, 6 mm, whose average yield stress and average tensile strength were 255 MN/m^2 and 314 MN/m^2 , respectively. All of the test slabs were cast simultaneously and were cured in air until the time of testing after 40 - 240 days since the casting.

4. OBSERVATIONS AND RESULTS

4.1 Static strength

The slabs IS and OS were tested under a static loading. The design load for the slabs allowable in the Japanese code, namely the load giving an allowable tensile stress, 138 MN/m^2 , in the bottom reinforcements, corresponds to 12.9 kN.

In the isotropic slab IS, initial cracking on the bottom side was observed at the design load mentioned above, while crack on the top side was first observed at the load, 39 kN. In the orthotropic slab OS, initial bottom surface cracking and top surface cracking were noted at the loads, 12.9 kN and 34.3 kN, respectively. The cracking patterns on the bottom surfaces were of a radial form, spreading from the loading point, and the collapse mode was of the

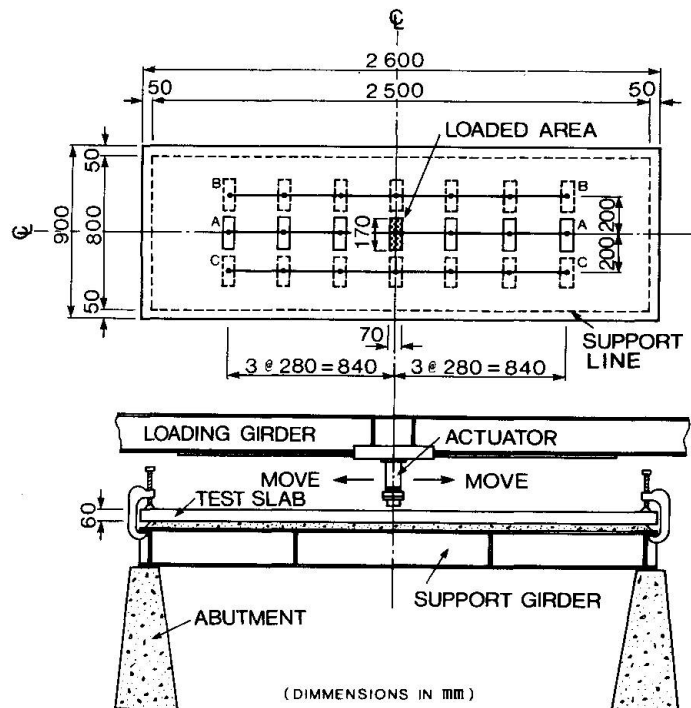


Fig. 1 Test Setup.



punching shear type following a flexural failure mode which had partially proceeded.

Since the collapse modes were located within the vicinity of the loading point, three tests about the center point and other two points of ± 70 cm away from this point on the transversal center line were carried out for each slab. The average value of the collapse loads obtained was 62.3 kN in the slab IS and 58.1 kN in the slab OS, theoretical values of which were 61.7 kN and 55.6 kN, respectively, using the yield line theory, assuming a circular or elliptical fan of yield lines, and considering the hogging plastic moment of cross section having effective depth 2.1 cm corresponding to the distance from the centroid of transverse reinforcement to the bottom surface of the slab.

4.2 Fatigue characteristics

In central pulsating loading, cracks that initially occurred beneath the center spread radially on the bottom surface and later some top surface cracks of a circular arc-form also appeared. The collapse mode was of the punching shear type without fracture of reinforcements. As the mode was quite similar to the static collapse mode, three tests about the same points in the static tests were carried out for each slab.

On the other hand, in repeated moving loadings on a single track, bottom surface cracks independently developed from each loading point and after these cracks crossed each other, the cracking pattern took on a tortoiseshell-like form. Severely cracking occurred only in the earlier stage of loading cycles. Behaviour of the bottom surface cracks was remarkable in that the cracks, parallel to the longitudinal reinforcements, opened considerably when a load situated just above them, but they closed completely when the load was taken away. Thus, by the action of alternate compression and twisting due to repeated movements of the load, the crack faces clapped together and rubbed against each other, so that the crack-widths, remaining with no loading, enlarged. The cracks on the top surface developed from the earlier stage of loading cycles were more numerous than those in the case of pulsating loading at a fixed point, and later on, small pieces of concrete fell due to the breaking of the lower edges of the cracked sections. Near the final stage of the loading cycles, a compressive fracture line resulting from the crushing of the concrete occurred along the transversal center line. Thus, the slabs seemed to collapse in a roof-like mode of yield lines, but they eventually collapsed in a punching shear mode without fracture of the reinforcements. The final cracking pattern and the collapse mode are shown in Fig. 2.

On the other hand, the behaviour under repeated moving loadings on three tracks was similar to that on a single track, but a different point was in that the cracking and the falling of small pieces of concrete rapidly developed just after the loading track was changed.

Table 1 Details of Test Slabs.

Type of Slab	Number of Slab	Sizes, Longl. x Trans. in cm	Depth in cm	Effective Depth in cm	Diameter of Reinforcing Bars in cm	Ratio of Reinforcement, in %	
						Longl.	Trans.
I	10	90 x 260	6	4.5	0.6	1.320	1.320
0	10	90 x 260	6	4.5	0.6	1.320	0.726

The relationship between load level (ratio of the load applied to the average value of static collapse loads) and the total number of loading cycles to failure is shown in Fig. 3. The fatigue life versus load level curves drawn in the figure are determined by the least-squares method, using the data given under identical loading conditions. These load level, R , versus fatigue life, N , curves can be expressed by the following equations:

For isotropic slabs under pulsating loading at a fixed point,

$$R = 1.08 - 0.086 \log N \quad (1)$$

For orthotropic slabs under pulsating loading at a fixed point,

$$R = 1.14 - 0.093 \log N \quad (2)$$

For isotropic slabs under moving loadings on a single track,

$$R = 0.93 - 0.076 \log N \quad (3)$$

For orthotropic slabs under moving loadings on a single track,

$$R = 0.99 - 0.102 \log N \quad (4)$$

If fatigue strengths at 2×10^6 in the total number of loading cycles are predicted from these equations, then the values, 0.54, 0.55, 0.45 and 0.35 are obtained for each case mentioned above.

Obviously, it can be seen that a fatigue life under the same load level is much shorter in the case of moving loadings than in the case of pulsating loading at a fixed point, and the effect of transverse reinforcements on the enhancement of fatigue strength is also greater in the case of moving loadings.

4.3 Stiffness degradation

Relationships between the increase in central deflection (the total amount of elastic and residual deflections) and the total number of cycles are shown in Figs. 4 and 5. Under central pulsating loading, the deflections became rather slow but began to increase rapidly near the time of collapse, and when the deflections reached within a range from 0.25 cm to 0.3 cm, corresponding to about 2.5 times of the theoretical value obtained by an elastic thin plate theory, top surface cracks occurred.

On the other hand, under repeated moving loadings, the deflections gradually progressed from the earlier stage of loading cycles, and when the deflections reached within a range from 0.32 cm to 0.48 cm, top surface cracks occurred; furthermore, when the deflections were within a range from 1.2 cm to 1.6 cm, corresponding to about 1/5 - 1/4 of the depth of the slabs, a compressive fracture line due to crushing of concrete occurred. The deflections just before collapse amounted to 1.7 cm - 2.2 cm under central pulsating loading and 2.1 cm - 3.0 cm under repeated moving loadings, respectively.

4.4 Strains in reinforcements

Variations of strains (excluding residual strains) in reinforcements at the center are indicated in Figs. 6 and 7. In the repetition of the higher load level, the strains of the longitudinal reinforcements happened to exceed to the yield strain at first one round of the movement of load, but there was virtually no subsequent growth. In the repetition of the lower load level, the longitudinal reinforcements did not yield and their strains were almost stable during

Table 2 Test Programs.

Slab	Number of test	Reinforcement	Loading Condition
IS	3	Isotropic	Static
ID	8	Isotropic	Pulsating at a fixed point
IM	5	Isotropic	Repeated Moving on a Single Track
IR	1	Isotropic	Repeated Moving on Three Tracks
OS	3	Orthotropic	Static
OD	6	Orthotropic	Pulsating at a fixed point
OM	5	Orthotropic	Repeated Moving on a Single Track
OR	2	Orthotropic	Repeated Moving on Three Track



all loading cycles. On the other hand, strains of the transverse reinforcements gradually decreased from the initial stage of loading cycles. Such behaviour seems due to the redistribution of stresses resulting from both the internal bond slips of reinforcements and the orthotropy of the flexural rigidity of the slabs. This behaviour was also consistent with the fact that no fracture of reinforcements occurred until the collapses of the slabs.

5. CONSIDERATION ON FATIGUE LIFE UNDER WHEEL LOADINGS

Moving loading used in these tests was performed by transferring, in turn, a loading point to seven discrete points in the transverse direction as shown in Fig. 1. Such a loading procedure was adopted to simulate the continuous movement of wheel loads since bending moment diagrams under loadings at adjacent points sufficiently overlap each other. However, a certain difference in the effect on fatigue failure between such a loading condition and the condition of wheel loading might arise because in the tests, the alternation of loading and unloading was performed at each loading point.

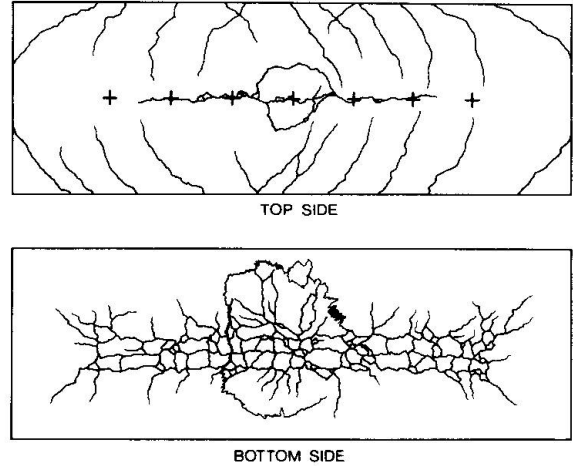


Fig. 2 Final Cracking Pattern in the Slab IM.

Assuming that the partial flexural failure preceding the punching failure controls the fatigue strengths of the slabs, we can examine the contribution of one cycle of loading at each discrete point to the fatigue life of a particular point by using Miner's hypothesis. Denoting the total amount of such contributions by α_j , we obtain,

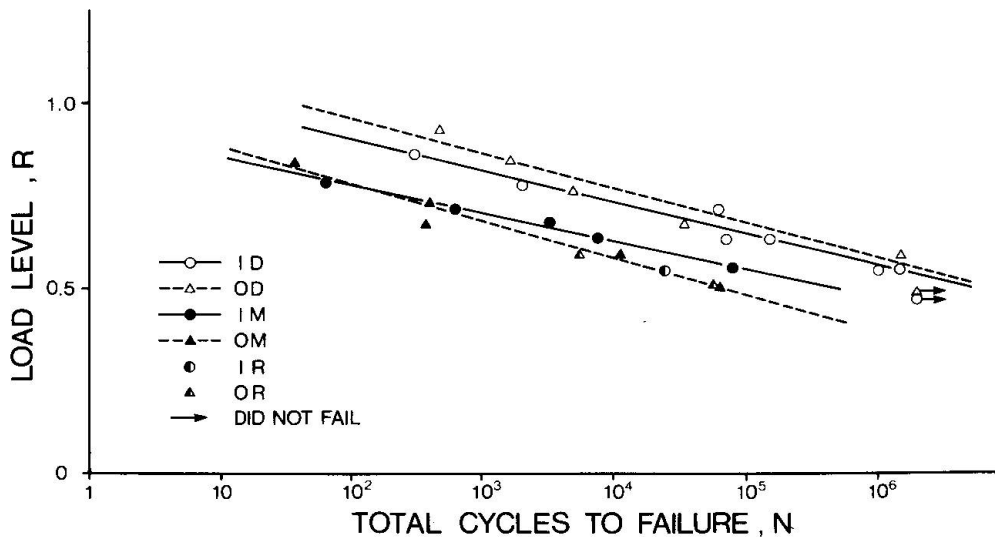


Fig. 3 Relation between Load Level Applied and Total Number of Cycles to Failure.

$$\alpha_j = \sum_{i=1}^r \frac{n_i}{N_{ji}} \quad (5)$$

where, r = number of loading point, N_{ji} = fatigue life of the particular point j under repeated loadings applied at an arbitrary point i , and n_i = cycles of loading applied at the point i . The variation of bending moment at the particular point can be obtained by the elastic thin plate theory,

$$M_j = M_{0j} f(y_j, y_i) \quad (6)$$

where M_{0j} = maximum value of bending moment and $f(y_j, y_i)$ = non-dimensional influence surface whose maximum intensity is reduced to unity, in which y_j and y_i indicate coordinates of the particular point and the loading point, respectively. Using the R-log N curves of Eqs. 1 and 2 for evaluating N_{ji} and using the relation, $R_j = R_0 f(y_j, y_i)$, where R_j = reduced load level to the point j and R_0 = applied load level, the factor, α_j , in Fig. 5 can be expressed as follows:

$$\alpha_j = \sum_{i=1}^r 10^{-M_{0j} [1-f(y_j, y_i)] / \beta K} \quad (7)$$

where $\beta = M_{0j} / R_0$ and K = the gradients of the R-log N curves.

Now, confining our attention on the center of slab and using $r = 7$, $K = 0.09$ obtained from Eqs. 1 and 2 and the influence surface obtained by the elastic thin plate theory, we obtain $\alpha_{j=4} = 1.0002$ and 1.02 for $R_0 = 1.0$ and 0.5 , respectively. Since for any discrete point, being away from the center, a similar result can be expected, it is concluded that the fatigue life of a particular point is scarcely influenced by the loading cycles at other points, and therefore the movement of a load on the seven discrete points aligned becomes equivalent to one passage of a wheel load for an effect on fatigue life.

Thus, from the data in Fig. 3, a comparison of fatigue life under pulsating loading at the center and repeated passages of a wheel load can be given as shown in Fig. 8. It is obvious that the fatigue life becomes much shorter under the condition of wheel-loadings than the condition of central pulsating loadings commonly used in the past studies. If a slab with an isotropic reinforcement fails at 1×10^6 cycles of central loadings, then the slab results in failure at about 1.3×10^4 times of wheel load passage. Further, in an orthotropic reinforcing slab whose transverse reinforcement is reduced to half the amount of the longitudinal reinforcement, a further reduction of fatigue life may be predicted under wheel-loadings.

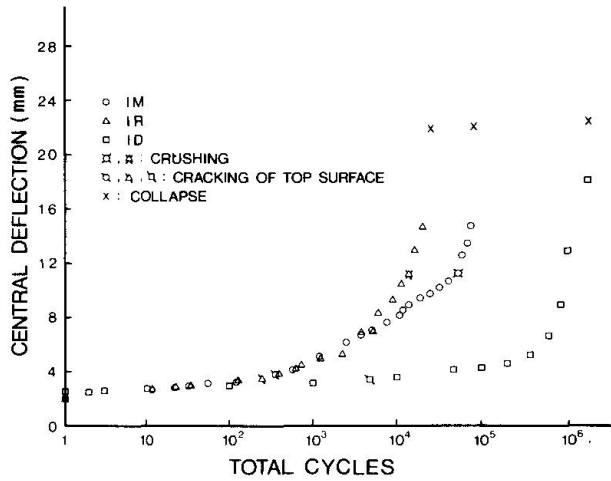


Fig. 4 Growth of Central Deflection under Load 34.3 kN.

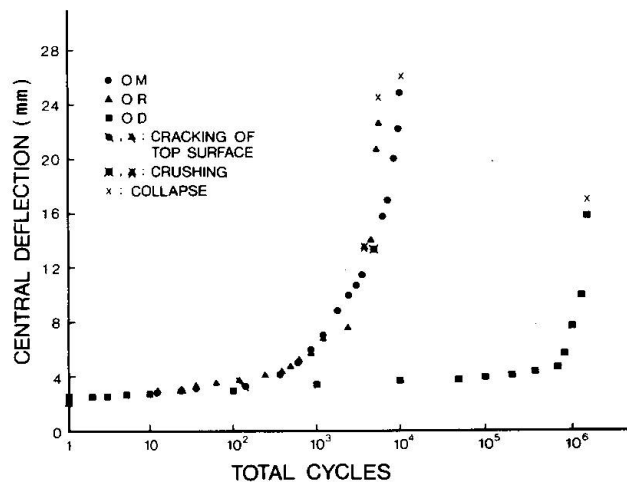


Fig. 5 Growth of Central Deflection under Load 34.3 kN.

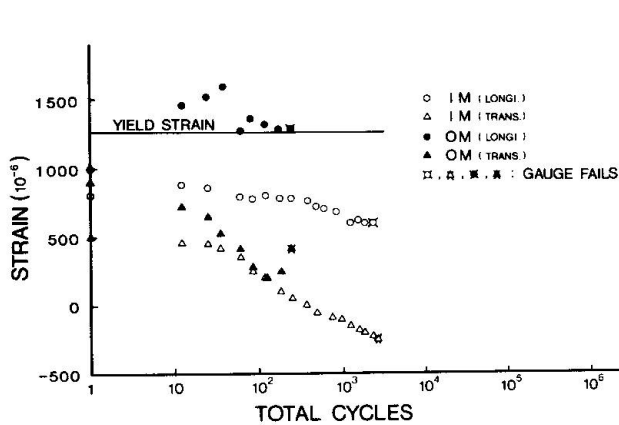


Fig. 6 Strain Variations under Load 39 kN.

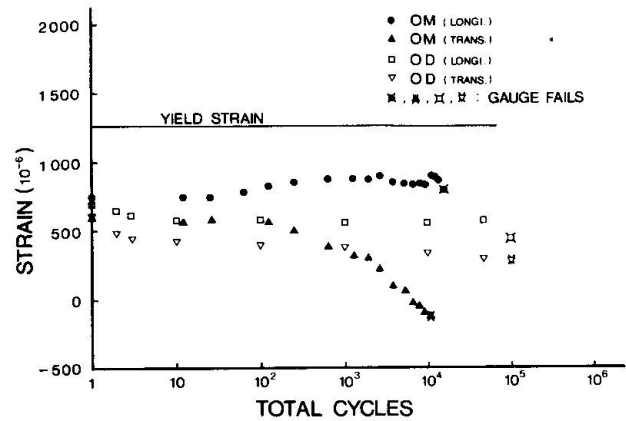


Fig. 7 Strain Variations under Load 29 kN.

6. CONCLUSIONS

The following conclusions can be made:

1. The static load carrying capacities can be predicted with sufficient accuracy by the yield line theory.
2. Damage associated with the development of cracking and the falling of small pieces of concrete occurs from the earlier stage of loading cycles in repeated moving loadings than in pulsating loading at a fixed point.
3. In pulsating loading at a fixed point, fatigue strengths at 2×10^6 cycles amount to more than a half of the static strength, while in repeated moving loadings, the fatigue strengths are predicted to be much lower than this.
4. The effect of transverse reinforcements on the enhancement of fatigue life becomes greater in repeated moving loadings than in pulsating loading at a fixed point.
5. The effect of one passage of a wheel load upon the fatigue failure of slab is equivalent to a range from 80 cycles to 600 cycles of central pulsating loadings.

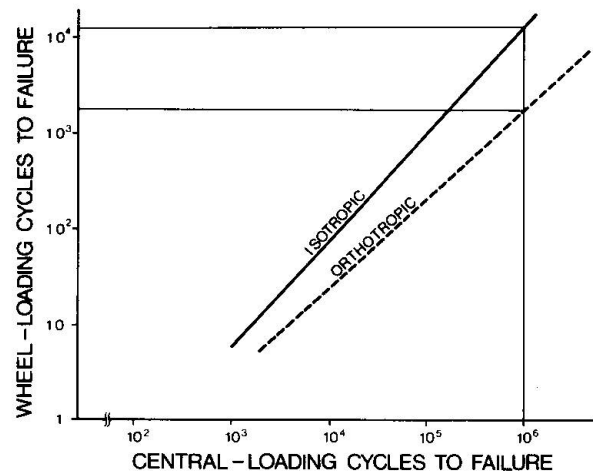


Fig. 8 Relation between Central Loading Cycles and Wheel Loading Cycles to Failure.

REFERENCES

1. Sawko, F. and Saha, G. P.: Effect of Fatigue on Ultimate Load Behaviour of Concrete Bridge Decks, American Concrete Institute Publication SP-26, Concrete Bridge Design, 1971.
2. Hawkins, N. M.: Fatigue Strength of Concrete Slabs Reinforced with Wire Fabric, American Concrete Institute Publication SP-41, Fatigue of Concrete, 1974.
3. Batchelor, B. dev. and Hewitt, B. E.: Are Composite Bridge Slabs Too Conservatively Designed? - Fatigue Studies, American Concrete Institute Publication SP-41, Fatigue of Concrete, 1974.

Fatigue of Anchor Bolts in Reinforced Concrete Foundations

Fatigue des boulons d'ancrage dans les fondations en béton armé

Ermüdung von Verankerungsbolzen in Stahlbetonfundamenten

LENNART ELFGREN

Associate Professor
University of Lulea
Lulea, Sweden

KRISTER CEDERWALL

Professor
University of Lulea
Lulea, Sweden

KENT GYLLTOFT

Sr Research Eng.
University of Lulea
Lulea, Sweden

CARL ERIK BROMS

Sr Project Eng.
AB Jacobson & Widmark
Stockholm, Sweden

SUMMARY

Analytical methods to design anchor bolts are compared to test results from 16 tests with cyclic loading. The level of prestress is the most important factor for the life length of a bolt.

RESUME

Des méthodes analytiques pour le dimensionnement des boulons d'ancrage sont comparées aux résultats expérimentaux de seize essais soumis à des charges cycliques. Le degré de précontrainte est le facteur de plus important qui influence la durée de vie des boulons d'ancrage.

ZUSAMMENFASSUNG

Analytische Methoden für die Dimensionierung von Verankerungsbolzen werden mit Ergebnissen aus sechzehn Versuchen mit zyklischer Belastung verglichen. Der Vorspanngrad hat den grössten Einfluss auf die Lebensdauer des Verankerungsbolzens.



1. INTRODUCTION

Machines are often anchored to reinforced concrete foundations by means of anchor bolts. It is desirable that these anchor bolts meet the following specifications:

- They are able to withstand static and cyclic loading
- They are able to anchor a load within a short anchor length even when the load is situated close to the edges of the concrete foundation
- They are easy to install in the foundation even long time after the foundation was cast.

These requirements have led to the development of various types of anchor bolts.

To be able to withstand cyclic loading, it is advisable to use prestressed bolts. In other cases very heavy bolts are required to withstand also relatively small cyclic loads. This is due to low fatigue capacity of bolts [1].

Two major types of anchor bolt arrangements are tested in this project [2]-[6]. In the first one, the recess for the bolt is provided by drilling a hole in the cast foundation, see Figure 1a. This type of recess has two main advantages. No special arrangements are needed during the design and the casting of the foundation and there is a complete freedom of where to drill the hole. On the other hand, this type of anchorage is likely to have a rather poor capacity for sustained load due to shrinkage of the mortar grouted in the hole.

In the other type, the recess for the anchor bolt is provided by a conical shell, which is placed in the foundation before casting; see Figure 1b [2]. The cone is provided with a spiral reinforcement which helps to carry the splitting forces in the concrete. This type has a good ability to carry sustained and cyclic loading although some more effort is needed during construction.

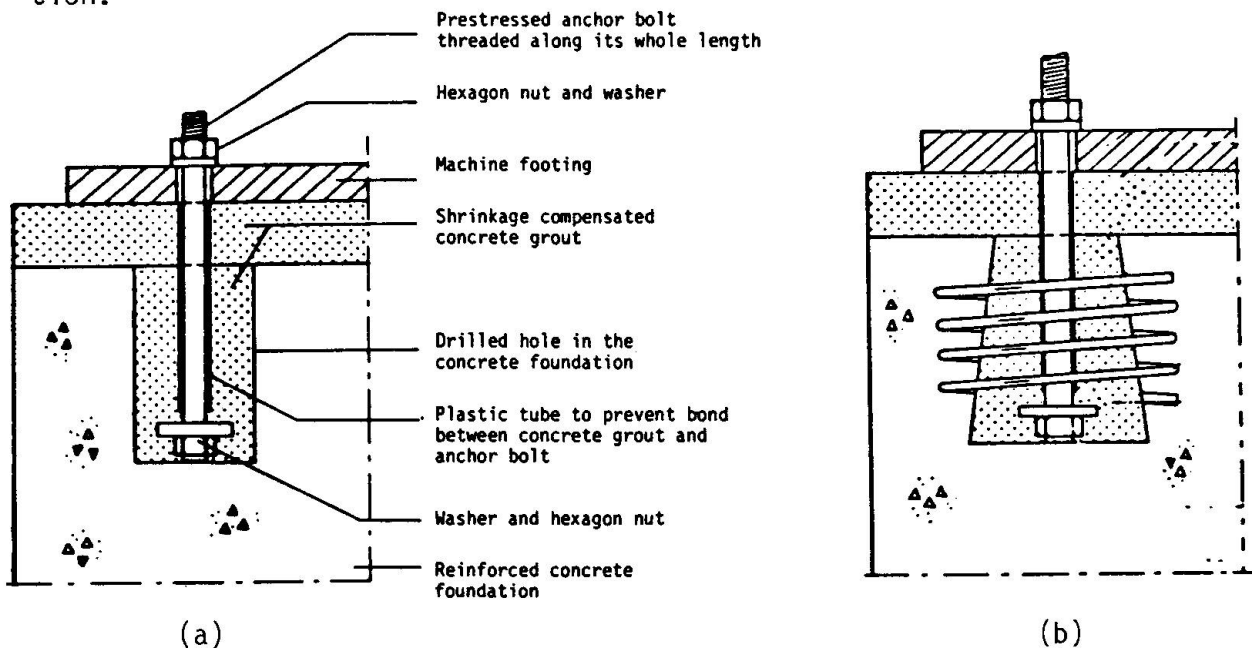


Fig 1 Tested anchor bolts. (a) Bolt placed in a cylindrical hole drilled into a reinforced concrete foundation. (b) Bolt placed in a cylindrical recess. The recess is formed by a 0.5 mm thick metal sheet



2. ANALYTICAL MODELS

2.1 Crack propagation

In order to study the propagation of a crack in the concrete, a fracture mechanics finite element model was used [6]-[8]. The model is illustrated in Figure 2 a, b and some results are given in Figure 2 c - f.

As can be seen from Figure 2, the fictitious (dashed line) and the real cracks (full line) grow as the load is increased. The cracks form a cone and the crack tip has to penetrate a larger area the more it grows. This implies that the crack is very stable also for fatigue loads. As soon as the crack tip penetrates a small distance, the stress in the zone around the crack tip will decrease and thus the crack propagation will be halted. For this reason there is usually no fatigue problems for the concrete [9], for a bolt which is loaded at a level reasonably below its static failure load.

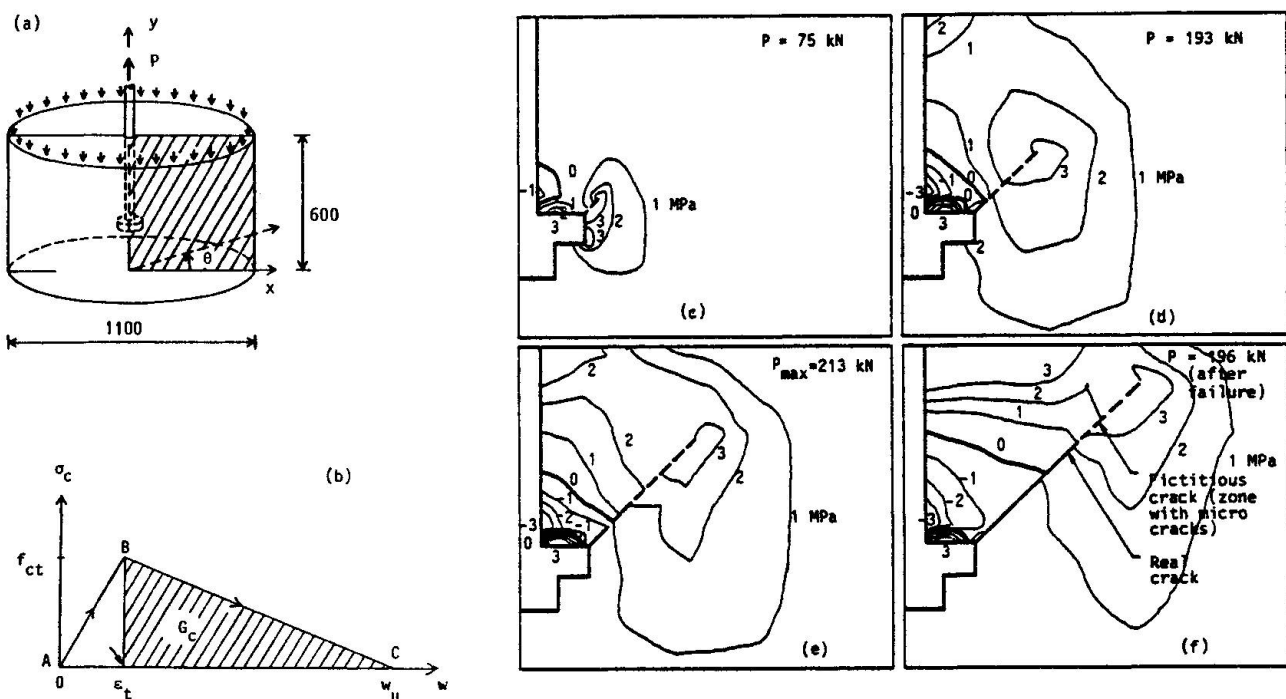


Fig 2 Fracture mechanics model used for study of crack propagation [4], [6]. (a) Dimension of finite element model (96 axisymmetric elements + 10 linear crack elements). (b) Material model for loading (AB) and unloading of crack element (BC), ϵ_t = tensile strain, w = crack width. The following material properties were used for steel and concrete $E_s = 210$ GPa, $\nu_s = 0.3$, $\rho_s = 7800$ kg/m³, $E_c = 30$ GPa, $f_{ct} = 3.0$ MPa, $\nu_c = 0.2$, $\rho_c = 2400$ kg/m³, $G_c = 60$ N/m (fracture energy) and $w_u = 40 \cdot 10^{-6}$ m (maximum fictitious crack width). (c)-(f) Isostress lines for maximum tensile stress for different load levels. A micro crack (fictitious crack) is marked with a dashed line and a real crack is marked with a full line. (c) $P = 75$ kN, (d) $P = 193$ kN, (e) $P_{max} = 213$ kN, maximum load, (f) $P = 196$ kN, after maximum load. The figure illustrates a test, where the anchor head deflection is the steering parameter.

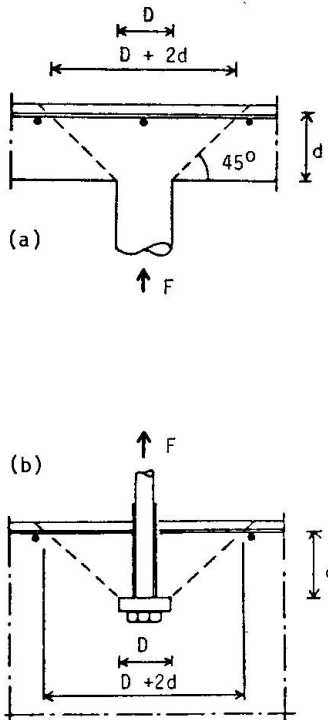


Fig 3 Comparison between punching (a) and anchor bolt failure (b)

2.2 Punching

The anchorage failure of a bolt is related to punching of slabs, see Figure 3. In codes, it is common to use a simplified calculation model for punching. An idealized failure cone is assumed, which is inclined 45° degrees to the horizontal plane. The area A of the cone is, see Figure 3, $A = \pi 0.5(D+D+2d) d\sqrt{2} = \pi(D+d) d\sqrt{2}$, where D is the diameter of the column or the washer and d is the effective depth of the slab or the foundation.

The shear stresses along the cone are often given a constant value f_v at failure. A vertical projection equation then gives

$$F = Af_v/\sqrt{2} = \pi(D+d)d f_v \quad (1)$$

In the 1978 CEB-FIP Model Code [10] the value of f_v depends on the concrete strength, the depth d , and the amount of the reinforcement in the top of the slab. In the United States a similar approach has been proposed [12].

2.3 Influence of prestress

A simplified model illustrating the influence of prestress is shown in Figure 4. A prestressing force P_0 gives rise to a strain ϵ_{s0} in the steel bolt and a strain ϵ_{c0} in the concrete grout under the machine footing. The bolt area is A_s , the effective concrete area is A_c , the length of the bolt is L_s , the effective length of the concrete is L_c , and the modulus of elasticity for steel and concrete grout are E_s and E_c , respectively. Equilibrium gives, see Figure 4a, $P_0 = E_s A_s \epsilon_{s0} = E_c A_c \epsilon_{c0}$. Here ϵ_{s0} and ϵ_{c0} can be written as $\epsilon_{s0} = v_{s0}/L_s$ and $\epsilon_{c0} = v_{c0}/L_c$, where v_s and v_c denote the elongation and the compression of the bolt and the concrete, respectively.

If now a force F (less than P_0) is applied to the machine footing, the bolt head will move a small distance v . The strain will increase in the bolt and it will decrease in the concrete grout. The applied force F can then be written as the difference between the tensile force F_s in the steel bolt and the compressive force F_c in the concrete grout, see Figure 4a and 4b, $F = F_s - F_c = E_s A_s v(r+1)/(L_s r)$, where $r = E_s A_s L_c / (E_c A_c L_s)$. This holds for $F < P_0$. If the applied force F is greater than P_0 , the concrete compressive force will be reduced to zero. The applied load will then be carried by the steel bolt alone, $F = F_s = E_s A_s (v_{s0} + v)/L_s$.

The applied force F , the tensile steel force F_s and the compressive concrete force F_c are shown in Figure 4b as functions of v . The numerical values are chosen to be representative for a bolt with dimension M 30. The applied force F is increasing steeply for small deformations v when $F < P_0$. When the concrete compressive stress disappears for $v = v_{c0}$ and $F = F_p = E_s A_s (v_{s0} + v_{c0})/L_s$ the applied load must be carried by the steel bolt alone. Accordingly, there is a change of the slope of the F - v -curve.

If the applied load F is varying with an amplitude $+\Delta F$ so that $F_0 + \Delta F < F_p$ only small variations ΔF_s will occur in the steel stress, see Figure 4b,

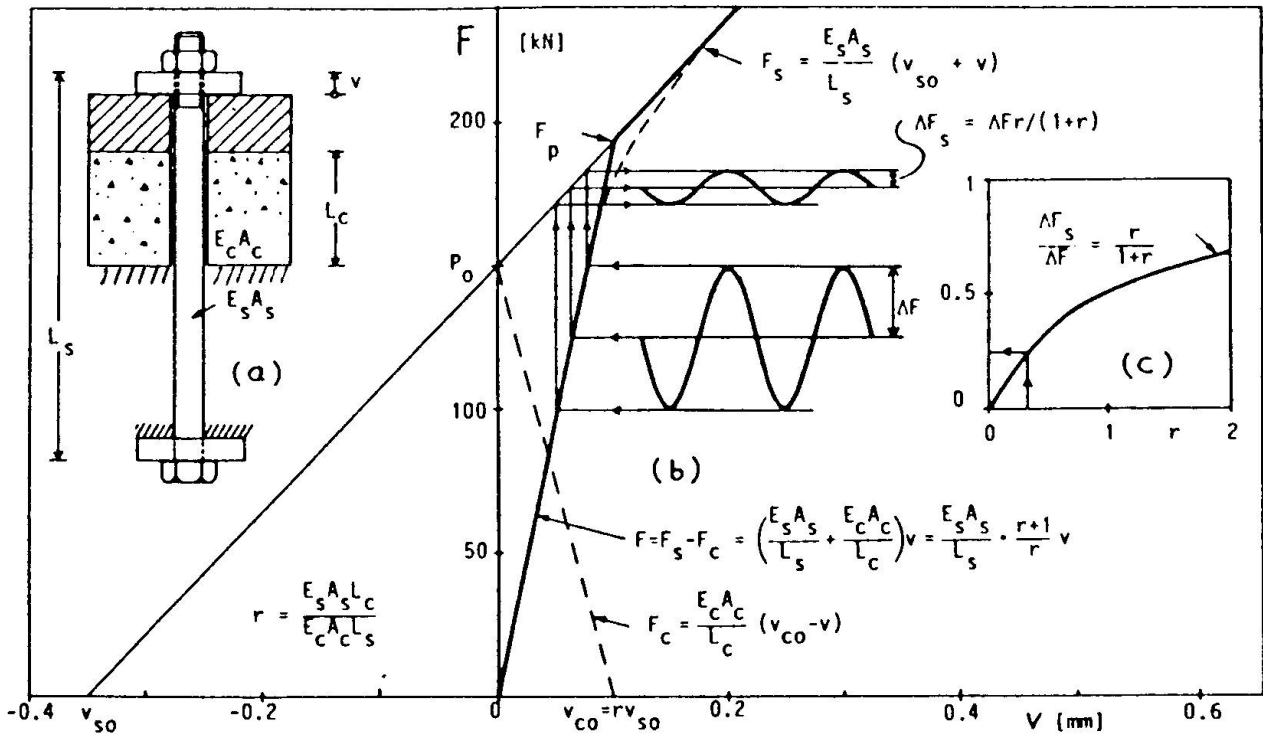


Fig 4 Prestressed anchor bolt. (a) Simplified theoretical model. (b) Applied force F , tensile bolt force F_s and compressive concrete force F_c as function of bolt displacement v . Numerical values: $E_s = 190$ GPa, $A_s = 561$ mm² (M 30), $L_s = 250$ mm, $E_c = 30$ GPa, $A_c = 2500$ mm², $L_c = 50$ mm, $P_0 = 150$ kN, $r = E_s A_s L_c / (E_c A_c L_s) = 0.284$, $v_{so} = P_0 L_s / (E_s A_s) = 0.352$ mm. (c) Relation between bolt steel stress range and applied stress range, $\Delta F_s / \Delta F$, as function of r .

$$\Delta F_s = \Delta F \frac{E_s A_s / L_s}{E_s A_s / L_s + E_c A_c / L_c} = \Delta F \frac{r}{r+1} \quad (2)$$

The ratio of $\Delta F_s / \Delta F$ is illustrated in Figure 4c as a function of r .

The model is simplified. The effective concrete area is a fictive concept and is in reality influenced by the prestressing. For this reason there will be no sharp change in the slope of the F - w -curve as shown in Figure 4b. Instead, there will be a gradual change from the slope of the F - w -curve to the slope of the F_s - w -curve (indicated as a dashed line in Figure 4b).

3. TEST RESULTS

3.1 Test program

A general view of the test set up is shown in Figure 5. The dimensions of the tested foundations were 1450x1450x650 mm³ with two to four bolts in each foundation in Tests Nos 1-6 and 400x400x400 mm³ with one bolt in each foundation in Tests Nos 7-9.

The test program for the fatigue tests [4] are summarized in Table 1. Two bolt dimensions were used, M30 and 1 1/4". They were both made of a material with a



nominal yield stress of 640 MPa. The nominal yield load was 359 kN for the M30 bolt and 400 kN for the 1 1/4" bolt. The M30 bolts were used in Tests Nos 1-6 and the 1 1/4" bolts were used in Tests Nos 7-9. The M30 bolts had washers $\phi 104 \times 24$ and the 1 1/4" bolts had washers $\phi 100 \times 8$ mm. The concrete strength in the foundations is given in Table 1. For grouting, a commercial grout was used in Tests Nos 1-6 ($f_{cc} = 50-60$ MPa, $f_{ct} = 2.5-3.5$ MPa) while a concrete made of Standard Portland cement was used in Tests 7-9 ($f_{cc} = 13-20$ MPa).

As a comparison, ultimate loads from equivalent static tests [3] are also given in Table 1 together with accompanying punching loads calculated according to Eq (1). The punching loads predict the ultimate loads with a reasonable degree of safety.

3.2 Stress range

Test results are summarized in Table 2. The ratio σ_r/σ_{r0} of the stress range with and without prestress varies between 0.04 (for a very low load level) to 0.63 (for higher load levels). The value of the ratio is linked to the value of the parameter r as discussed in section 2.3. For example, if the bolt length L_s is doubled, the parameter r will be half as big as before and the ratio σ_r/σ_{r0} will be reduced considerably. This phenomenon can be seen in Table 2 if tests Nos 2A and 2B with $L_s = 250$ mm are compared to Tests Nos 3 and 4 with $L_s = 450$ mm. The ratio σ_r/σ_{r0} is here reduced from 0.53 and 0.43 to 0.29 and 0.26.

To be able to determine r one must know the parameter A_c/L_c of the effective concrete. Using the relationship $\sigma_r/\sigma_{r0} = r/(1+r)$ and the test values for σ_r/σ_{r0} , we calculated the value of A_c/L_c for the different tests. We got low values, $A_c = 10 L_c$ to $75 L_c$. Consequently, to be on the safe side a low value should be used for design purposes, e.g. $A_c/L_c = 5$ to 10 mm.

The test results are plotted in a Wöhler diagram in Figure 6. In the figure is also drawn a line which represents the Swedish Code for bolts [11]. There is a fair agreement between the test results and the code.

The level of prestress is reduced with time due to shrinkage and creep in the grout. Tests on four commercially manufactured so called non-shrinkage grouts show larger reductions in prestress force than normal concrete under equal conditions [5]. In most of the tested bolts the ratio of σ_r/σ_{r0} has increased with time. However, for some of the short bolts the opposite phenomenon appeared. The maximum stress level in a cycle here remained constant whereas the minimum stress level increased slightly. This was probably due to some interlocking effect which prevented the bolt to unload completely.

3.3 Conclusions

No concrete fatigue failures have appeared for prestressed anchor bolts (except for cyclic loads on a very high level close to the ultimate static load for the bolt). Consequently, there is no fatigue problem for the concrete.

Steel fatigue failures have appeared in several tests. The most important factor governing the life length of a prestressed bolt is the stress range in the bolt. The stress range can be reduced by prestressing the bolt. Reductions of 50 to 75% of the stress range can be achieved. The magnitude of the reduction depends on the length of the bolt and the level of prestressing.

It is important to use a grout with a small shrinkage and it is advisable to check the level of prestress periodically in order to ensure a low stress range.



Table 1 Test program

Test No	Depth of hole or recess	Diameter of hole or recess	Distance to edge of foundation	Spiral reinforcement	Concrete strength		Results from equivalent static tests		
					Compression f_{cc}	Tension f_{ct}	Punching load (Eq 1) F_{th}	Ultimate load F_u	Bolt No Ref [3]
					MPa	MPa	kN	kN	
1 A-B	200	$\phi 120$	150	-	35	3.0	48	147	SD 3:1
2 A-B	200	$\phi 120$	300	-	35	3.0	59	206	SD 3:2
3	400	$\phi 120$	150	-	35	3.0	151	344	SD 3:3
4	400	$\phi 120$	300	-	35	3.0	191	>400	SD 3:4
5	250	$\phi 120/200$	150	(a)	35	3.0	86	418	SC 3:1
6	250	$\phi 120/200$	300	(a)	35	3.0	95	425	SC 3:2
7 A-B	200	$\phi 150/200$	200	(b)	65	4.0 (d)	-	300	ML III
8 A-D	200	$\phi 150/200$	200	(c)	23	2.0 (d)	-	190	ML 3:1
9 A-B	200	$\phi 150/200$	200	-	28	2.5 (d)	-	-	-

Notes: (a) 4 $\phi 10$ Ks400, $f_y = 400$ MPa; (b) 5 $\phi 10$ Ss260, $f_y = 260$ MPa; (c) 4 $\phi 10$ Ss 260, $f_y = 260$ MPa; (d) The value f_{ct} is an estimation based on f_{cc}

Table 2 Test results

Test No	Prestress force P_o	Applied load F	Stress range		$\frac{\sigma_r}{\sigma_{ro}}$	Number of cycles	Mode of failure	
			Without prestress σ_{ro}	With prestress (measured) σ_r			Ultimate load F_u after fatigue loading [kN]	
			MPa	MPa				
1A	102	62.5 \pm 27.5 (a)	98.0	16.2	0.17	8.556	Run out	$F_u = 153$
1B	100	5.0 \pm 5.0 (b)	(17.8)	(0.7)	(0.04)	<0.001	Concrete spalling	$F_u = 138.5$
2A	143	142.8 \pm 20.4	72.7	38.0	0.53	>13.000	Run out	$F_u = 252$
2B	150	125.0 \pm 25.0 (c)	89.1	38.0	0.43	2.040	Concrete spalling	$F_u = 225$
3	180	125.0 \pm 55.0	196.1	57.0	0.29	>4.000	Run out	$F_u = 296$
4	220	137.5 \pm 82.5	294.1	76.0	0.26	>0.937	Run out	
5	287	172.5 \pm 42.5	151.5	95.0	0.63	>3.780	Run out	$F_u = 433$
6	215	161.0 \pm 54.0	192.5	120.0	0.62	0.671	Bolt fatigue failure	
7A	-	112.5 \pm 37.5	120.0	-	-	1.700	Bolt fatigue failure	
7B	-	112.5 \pm 37.5	120.0	-	-	>2.000	Run out	$F_u = 285$
8A	-	112.5 \pm 37.5	120.0	-	-	0.600	Concrete spalling	
8B	-	112.5 \pm 37.5	120.0	-	-	0.250	Bolt fatigue failure	
8C	-	112.5 \pm 37.5	120.0	-	-	0.750	Bolt fatigue failure	
8D	-	112.5 \pm 37.5	120.0	-	-	0.820	Bolt fatigue failure	
9A	-	112.5 \pm 37.5	120.0	-	-	>1.000	Run out	$F_u = 200$
9B	-	112.5 \pm 37.5	120.0	-	-	0.525	Bolt fatigue failure	

Notes (a) After 3 megacycles increased to 82.5 \pm 27.5 kN; (b) Gradually increased to 65.0 \pm 65.0 kN with load steps of 5 kN after 10 cycles (c) After 2 megacycles increased with steps of 7.5 kN after every 10 000 cycles up to 162.5 \pm 62.5 kN

ACKNOWLEDGEMENT

The project is sponsored by the Swedish Council for Building Research (Grant No 780949-3)

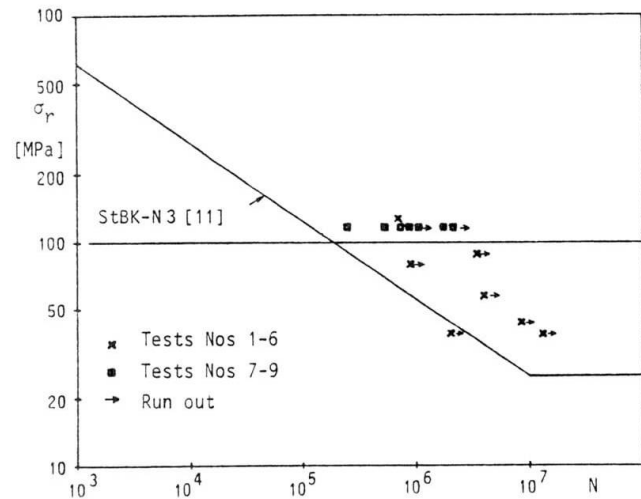
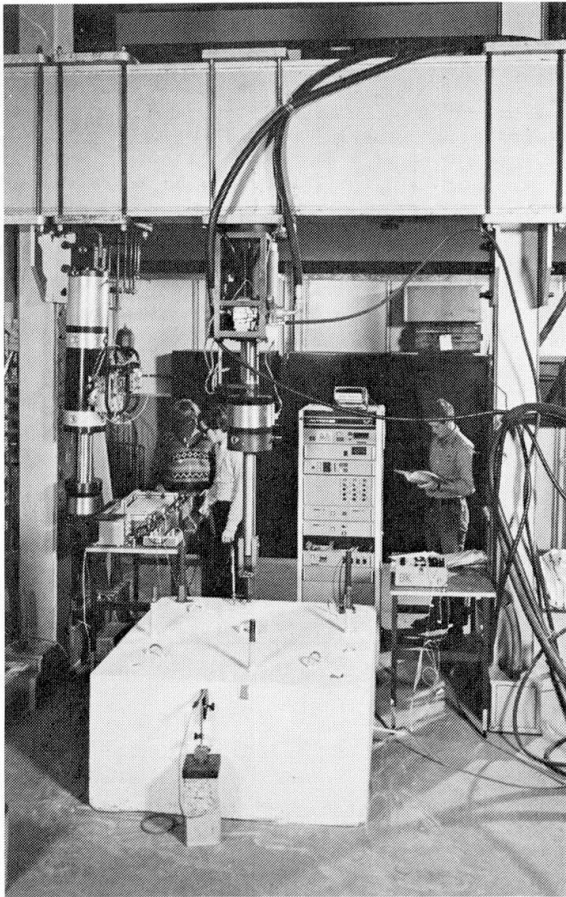


Fig 5 (left)

General view of test set-up

Fig 6 (above)

Wöhler curve for tested bolts. The stress range σ_r is based on measured strain rates

REFERENCES

- 1 GYLLOFT, KENT - ELFGREN, LENNART: Utmattningshållfasthet för anläggningskonstruktioner. En inventering (Fatigue of civil engineering structures. A state of the art report. In Swedish). Bygghögskolan, Rapport R68:1977, Stockholm 1977, 160 pp
- 2 LORENTSEN, MOGENS: Dragförsök med skruv i igjuten betongursparing (Pull-out tests on anchor bolts embedded in concrete. In Swedish with English captions and summary). Nordisk Betong (Stockholm), 1971:1, pp 191-201
- 3 ELFGREN, LENNART - BROMS, CARL ERIK - JOHANSSON, HAKAN E - REHNSTRÖM, ARNE: Anchor bolts in reinforced concrete foundations. Short time tests. University of Luleå, Div of Structural Engineering, Research Report TULEA 1980:36, Luleå 1980, 117 pp
- 4 ELFGREN, LENNART - BROMS, CARL ERIK - JOHANSSON, HAKAN E - JOHANSSON, HAKAN V: Anchor bolts in reinforced concrete foundations, Fatigue tests. University of Luleå, Div of Structural Engineering, Research Report, Luleå 1981 (to be published)
- 5 HAKANSSON, MATS - JOHANSSON, HAKAN E - BROMS, CARL ERIK - ELFGREN, LENNART: Ingjutfningsbruk. Hållfasthet, krympning och krypning hos ingjutfningsbruk för förankringskravar i betongfundament (Strength, shrinkage and creep of grout for anchor bolts in reinforced concrete foundations. In Swedish with English summary). Högskolan i Luleå, Avd för Konstruktionsteknik, Teknisk Rapport 1981:47T, Luleå 1981, 50 pp
- 6 HAKANSSON, MATS - NILSSON, ROGER: Förankringar i betongfundament. Beräkningar med finit elementmetod. Försök med statiska och dynamiska laster. (Anchor bolts in reinforced concrete foundations. Calculations with finite element methods. Tests with static and dynamic loadings. In Swedish with English summary). Högskolan i Luleå, Avdelningen för Konstruktionsteknik, Examensarbete 1981:011E, Luleå 1981, 71 pp
- 7 HILLERBORG, ARNE - MODEER, MATS - PETERSSON, PER-ERIK: Analysis of crack formation and crack growth in concrete by means of fracture mechanics and finite elements. Cement and Concrete Research, Vol 6, 1976, pp 773-782
- 8 GYLLOFT, KENT: Bond failure in reinforced concrete under cyclic loading. A fracture mechanics approach. University of Luleå, Div of Structural Engineering, Research Report TULEA 1980:29, Luleå 1980, 89 pp
- 9 GYLLOFT, KENT - CEDERWALL, KRISTER - ELFGREN, LENNART: Fatigue strength of reinforced concrete structures. Nordisk Betong, Journal of the Nordic Concrete Federation (Stockholm), 1979:6, pp 27-32
- 10 CEB-FIP: Model Code for Concrete Structures. 3rd Ed., CEB (Comité Euro-International du Béton), Paris 1978, 348 pp
- 11 STATENS STALBYGGNADSKOMMITTE. Skruvförbandsnorm 76, StBK-N3 (Regulations for bolted connections 1976, StBK-N3, In Swedish), AB Svensk Byggtjänst, Stockholm 1977, 80 pp
- 12 CANNON, ROBERT W - GODFREY, DWAIN A - MOREADITH, F L: Guide to the design of anchor bolts and other steel embedments. Concrete International, Design and Construction (Detroit), Vol 3, No 7, July 1981, pp 28-41

Fatigue Testing of Reinforced Concrete Beam to Column joints

Essais de fatigue sur des joints poutre-colonne en béton armé

Ermüdungsversuche an Träger-Stützen-Verbindungen aus bewehrtem Beton

Y. NAGAI

Manager of Techn. Research
Kobe Steel Ltd.
Kobe, Japan

Y. YAMAGATA

M. Eng.
Kobe Steel Ltd.
Kobe, Japan

T. KARATSU

M. Eng.
Kobe Steel Ltd.
Kobe, Japan

SUMMARY

This paper presents experimental studies relating to the fatigue strength of reinforcing bars and anchorages in concrete structures. Beam to column joint specimens were given up to 10 million cycles of loading to study bar strength and enable the development of a reliable mechanical anchorage for repeated severe loads.

RESUME

Cet article présente des études expérimentales sur la résistance à la fatigue de barres d'armature et d'ancrages dans les structures en béton. Des échantillons de joints poutre-colonne ont subi jusqu'à 10 millions de cycles de charges pour étudier la résistance des barres et permettre le développement d'un ancrage mécanique sûr pour des charges répétées.

ZUSAMMENFASSUNG

In diesem Artikel werden Ermüdungsversuche an Armierungsstäben und an Verankerungen in Betonkonstruktionen beschrieben. Probekörper von Träger-Stützen-Verbindungen wurden bis zu 10 Millionen Mal belastet, um das Ermüdungsverhalten der Armierungsstäbe zu untersuchen. Zudem wurde versucht, eine mechanische Verankerung für wiederholte Belastungen zu entwickeln.



1. INTRODUCTION

Thread-like deformed bars which are formed by hot-rolling are anchored by a mechanical method. Anchor plates and anchor nuts are used in this method. Anchorage of reinforcing bars is the result of a coupled effect which consists of bond stress and bearing stress. Under the tensile stress state of reinforcing bars bond stress occurs between the bars and the concrete, and bearing stress on the concrete occurs through anchor plates and anchor nuts.

The method described above is different from conventional ones, such as bending or hook anchorage, and it is very useful for rationalization and saving on the expense of the field practice of reinforcement. When there are many frames with the same dimensions and details in concrete structures, for example the frames of overhead railroad bridges, this mechanical method may be of good use. Here, fatigue, caused by trains' passing through, should be discussed. However, there has as yet been little research on the fatigue of reinforced concrete structures under cycles as high as 10^7 cycles.

The purpose of this research is to investigate the applicability of this mechanical anchoring method to concrete structures under dynamic loads by carrying out fatigue tests, using reinforced concrete L-shaped frames with the mechanical anchors in beam-column joints.

2. OUTLINE OF TEST

2.1 Specimens

To investigate the fatigue behaviour of mechanical anchorage in beam-column joints of reinforced concrete L-shaped frames, six specimens for the fatigue test at six stress levels, and a specimen for the static test were prepared. Through the static test the stress of reinforcing bars imbedded in concrete and deflections of the beams were determined for the fatigue test.

The details of specimens, the list of specimens and the mechanical properties of reinforcing bars are shown in Fig. 1, Table 1 and 2, respectively.

Dimensions of the beams were 290mm x 470mm (defined as a model with about one third the scale of actual structures). The flexural tension reinforcement ratio was 0.89% (four thread-like deformed bars with a nominal diameter of 25mm). Dimensions of the columns were 500mm x 500mm. The flexural tension reinforcement ratio was 1.9% (twelve thread-like deformed bars with a nominal diameter of 35mm). Because of the placement of the bars, when the stress on the main bars in the beams reached $1,800 \text{ kgf/cm}^2$ at the critical section, the stress on the main bars in the columns went under 500 kgf/cm^2 at the critical section. This is the reason why it was considered that the stress on the main bars in the columns was to be under a quarter of the allowable stress of reinforcing bars (f_t) ignoring the effects of fatigue in the design of the overhead bridges of super express "Shinkansen" railroad (under 500 kgf/cm^2 in case of Grade SD35, $f_t=2,000 \text{ kgf/cm}^2$).

2.2 Loading and Measuring

The loading point was near the end of the beams as shown in Fig. 1. In the static test for specimen No. D-AS, load reversals were controlled by the stress at the end of the top reinforcements of the beams (${}_s\sigma$) and the deflection at the loading point (δ), that is, five cycles at ${}_s\sigma = 1,800 \text{ kgf/cm}^2$, five cycles

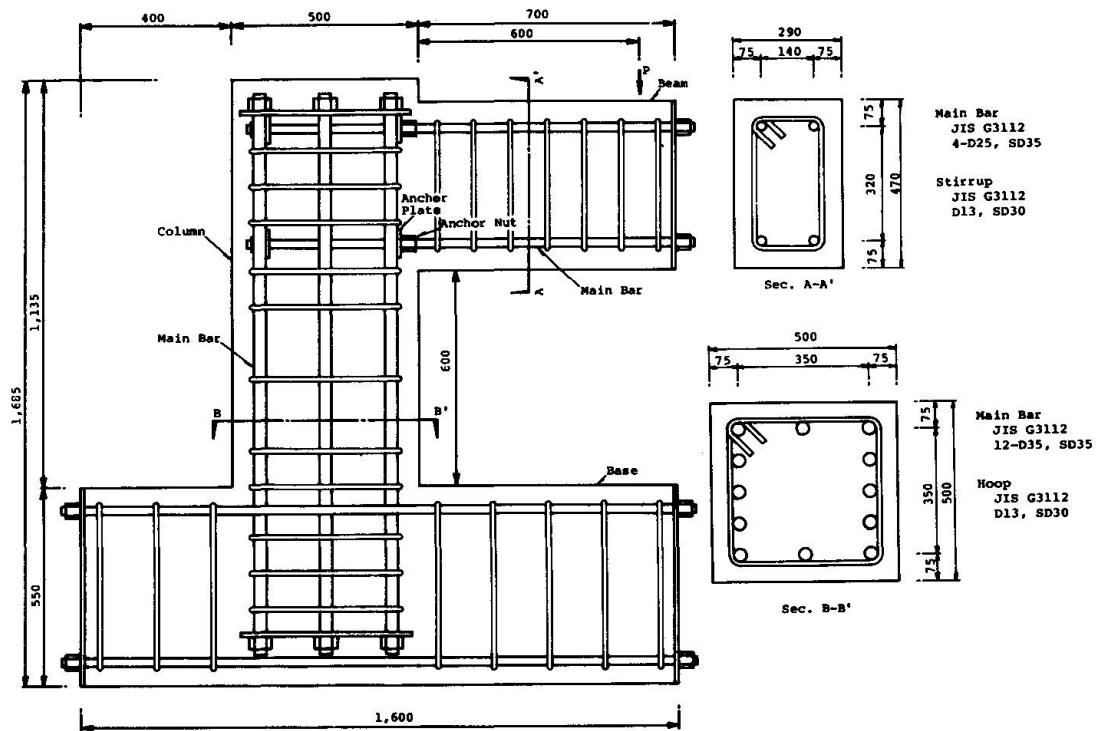


Fig. 1 Details of Specimens (in mm)

Table 1 List of Specimens

Specimen No.	Loading pattern	Beam				Column			
		Main bars	Flexural tension reinforcement ratio (%)	Stirrups	Web reinforcement ratio (%)	Main bars	Flexural tension reinforcement ratio (%)	Hoops	Web reinforcement ratio (%)
D-AS	Static	4-D25 Thread bar	0.89	D13 Spacing 100 mm	0.88	12-D35 Thread bar	1.91	D13 Spacing (mm)	Upper 0.51 Mid. 0.25 Lower 0.51
D-Al ^o 6	Partial pulsating fatigue							Upper 100 Mid. 200 Lower 100	

Table 2 Mechanical Properties of Reinforcing Bars

Size	Grade	Section area (cm ²)	Yield strength (kgf/cm ²)	Tensile strength (kgf/cm ²)	Elongation (%)	Young's modulus (x10 ⁶ kgf/cm ²)
D35	SD35	9.57	3,950	5,750	32.4	2.06
D25	SD35	5.07	4,090	6,000	27.8	2.07
D13	SD30	1.27	3,520	5,410	28.1	2.10

at $s\sigma = \sigma_y$ (σ_y = yield stress of reinforcing bars), to $\delta = 7\delta_y$ (δ_y = yield deflection defined as the deflection corresponding to yielding of top reinforcements).

In the fatigue tests for specimens No. D-A1 ~ A6, repeated loads by partial pulsating were applied at six stress levels by the electro-hydraulic fatigue testing machine (Photo. 1).

Deflections at the loading point, strains in the reinforcing bars and crack patterns were measured.

3. TEST RESULTS AND DISCUSSION

3.1 Static Test

Fig. 2 shows the load-deflection relationship obtained from the static test for specimen No. D-AS. Fig. 3 shows the measured strain distribution through the main bars of the beams and the columns ((a): at $s\sigma = 1,800 \text{ kgf/cm}^2$, (b): $s\sigma = \sigma_y$). Fig. 4 shows the crack patterns under the yielding state of the beam (at $\delta = 4\delta_y$).

Typical flexural behaviour is represented in the load-deflection curve (Fig. 2). That is to say, the stiffness decreased a little when flexural tension cracks appeared. Yielding of the top reinforcements of the beam occurred and simultaneously the beam yielded. After that the frame showed much ductility.

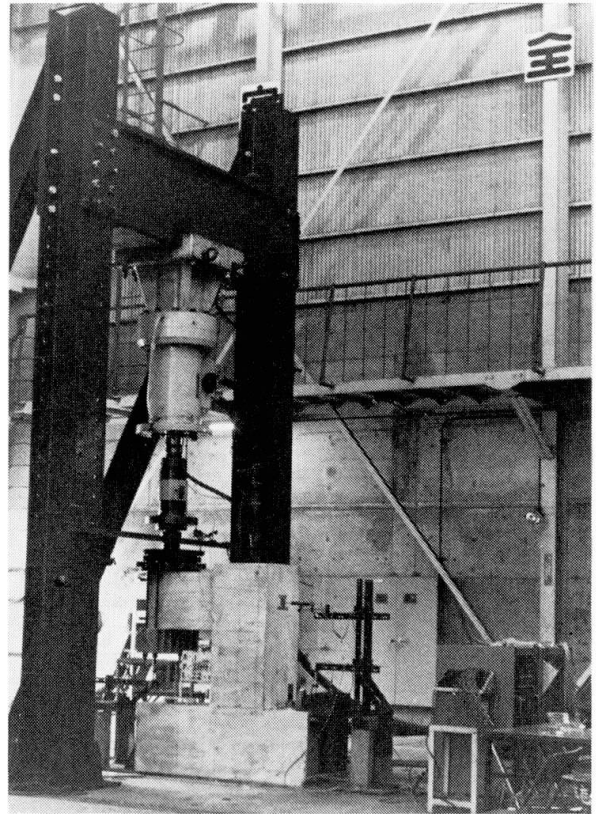


Photo. 1 Test Set-up

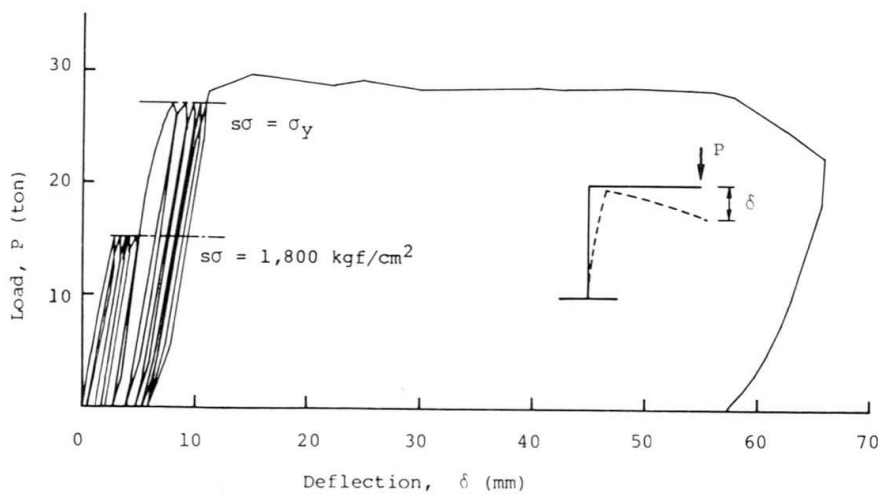


Fig. 2 Load-Deflection Curve (Static Test)

The strains in the top re-inforcements in beam-column joints show triangular distribution which indicates almost no stress at the anchor nut. This proves that the anchorage of re-inforcements was performed completely under cyclic loading at either $s\sigma = 1,800 \text{ kgf/cm}^2$ or $s\sigma = \sigma_y$. And the strains in the main bars of the column remain at the level of 200×10^{-6} ($s\sigma < 500 \text{ kgf/cm}^2$) when the stress of the beam was $1,800 \text{ kgf/cm}^2$ (Fig. 3). This shows very clearly that the stress transmission from the beam to the column was performed smoothly by this mechanical anchorage.

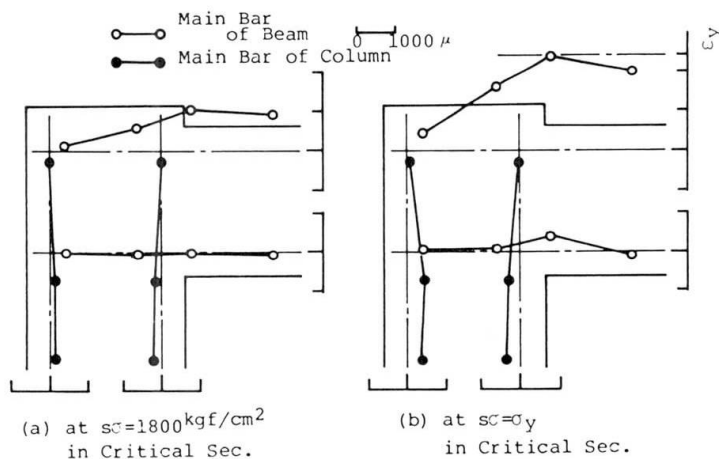


Fig. 3 Strain Distribution through Main Bars in Static Test

3.2 Fatigue Test

Table 3 indicates the results of the fatigue tests for specimens No. D-A1 ~ A6 which were carried out at six amplitude levels.

The stress on the bars was determined by using the results of specimen No. D-AS and the results of the standard tensile test of reinforcing bars in the air. Table 4 indicates the results of the fatigue tests for reinforcing bars with a nominal dia. of 25mm and Grade SD35 in the air as compared to in concrete.

Several cracks were observed in the beams of each specimen and their distribution was almost the same. Diagonal cracks did not appear in the concrete web panels of the joints. As a matter of course the top reinforcements of the beams fractured near the critical section (see Photo. 2).

Fig. 5 shows the S-N relationship between stress amplitude (σ_R) in ordinate and number of cycles to failure (N) in abscissa. In the diagram the '●' shows the test results in concrete and the '○', those in the air.

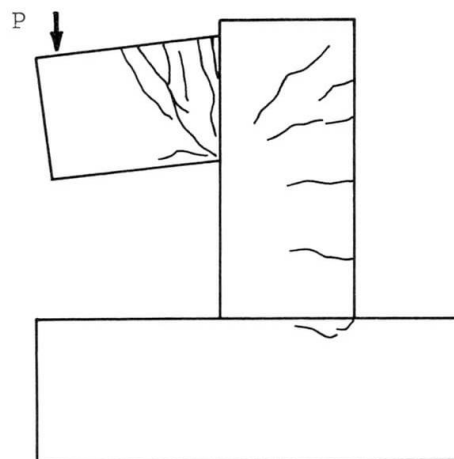


Fig. 4 Crack Pattern (at $\delta = 4\delta_y$)



Photo. 2 Fracture Surface of Bar



The fatigue strength of bars imbedded in concrete was 18.0 kgf/mm^2 at 2×10^6 cycles, and 17.0 kgf/mm^2 at 10^7 cycles. There is no significant difference between the test results in concrete and those in the air.

Fig. 6 shows the strain distribution through the top and bottom reinforcements in the beam of specimen No. D-A2, which was measured at the upper limit stress of the first, of the 50×10^3 th, then of the 100×10^3 th and finally of the 200×10^3 th cycle. According to Fig. 6 the strains in the reinforcing bars in the joints were nearly constant, independent of the increase in the number of cycles and they were about zero at the end of anchorage. This shows that the deterioration of the performance of the anchorage in the joints never occurred and the reinforcing bars didn't slip even under dynamic-repeated loads.

It may be concluded that this mechanical anchorage with thread-like deformed bars, anchor plates and anchor nuts is excellent and appropriate from the point

Table 3 Results of Fatigue Tests (in Concrete)

Specimen No.	Concrete Compressive Strength (kgf/cm^2)	Load (ton)		Stress of bar at critical section (kgf/mm^2)			Repetition frequency (Hz)	Number of cycles to failure ($\times 10^3$ cycle)
		P max.	P min.	σ max.	σ min.	σ_R		
D-A1	409	22.6	1.0	28.17	1.17	27.00	1.5	172
D-A2	360	20.0	1.0	24.89	1.17	23.72	1.5	559
D-A3	413	17.1	1.0	21.19	1.17	20.02	1.5	798
D-A4	364	16.3	1.0	20.17	1.17	19.00	1.5	1,470
D-A5	428	15.4	1.0	19.16	1.17	17.99	2.5	8,380
D-A6	416	13.5	1.0	17.17	1.17	16.00	2.5	over 10,000

Table 4 Results of Fatigue Tests (in the Air)

Specimen No.	Section area (mm^2)	Load (ton)		Stress of bar (kgf/mm^2)			Repetition frequency (Hz)	Number of cycles to failure ($\times 10^3$ cycle)
		P max.	P min.	σ max.	σ min.	σ_R		
S-A1	506.7	15.0	0.1	29.6	0.2	29.4	5	224
S-A2		14.2	0.1	28.0	0.2	27.8	5	289
S-A3		13.2	0.1	26.0	0.2	25.8	8	428
S-A4		12.0	0.1	23.7	0.2	23.5	8	692
S-A5		11.2	0.1	22.1	0.2	21.9	8	1,226
S-A6		10.3	0.1	20.3	0.2	20.1	10	over 2,220

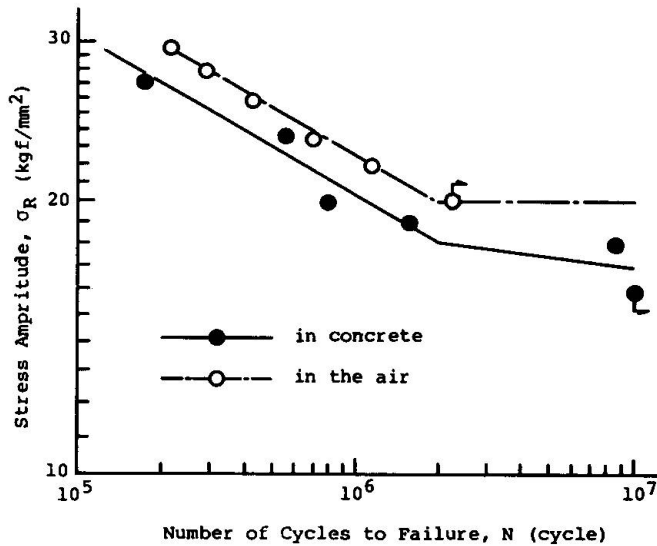


Fig. 5 S-N Diagram

of view of structural performance, and that the mechanical device for anchoring reinforcements is applicable to structures under repeated loading, such as overhead railroad bridges, as a result of the high efficiency in field practice.

4. SUMMARY AND CONCLUSIONS

The fatigue tests using reinforced concrete L-shaped frames with mechanical anchors in the beam-column joints were carried out in order to make clear the fatigue strength of bars and performance of anchorage in concrete structures under dynamic loads. On the basis of the test results presented herein, the following conclusions can be made;

- The mechanical anchoring method conducted surely the L-shaped frames to the mode of flexural failure in the beams.
- The fatigue strength of the bars imbedded in concrete is nearly equal to that of those tested in the air.
- The fatigue strength of the bars imbedded in concrete is 17.0 kgf/mm² at 10⁷ cycles.
- The deterioration of the performance of the anchorage in the joints never occurred.

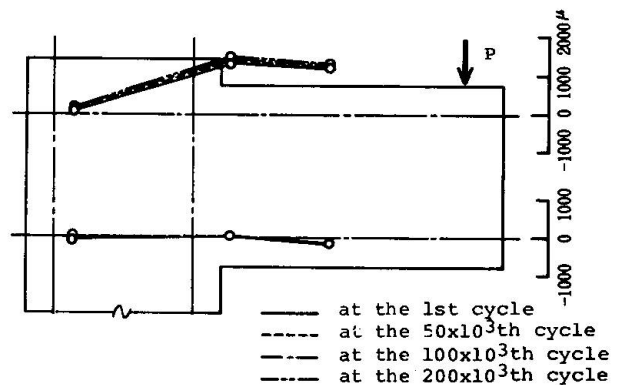


Fig. 6 Strain Distribution through Main Bar of Beam (Fatigue Test)



- It was clarified that the mechanical anchoring method was applicable to concrete structures subjected to dynamic loads.

NOTATIONS

P	applied load	ϵ_y	strain in steel bar at yielding
N	number of cycles to failure	σ	stress
f_t	allowable stress of steel bar	$s\sigma$	stress on steel bar
δ	deflection at loading point	σ_y	yield stress
δ_y	yield deflection	σ_R	stress amplitude

REFERENCES

MIYAZAKI, S., INOUE, H.: Building Requirements of Concrete Structures in TOHOKU-SHINKANSEN, Building Code of JNR, No.37, Mar., 1971.

Miami Guideway: Testing of Prestressed Twin-Tee Girders

Voie ferroviaire de Miami: essais de poutres précontraintes

Miami Guideway: Versuche an vorgespannten zweifach-T-Trägern

S. DHONDY

M. Sc.

Carr Smith & Assoc.

Miami, FL, USA

SUMMARY

Over 2 300 precast, pretensioned, twin-tee guideway girders are being fabricated for Miami's Rapid Transit. Two full size, 85-tonne girders were precracked with 60% overload and then subjected to 6 million cycles simulating 60 years of service life under combined bending, shear and torsion. No crack propagation was observed; this exemplary behaviour is due to the "zero service tension" design and stabilized strands.

RESUME

Plus de 2 300 poutres précontraintes à section en T jumelés ont été fabriquées pour supporter la voie de roulement du "Rapid Transit" de Miami. Deux poutres grandeur nature de 85 tonnes furent pré-fissurées sous une surcharge de 60% et furent ensuite soumises à 6 millions de cycles simulant 60 années d'utilisation sous flexion, effort tranchant et torsion. Aucune propagation des fissures ne fut observée; ce comportement exemplaire est dû au dimensionnement pour des tractions de service nulles et aux torons faits à partir de fils stabilisés.

ZUSAMMENFASSUNG

Über 2 300 vorgespannte zweifache-T-Träger werden als Fertigteile für die Miami "Rapid Transit" hergestellt. Zwei der 85t schweren Träger wurden mit 60% Vorlast angerissen und anschliessend dynamisch belastet. Die 6 Millionen Lastwechsel entsprechen dabei einer Betriebsdauer von 60 Jahren unter Biege-, Torsions- und Querkraftbelastung. Dabei konnte kein Fortschreiten der Risse festgestellt werden. Dieses Resultat ist auf die Tatsache zurückzuführen, dass einerseits im Gebrauchszustand im Betonquerschnitt keine Zugspannungen auftreten und andererseits die Vorspannlitzen aus stabilisierten Drähten bestehen.



1. INTRODUCTION

Stage I of the Miami Rapid Transit System, scheduled for operation in 1984, is a 36km, heavy rail line, with more than 34km. of elevated dual-track guideway. The precast prestressed concrete industry is very active in Miami and this transit alignment had obvious potential for repetitive span layout. Thus, as expected, a design and cost study established that the most economical aerial guideway superstructure would be a two-ribbed, simply supported prestressed girder, one for each track, precast as a single unit complete with deck slab and end diaphragms, and transported to job site for erection by cranes, one crane in most cases. Optimum spans were set at about 24m and over 2300 standard girders are required.

As an alternate to the conventional, relatively costly, single-cell box girder with its expensive inside formwork and complex concreting operation, the Consulting Engineers (Kaiser Transit Group) introduced a large precast pretensioned double tee as a guideway girder; this was a 'first' for any U.S. transit system. Besides an impressive saving of over 25% in fabrication cost, mainly due to fixed forms and simple concreting and stripping operations, the open-bottom section was also preferred architecturally as it imparted lightness compared to the massive look of the closed box, supported on relatively short columns.

2. OBJECTIVES OF DEMONSTRATION TESTS

It is prudent to design any guideway girder to have sufficient torsional and flexural strength and ductility to resist abnormal torsional and impact overload caused by the extremely rare case of eccentric loading, initiated by high speed derailment. Under such preset 'design' condition (maximum transverse eccentricity of 92 cm. and arbitrary 100% impact for Miami system), the girder should not crack extensively and remain 'serviceable' thereafter, hopefully without any repairs or with minor repairs. Adequate torsional and bending stiffness and adequate fatigue resistance of girder under repetitive operational (service) dynamic moving loads causing combined bending, shear and torsion are principle criteria of 'serviceability', both for uncracked and cracked girders.

Before the design could be safely endorsed for competitive bidding, test verification was required of all the criteria defined above, and also the following most important design and fabrication aspects:

- Verification of complex elastic (precracking) and postcracking mixed torsion (St. Venant and warping torsion) analyses by special torsion consultant Dr. T. Hsu [1], predicting girder behaviour under operational and derailment loading.
- Verification of design and reinforcement detailing of articulated ends (dapped for one-half overall depth) required for nearly 30% of the girders.
- Verification of an exhaustive analysis computing loss of prestress in Miami environment. Adequate fatigue resistance of the girder was ensured by a design prohibiting any longitudinal flexural tension in the bottom fibre under 'normal' operational load (89% of crush live load and coexisting nosing and centrifugal forces) and permitting a small bottom fibre tensile stress of 1240kN/m^2 (180psi) for the very rare case of 'abnormal peak' operational load (100% crush live load maximum nosing and centrifugal forces and peak prevailing winds of 100kmph). Any significant underestimate of loss of prestress will lead to pronounced violation of 'zero service tension' design criterion of fatigue resistance which ensured that cracks due to accidental overload would not reopen under normal loads.
- Verification of stress concentration effects in concrete and steel at and between hold-down points. Fig. 1 is detail of a 'hold-down' located at each of 4 deflection points (0.37L & 0.63L in each stem) of the harped strands; these hold-downs anchor tensioned strands to form and stressing bed.

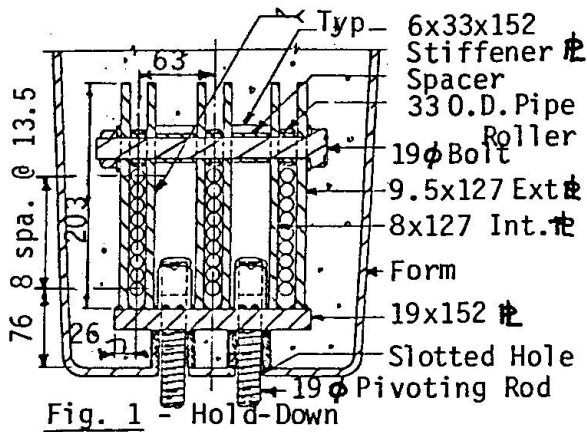


Fig. 1 - Hold-Down

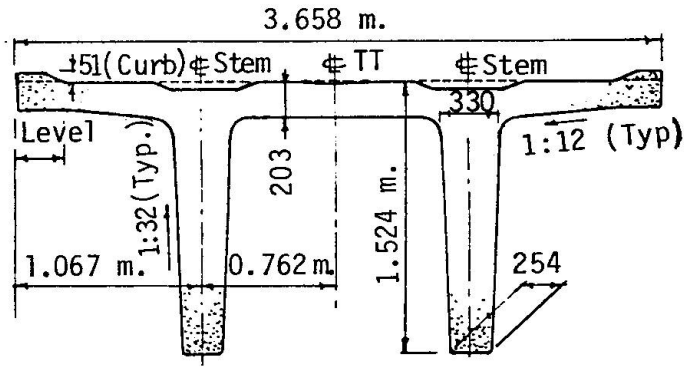


Fig. 2-Double Tee Girder-X Section.

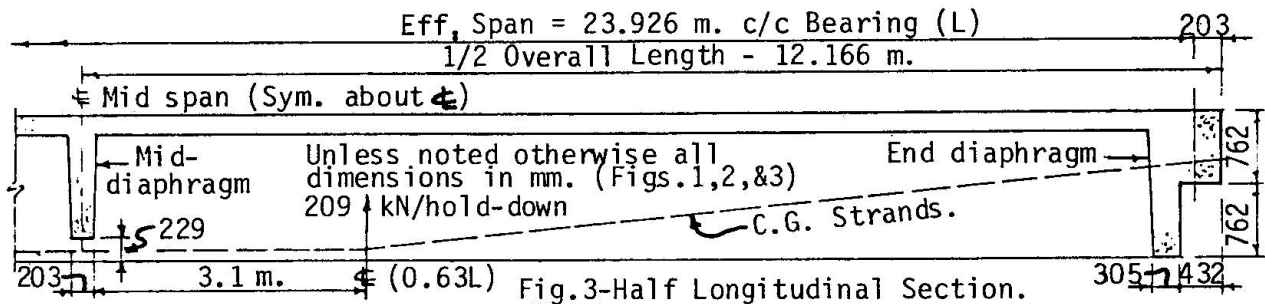


Fig. 3-Half Longitudinal Section.

The 54-12.7mm dia. 1,860MN/m² stabilized pretensioned strands were divided into 6 vertical columns (3 per stem) of 9 strands each, in contact with each other between hold-down points; the strands are progressively spaced apart to provide a clearance of 85mm between strands at girder ends. Strand contact between hold-downs introduced considerable economy by attaining gain of eccentricity of prestress in the bulbless stem. This hold-down detail was used in the 3 test girders and over 1000 girders fabricated up to October '81. Some engineers felt that the sharp radius of bend at deflection points and the possible rubbing of contact strands over each other may reduce ultimate and fatigue strengths. Yet, the designers were convinced that the 'zero service tension' design and the very small calculated stress fluctuation in the uppermost strands, with the sharpest radius of bend of 17mm and a deflection angle of only 0.12 rad. would guarantee adequate fatigue resistance; note that the second row of strands from bottom had a radius of bend of 110mm (8.7d) for a deflection angle of only 0.01 rad. and a calculated stress fluctuation of only 70MN/m² (10ksi). The fatigue behaviour of stabilized strands has been established to be significantly superior to stress-relieved strands [2]. The precautions of using stabilized strands and adopting a 'zero service tension' design were strong antidotes used in light of reported fatigue fracture of stress-relieved strands after subjecting precracked State of Louisiana AASHTO type II test beams to only 3 million cycles of repetitive loads creating a design concrete tensile stress of 3100 kN/m² (450 psi) [3]; the calculated strand stress fluctuation of 62MN/m² (9ksi) matched the calculated value of the Miami girders closely, whereas the calculated minimum strand stress of Louisiana girders (980MN/m² = 142ksi) was 10% lower than the Miami girders.

To summarise, the test objectives were to verify all design methods, to confirm fabrication details and to verify the dynamic behaviour of the girders. After extended discussion, it was determined by a blue-ribbon review panel of well-known U.S. experts that only full-size girder testing, as opposed to 1/4 or 1/2 scale models, would yield convincing results for the complex issues involved. As immediate short-term savings of over 10 million dollars were envisaged, and in view of the potential for tapping multiple amounts in future transit systems, a grant of U.S. \$350,000 was sanctioned from Research and Design funds of U.S. Department of Transportation for Fabrication and Demonstration Static and Dynamic Tests of two full-size girders and monitoring of a third full-size



companion girder for camber and loss of prestress in Miami environment. This paper gives highlights and some details of fatigue testing under repetitive dynamic cyclical loading, tests which are reputed to be the most exhaustive tests in the world on such large full-size girders.

3. TEST SPECTRUM

Special consultant, Dr. J. Fisher of Lehigh University, assisted the Engineers (KTG) in developing suitable test loading spectra of constant stress cycles, which would represent the actual variable stress spectrum of the rapid transit girder. To reduce testing time and costs, it was imperative to reduce the test spectrum to a maximum of 6 million cycles of loading (28 days of continuous loading at 2.5 Hertz average) imposing on the test girder the same cumulative damage as the 16.3 million cycles of actual loading; some basic operational data and the logic of Dr. Fisher's approach [4] is summarised in this chapter.

3.1 Actual Stress Spectrum

The transit system is designed for operation of 2, 4, 6, and 8-car (future option) trains, each 22.85m long, moving on two dual-axle trucks spaced 16.45m apart, with 2/4 car trains used for off-peak and mid-peak hours and 6/8 car trains used for peak hours. Progressive preliminary operating schedules over the projected life of 60 years were analyzed to develop the fatigue design criterion that the girder should sustain loading of 3 million 6-car trains and 1.3 million 2-car trains. Note that for fatigue design purpose, on the conservative side, only 6-car trains were used for peak and mid-peak hours, as these trains cause more cumulative fatigue damage than 8-car trains, for the same total number of cars crossing a girder in any given time. This comparison is based on the premise that a $(x+1)$ - car train with (x) couplers will cause a total of (x) cycles, two 'major' or 'high-loading' cycles (one each on loading and unloading) with maximum fluctuation of strand stress/bending moment/deflection and $(x-2)$ 'minor' or 'low-loading' cycles with only 57% maximum stress fluctuation, neglecting two very minor stress fluctuations; based on Miner's Rule of Cumulative Damages and a conservative low value of $n = 3$ for the slope of the $\log S - \log N$ curve, the total cumulative damage of a $(x+1)$ - car train is that due to $[2+(x-2)(0.57)^3]$ major cycles. These general equations are invalid for a 2-car train which creates only one major cycle and no minor cycles; thus, sixteen 6-car trains (96 cars/hour at 3-3/4 mins. headway) would create the cumulative damage of about 41 major cycles, compared to 35 major cycles for twelve 8-car trains (96 cars/hour at 5 mins. headway) handling the same volume of passenger traffic. On this basis, the fatigue design loading of 3 million 6-car trains and 1.3 m. 2-car trains, created 7.3 m. major and 9 m. minor cycles or a major:minor distribution ratio of 55:45. Further the design load distribution specifies 3 subclasses:

- 125,000 six-car trains of abnormal crush load (250 passengers/car), each car weighing 52.4 tonnes (100%), including empty car weight of 35.4 tonnes.
- 1,075,000 six-car and 500,000 two-car trains of 'normal' full load (166 passengers/car) with loaded car weight of 46.7 tonnes (89%) per car.
- 1,800,000 six-car and 800,000 two-car trains of 'mid-peak' load with loaded car weight of 40.7 tonnes (78%) per car.

The 'zero service tension' design criterion applies to 'normal' full loading. The 3 subclasses, when combined with the 57% ratio of major:minor cycle load fluctuation, give an actual spectrum of fatigue load consisting of 6 load ranges (100%, 57%), (89%, 51%) and (78%, 45%), where 100% load or moment fluctuation range is 2827 kN-m (=1.0M) for the major cycle due to abnormal crush load. Using the preceding equations, the actual spectrum consists of 0.25m. cycles of 1.0M moment range, 2.65m. cycles of 0.89M, 4.4m. cycles of 0.78M, 0.38m. cycles of 0.57M, 3.3m. cycles of 0.51M and 5.4m. cycles of 0.45M, a total of 16.3m cycles.



3.2 Fatigue Testing Load Spectra

The basic concept used for the transformation of the actual stress spectrum into equivalent testing load spectra is Miner's Rule of Cumulative Damages predicting specimen fatigue failure when the cumulative total $\sum f_i N_i$ equals unity, where f_i =number of applications of stress range S_i in the spectrum, and N_i =number of cycles of this same range S_i which alone will cause fatigue failure. When the well-known linear logS-logN relationship (slope=n) for various stress ranges S_i is superposed on Miner's Rule, it can be easily established that any two loading spectra having equal cumulative indices of $(\sum f_i S_i^n)$ will cause the same degree of fatigue damage in the specimen. Note that although values of $n=3.56$ and 4.53 have been derived from previous tests, a lower value of $n=3$ was selected, as the consequently steeper slope gives a larger number of test cycles of amplified loading. Further, bending moment fluctuation range ΔM was used in place of stress-range S_i so that the Index of Cumulative Damages for the actual and test loading spectra was taken as $\sum f_i (\Delta M)^3$ which totalled $(114.5 \times 10^3) (\text{MN-m})^3$ for the actual variable stress spectrum defined in 3.1 above. The following 3 equivalent test loading spectra were determined to generate the same index.

Test Spectrum	Total No. of Cycles	No. of Cycles-Range M	No. of Cycles-Range 0.89M
Alternate A	5.05 Million	5.05 Million	None
Alternate B	6.00 Million	3.20 Million	2.80 Million
Alternate C	7.07 Million	0.25 Million	6.82 Million

A cycle of range $M=2.827\text{MN-m}$ corresponds to the moment fluctuation range of the major cycle caused by 100% abnormal crush load, whereas the $(0.89M)$ fluctuation range cycle corresponds to the major cycle of 'normal' full loading. Note that the substitution of (S_i) by (ΔM) in the equation for Index of Cumulative Damages is permitted because of the linear relationship between fibre stress and bending moment over virtually the entire loading range concerned. Based on uncracked section properties, the maximum bottom fibre tensile stress under 100% abnormal crush load is only about 800kN/m^2 (120psi), including the longitudinal tension in the bottom of one stem of the girder due to warping torsion bimoment created by coexisting additive transverse horizontal forces (nosing, centrifugal force and a sustained wind of 20 kmph). Thus, even if the section has been previously cracked by an extreme overload, the reopening of the crack under 'abnormal crush load' will be very small and the penetration of the crack will be very shallow. In this way, it was reasoned that treating the behaviour as linear throughout would introduce only negligible errors, on the conservative side, in determining alternates A and B; of course alternate C, which retained the 0.25m. cycles of range M, would generate more exact equivalence between actual and test spectra.

4.0 FABRICATION OF TEST GIRDERS

Figs. 2 and 3 give the cross-section and one-half longitudinal section of a prototype standard girder designed for tangent track with webs stiffened by a midspan diaphragm and dapped end diaphragms, all precast as a single unit. Three full-size test double-tees, 24.34m long by 3.66m wide by 1.52m deep were made to dimensions identical to the prototype with the exception that the complex contoured top surface, with edge curbs and recesses, was replaced by a level surface (shown dotted in Fig.2) to facilitate installation of test loading equipment and to reduce cost of fabrication; this minor change made a nominal difference in the critical flexural stress history of the bottom fibre. The test girders were fabricated by Stresscon, Miami, using a special, relatively inexpensive, self-stressing concrete and steel form. Although Miami did not have a suitable testing laboratory, the test girders were made in Miami rather than at a casting yard near five potential laboratories located in California, Illinois, Pennsylvania and Texas, due to the following reasons:

- The 2,300 prototype girders would most likely be made in Miami using local South Florida oolitic limestone coarse and fine aggregates for the concrete.



- Fabrication of test girders outside South Florida necessitated shipping of local aggregate to a casting yard near the potential testing lab, to match relatively low moduli of elasticity and rupture and high specific creep strain of oolitic concrete. Also, one test girder (No. 1) would have to be shipped to Miami to simulate actual storage conditions of temperature and humidity.
- Inspection for total conformance of details and specifications was essential.
- Total costs were the least for girders made in Miami and shipped to test lab.

The strands of test girder No. 1 were initially tensioned to the full design value of 130 kN per strand between hold-downs, as per prototype design, computed to give corresponding prestress of 101 kN after all losses. Strands of test girders No. 2 and 3 were initially tensioned to lower values of 123 kN and 127 kN respectively, computed so that prestress available at the scheduled time of commencement of fatigue testing, is 101 kN per strand.

The following special test equipment was incorporated in the test girders:

- Load cells mounted on the strands between anchorage and stressing abutment monitored loss of tension between initial tensioning and start of transfer of prestress. Thereafter, the actual loss of prestress was computed from change in strain recorded by Whittemore and Demec demountable mechanical strain gauges, applied to surface discs preglued on gauge lengths, located on both webs at the c.g. of strands and 3'-6" either side of midspan. The observed readings were compensated for changes in temperatures of the concrete surface and the gauges.
- Twentyfour SR-4 electrical resistance strain gauges were epoxy glued to the first, second, fourth, sixth and top row of the inner column of tensioned strands of both webs of test girder No 2 only; these strain gauges were also located 3'-6" from midspan. Five of these gauges were continuously monitored during the fatigue test. To force cracks at gauge lengths, a crack former steel plate was placed at each location between web soffit and underside of strands.
- Thirtyone SR-4 gauges were epoxied on stirrups in stems between 0.05L and 0.20L and in an end diaphragm (0.0L) of test girder No 3 only.

5.0 DYNAMIC TESTS

Transportation of girders from Miami to California or Pennsylvania presented almost insurmountable problems. After extended evaluation of all parameters, it was decided to test Girders Nos. 2 & 3 at Portland Cement Association, Skokie, Illinois; these girders were transported by rail from Miami to Skokie siding.

5.1 Test Loading and Monitoring Equipment

Two MTS 490 kN (110 kips) actuators, each representing loading from a dual-axle truck located nearest the coupler of a pair of married cars, were used for repetitive loading. The piston of each actuator was clamped to the girder as shown in Fig 4; note that swivel heads were used at top and bottom ends of the actuator and connected to steel cross heads, with the top cross head clamped to the girders by tie-rods and the bottom cross head anchored to laboratory floor. This efficient arrangement enabled use of the available actuators and reduced the cost of the hydraulic system. For girder No. 2, with actuators located 3.20m on either side of midspan, each tie-rod was prestressed to 266 kN and thus will not affect the results of the symmetrically loaded girder with 'coupler at midspan'. However, as the coupler is located at 0.21 L for girder No 3 providing unsymmetrical load, the rods were not prestressed, but a different clamping system devised to avoid external prestressing forces on the girder webs. The girder is under flexure and vertical shear when the centre-lines of the actuator and the girder are aligned; transverse 'eccentricity' of the girder makes P1 and P2 unequal and then the girder is also subjected to torsion.

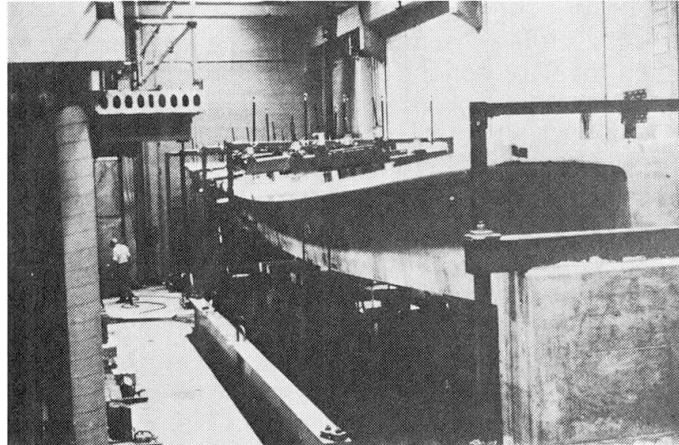
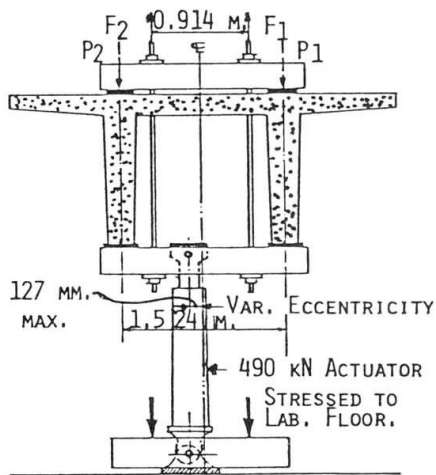


Fig. 4 - Repetitive Loading Setup Fig. 5 - Girder No. 2 at Ultimate Load.

The computed first mode natural frequencies of the girder, without the mass of the design superimposed load which was applied as external test loading, are 4.5 cycles per second in flexure (vertical impulse) and 5.9 cps in torsion (horizontal impulse) ignoring, on the safe side, warping torsion stiffness. The 490 lpm (120 U.S. gpm) hydraulic system was estimated to move enough oil to pulsate girder No 2 at 2.4 to 2.7 Hertz under maximum loading, with a calculated dynamic deflection range of 18 mm, and to pulsate girder No. 3 at 3.0 to 4.0 Hz with a smaller deflection range; so, no resonance problems were expected. However, during testing of girder No 3 at 3.3 Hz, there was some minor resonance with the laboratory building and this particular frequency was avoided thereafter.

Precracking of girder No 2, preceding flexural fatigue testing, was done with loads applied at 0.37 L and 0.63 L through a system of cross heads and the rods, without using the actuators. Precracking of girder No 3, which required larger loads applied at 0.08 L and 0.34 L to produce cracking, was done by using the actuators together with an auxiliary ram applying loads through cross-heads.

Monitoring of fatigue tests was done as follows:

- Cracks were marked with black felt tip pens, photographs taken and widths measured by illuminated hand microscopes.
- Demountable mechanical strain gauges were used to compute available prestress.
- A linear variable differential transformer (LVDT) was attached to brackets glued to the concrete surface on either side of the worst crack of girder No. 2.
- A six-channel Sanborn strain recorder monitored SR-4 gauges and LVDT.
- Minimum and maximum loads, corresponding deflections sensed by 50mm travel potentiometers, and cyclic frequency were registered on MTS digital indicators.
- During precracking, data from load cells, rotation gauges, potentiometers and SR-4 gauges was recorded by a Vidar digital data acquisition system and fed into a mini-computer for conversion into engineering units.

5.2 Test Loading of Girder No. 2

This is a test load creating maximum flexure with corresponding shear and torsion. The girder was precracked under a total symmetrical load of 1192 kN, applied equally to both webs at 0.37L and 0.63L, which equals superimposed dead load plus 1.6 times abnormal crush load including impact. This overload cycle, which caused several cracks up to 0.5m long and 0.15 mm wide within the constant moment zone, was repeated 5 times to stabilize strand movements. Thereafter, this girder was subjected to 6 million cycles of loading as per test spectrum alternate B; transverse eccentricities imposed torsion as required and direction



of torsion was reversed after 50% of the cycles. There were 6 loading stages, with maximum moment range cycle 1.0 M used for the commencement and at the end of the test. The large mass of the girder necessitated a dynamic correction accounted for by controlling the loads such that the deflections produced by cyclic loading matched measured minimum and maximum static deflections of both webs. Control static deflections were remeasured several times.

5.3 Test Loading of Girder No. 3

This load created maximum combined shear stress (due to vertical shear and St. Venant torsion) with coexisting flexure. Precracking loads of 436 kN were applied through each of the two actuators kept at 0.08L and 0.34L, augmented by an auxiliary load of 427 kN applied at 0.375L. This process produced several flexural cracks between 0.28L and 0.44L, the largest being about 0.6 m long and 0.2 mm wide. Thereafter, the auxiliary load was removed, actuator positioned to required transverse eccentricities and the girder subjected to 5.05 million cycles of 100% crush loading with coupler located at 0.21L (Test Spectrum A).

6.0 FATIGUE TEST RESULTS

6.1 Test Girder No. 2

Results of fatigue test on girder No 2 are summarized below:

- Static deflection tests conducted periodically during fatigue testing showed no apparent deterioration of flexural stiffness.
- The maximum crack width of 0.035 mm under maximum moment range increased to only 0.05 mm after 6 million cycles of loading.
- The maximum measured strand stress increase was about 50 MN/m² (8ksi) matching calculated values closely.
- After fatigue testing, the girder was subjected to a static load equal to 2.25 design derailment load or 1.6 times the required ultimate strength. Figure 5 is a photograph of the twisted girder at incipient failure.

6.2 Test Girder No. 3

Results of fatigue test on Girder No 3 are summarized below:

- There was no apparent deterioration of torsional or flexural stiffness.
- Flexural cracks did not propagate during the fatigue test.
- Measured stirrup strains showed that concrete did not crack in combined shear.
- Ultimate strength was 2.5 times derailment load with coupler at 0.21L.

7.0 CONCLUSION

Flexural fatigue resistance was fully established by Girder No 2. Test data provided by Girder No 3 clearly established torsional fatigue resistance.

REFERENCES

1. HSU, T.T.C: Torsion Analysis of DCRT Aerial Guideways - Report to Kaiser Transit Group, April 12, 1977.
2. PRESTON, H. Kent: Comments in PCI Journal May-June 1977.
3. RABBAT B.G., KAAR, P.H., RUSSELL H.G, and BRUCE R.N.: PCA Report-Fatigue Tests of Full-Size Prestressed Girders, July 1978.
4. FISHER, J.W., HWANG, T. and SLUTTER, R.G.: Selection of a Fatigue Load Spectrum-Report to Kaiser Transit Group, March 1978.

Fatigue Considerations in the Design of Concrete Offshore Structures

Fatigue et conception des structures offshore en béton

Ermüdungsfestigkeit und Konstruktion von Offshore-Betonbauten

W.I.J. PRICE

Partner
Gifford and Partners
Southampton, UK

A.H. TRICKLEBANK

Associate
Gifford and Partners
Southampton, UK

E.C. HAMBLY

Consulting Engineer
Berkhamsted, UK

SUMMARY

Fatigue analyses were carried out on three types of oil production platforms and a pontoon type hull using a North Sea wave climate. Two types of floating wave energy converters were analysed using a North Atlantic wave climate. Fatigue criteria were only important for oil production platforms at stress concentrations and on components sensitive to smaller waves. However, they have a strong influence on the design of main members of wave energy converters and make a reinforced concrete hull uneconomic.

RESUME

Des analyses de fatigue ont été effectuées sur trois types de plateformes pétrolières et sur une coque de bateau-ponton sollicités par un régime de vagues type Mer du Nord. Deux types de convertisseurs d'énergie flottants ont été sollicités par un régime de vagues type Atlantique Nord. Les critères de fatigue pour les plateformes pétrolières ne se sont révélés importants que pour les concentrations de contrainte et pour les éléments sensibles aux petites vagues. Cependant, ils ont une forte influence sur la conception des éléments principaux des convertisseurs d'énergie des vagues et ils rendent une coque en béton armé non économique.

ZUSAMMENFASSUNG

Es wurden verschiedene Ermüdungsuntersuchungen durchgeführt, nämlich an drei Erdölplattformen und einem pontonartigen Schiffsrumpf, wobei ein Nordseewellenklima verwendet wurde. Für zwei verschiedene schwimmende Wellenenergiewandler wurde ein Nordatlantikwellenklima angenommen. Bei den Erdölplattformen spielten die Ermüdungskriterien nur an Spannungskonzentrationen sowie an gegen kleinere Wellen empfindlichen Bauteilen eine Rolle. Bei der Konstruktion der tragenden Bauteile von Wellenenergiewandlern gewinnen sie jedoch stark an Bedeutung und machen einen Eisenbetonrumpf unwirtschaftlich.



1. INTRODUCTION

The design study described in this paper was undertaken as a part of the Concrete in the Oceans programme funded by the Department of Energy and the UK Offshore Industry, to determine how serious a problem fatigue is in the design of offshore structures. It is published by permission of the Management Committee. The structures analysed are shown in FIGS 1 and 2. They are:

- Prestressed and Reinforced Concrete Tower Platforms
- Prestressed Concrete Articulated Column Platform
- Prestressed Concrete Pontoon Hull for Petrochemical Plant
- Wave Energy Converter (WEC) with a Reinforced Concrete Raft Hull
- Wave Energy Converter (WEC) with a Prestressed and Reinforced Concrete Spine Hull

This paper outlines the methods used and the assumptions made, and summarises the main conclusions. A fuller version of it is contained in reference [1].

2. LOADING

In the fatigue calculations only wave loading has been considered as fluctuating because it created the most arduous conditions. However, in more rigorous analyses it may be necessary to consider additionally several combinations of fluctuating loads from currents, wind, hydrostatic pressures, temperature effects, machinery, plant and moorings.

The stresses for various levels of loading were calculated deterministically for the oil platforms and pontoon hull, using eight blocks of waves which describe the wave climate in the North Sea. Their range and occurrences for a 100 year period are plotted in FIG 4(i). Damaging stresses in a structural detail may only be caused by waves from a limited number of directions, so the simplifying assumption has been made that only 50% of the waves pass in the particular directions most critical to the detail under consideration.

For the raft form of the wave energy converter, FIG 2(a), the loading is obtained from the wave height/exceedance data for the North Atlantic near the island of South Uist off the west coast of Scotland [2]. The number of occurrences, n , in a period of 25 years derived for each block with a mean wave height, H , is given by: $\text{Log } n = 8.5 (1-H/23.5)$ - (1)

The shorter return period of 25 years reflects the shorter nominal life of wave energy structures compared with petrochemical structures. No reduction for directionality is taken, as the directional spread for the larger waves is likely to be confined mainly to the forward quarter directions because of the location. Greater directional spread may be expected from smaller waves but the panel loadings which they produce are not strongly dependent on heading to the waves.

In the case of the wave energy converter with the spine hull, FIG 2(b), a spectral analysis was undertaken based on the response in bending of a hydrodynamic model to random fully developed seas, with a Pierson-Moskowitz spectrum and suitable spreading function, in a three dimensional wave tank.

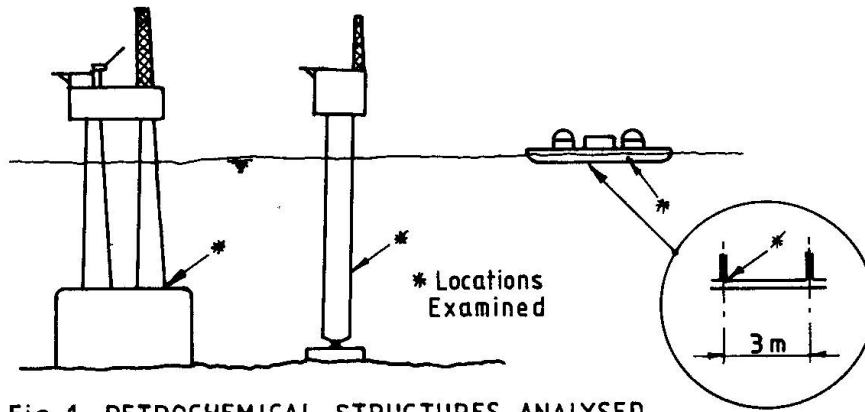
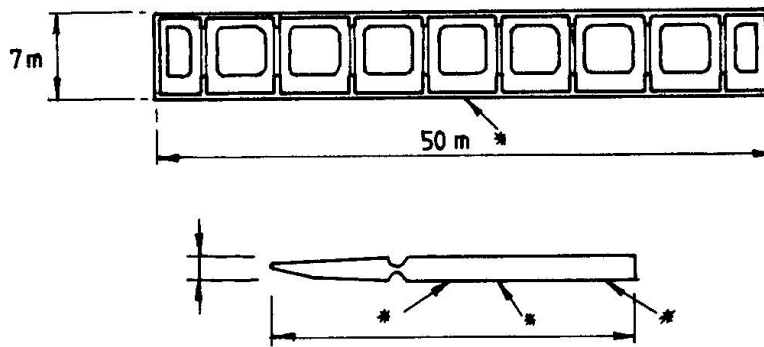
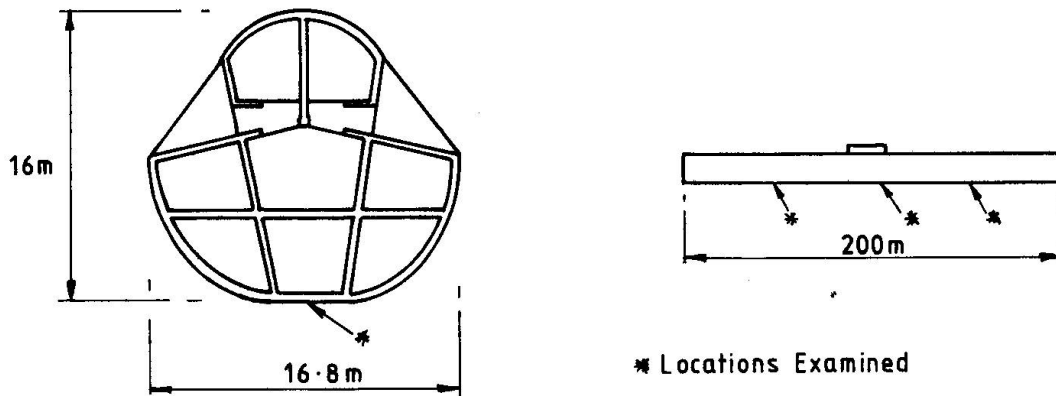


Fig.1, PETROCHEMICAL STRUCTURES ANALYSED



(a) Wave energy converter - Raft.



(b) Wave energy converter - Spine hull.

Fig.2 WAVE ENERGY STRUCTURES ANALYSED

From this analysis a bending moment exceedance curve was produced and this was used to determine the most probable number of stress occurrences in any given period of time.



3. FATIGUE CHARACTERISTICS OF MATERIALS

3.1 Concrete

If the fatigue strength of normal portland cement concrete is expressed as a fraction of the static strength, S_0 , it can sustain repeatedly for a given number of cycles, then this strength is essentially the same whether the stress regime is tension, compression or flexure. The S-LogN or Wohler curve of normal portland cement concrete in tension, compression and bending, is approximately linear, as also is the Goodman diagram, so that they can be represented by a single diagram for which the equation is:

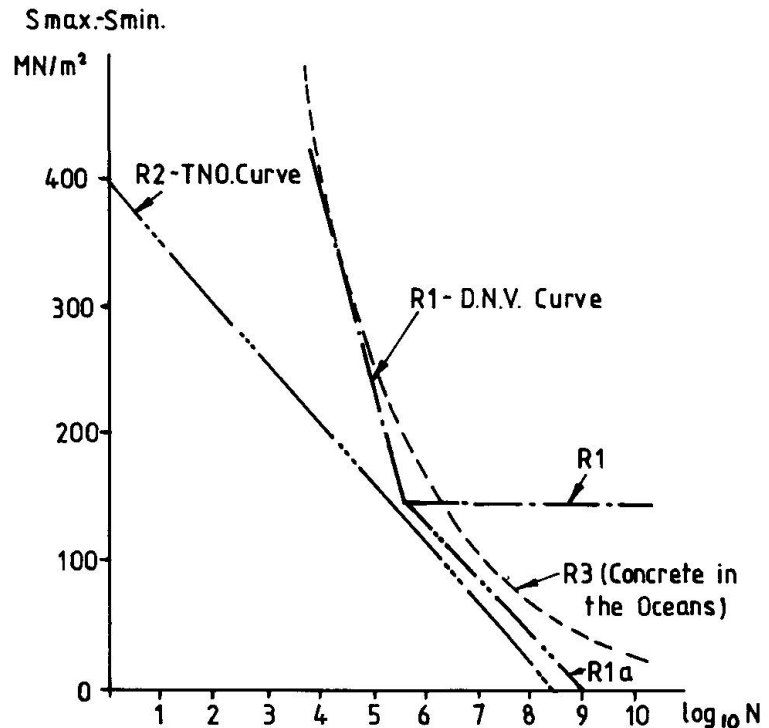


FIG.3 S-N CURVES FOR STEEL REINFORCEMENT

$$\log N = C(1 - (S_{max}-S_{min})/(S_0-S_{min})) \quad - \quad (2)$$

Where S_{max} and S_{min} = Maximum and minimum of stress range, S_r ,
 S_0 = factored static strength

$$= \alpha f_k / \gamma_m$$

α = stress gradient factor (unity for uniform stress)

f_k = characteristic strength

γ_m = partial safety factor for materials

The calculations were carried out for two forms of this relationship. One based on TNO procedures [3], with $C = 12.6$ and an endurance limit at $N = 2 \times 10^6$ of $(S_{max}-S_{min})/(S_0-S_{min}) = 0.5$ [Curve C1 in FIG 4 (iv)]. The other is based on DNV rules [4], with $C = 10$ and no endurance limit [Curve C2 in FIG 4 (iv)]. Curves V1 and V2 used for shear calculations are similar to C1 and C2 with shear force replacing tensile or compressive forces.

3.2 Reinforcing Steel

The S-LogN curves given in design codes take the forms of R1 (DNV ref [4]) and R2 (TNO ref [3]) (FIG 3). The equation for R1 is:

$$\log N = 6.5 - (2.3(S_{max}-S_{min})/S_0) - 0.002 S_{min} \quad - \quad (3)$$

where $S_0 = f_{sy} / \gamma_m$

f_{sy} = yield strength of steel

It has an endurance limit of $(S_{max}-S_{min}) = (165/\gamma_m) - 0.33 S_{min}$.

The equation for R2 is:

$$\log N = 8.4 (1 - (S_{max}-S_{min})/400) \quad - \quad (4)$$



Recent experimental work on the fatigue of reinforcement in concrete beams subject to bending and immersion in sea water, carried out as part of the Concrete in the Oceans programme, demonstrated the influence of crack blocking and corrosion [5]. The results fit a linear LogN-LogS relationship of the form:

$$\text{Log } N = 17.464 - 4.83 \text{ Log } S_r \quad - \quad (5)$$

where S_r is the initial stress range. The 97.5% survival limit is given by:

$$\text{Log } N = 17.088 - 4.83 \text{ Log } S_r \quad - \quad (6)$$

Curve R1a is a suggested compromise for a design curve whose upper portion is the same as R1 (DNV rules) and whose lower portion lies between R2 (TNO procedures) and R3, without a fatigue limit. The equation of the lower portion is:

$$\text{Log } N = 9 - 0.0237 (S_{\text{max}} - S_{\text{min}}) \quad - \quad (7)$$

3.3 Prestressing Steel

Only fully bonded prestressed designs have been considered in this analysis with the concrete section remaining uncracked, except for a single occurrence of extreme loads. Taking a modular ratio in the range of 4.5 to 7, the stress ranges in the tendons usually fall below the values regarded as significant for fatigue according to present rules [4][6]. The question may be raised whether complete bonding is achieved in practice under difficult grouting conditions and whether the assumption of full bonding is appropriate in all circumstances.

4. CUMULATIVE FATIGUE DAMAGE

The cumulative damage that is suffered as a result of all the stress blocks, "a" to "h" in FIG 4 is calculated using Miner's Sum:

$$\sum_{i=a}^h n_i / N_i \leq K \quad - \quad (8)$$

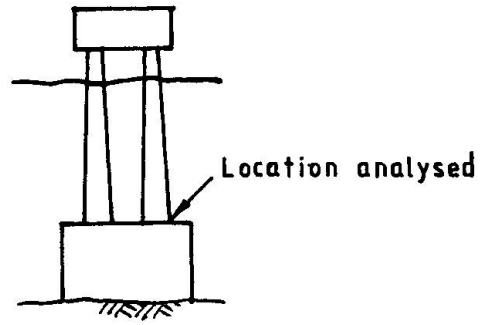
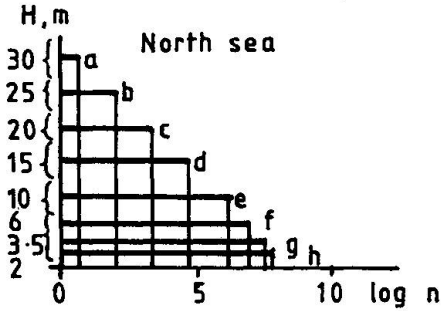
To avoid fatigue problems the value of K must not be exceeded. For steel members K is usually taken as 1. Tests on plain concrete have shown that Miner's sum gives a scatter of values with a log-normal distribution with a mean value generally less than 1 [7]. Waagard suggests that values between 0.2 and 0.5 are appropriate [8] and DNV rules take the lower value [4].

5. FATIGUE LIMIT STATES

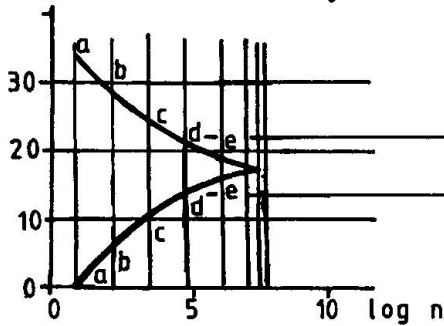
The Miner's sums were calculated for actual designs of several types of structures shown in FIGS 1 and 2. Some of the analyses and results are illustrated in diagrammatic form in FIG 4 for specific conditions and locations. In the deterministic calculations (FIG 4), wave heights in diagram (i) have been translated into stresses in the more vulnerable locations in diagram (ii). These stresses have been combined with frequency, n , in diagram (iii) and related to S-logN curves in diagram (iv). The values of n/N for each wave height range are plotted in diagram (v) and summed for each appropriate fatigue damage curve. In FIG 4, large values of the Miner's Sum were obtained, but without the "hot spot" and its stress concentration effect, the fatigue damage was generally small (see Table 2).



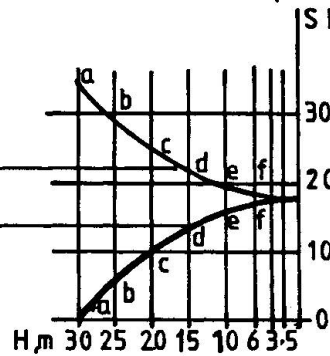
(i) Wave incidences (100 years)



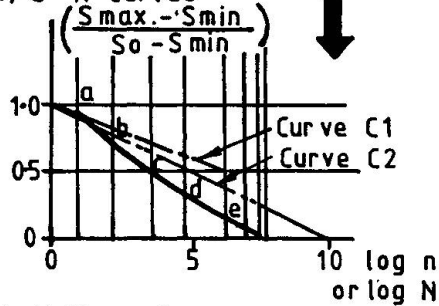
(ii) Stress incidences
S MN/m²



(iii) Structural response to waves
S MN/m²



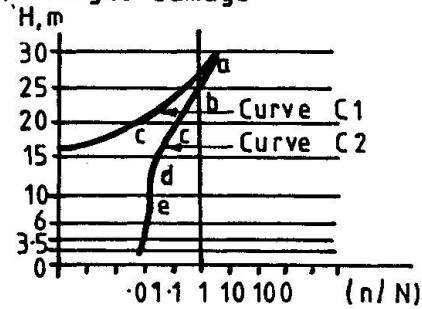
(iv) S-N Curves



$$S_o = \frac{1.0 \times 45}{1.25} = 36 \text{ MN/m}^2$$

Stress Concentration Factor = 2

(v) Fatigue damage



$$\text{Curve C1 } \sum \frac{n}{N} = 5.3 \text{ in 100 years}$$

$$\text{Curve C2 } \sum \frac{n}{N} = 6.2 \text{ in 100 years}$$

Fig.4 P.S.C. TOWER PLATFORM : HOT SPOT IN CONCRETE AT BASE OF TOWER.

For the case illustrated in FIG 4, a simultaneous disadvantageous change of 20% to the number of waves, the mean stress level, the stress range, the characteristic strength and the S-N curve changed the value of Miner's Sum by five orders of magnitude.



In the spectral analysis of the spine hull the input of load effect is in the form of bending moment or shear force occurrences. This has been translated into effective stress ranges for various values of the partial load factor, γ_f . Calculated fatigue damage was plotted logarithmically against γ_f , to show that a load factor in excess of 2.04 would be required to satisfy the criterion of $n/N \leq 0.2$.

6. CONCLUSIONS

The main results of all the analyses are summarised in Table 2. In general terms, fatigue strengths of the oil platforms and pontoon hull were adequate, except perhaps at stress concentrations and in components that may be as sensitive to the action of small waves as to the action of large waves.

Floating wave energy structures are more vulnerable to fatigue. Prestressed hulls suffered little fatigue damage under overall bending, but areas which are difficult to prestress, such as corners, where the strength may be provided by conventional reinforcement, may be critical. Hulls made of reinforced concrete will require a substantial increase in the proportion of reinforcement to avoid premature fatigue damage and the need for welding and lapping of bars for economical construction will exacerbate the fatigue problem and make such structures impracticable.

7. REFERENCES

1. Price W I J, Hambly E C and A H Tricklebank: Review of Fatigue in Marine Structures. CIRIA/UEG, Concrete in the Oceans; P5/Final Report, London 1981.
2. Tann H M: The Estimation of Wave Parameters for the Design of Offshore Structures. Institute of Oceanographical Sciences, Report No 23, Taunton 1976.
3. Monnier T: Fatigue Strength Procedure for Concrete Offshore Structures. TNO Report Delft October 1975.
4. Det Norske Veritas: Rules for the Design, Construction and Inspection of Offshore Structures, Appendix D Oslo 1977.
5. Paterson W S, Dill M J and R Newby: Fatigue Strength of Reinforced Concrete in Sea Water, CIRIA/UEG, Concrete in the Oceans, P6/Final Report, London, April 1981.
6. Hawkins N M: Fatigue Considerations for Concrete Ships and Offshore Structures. Proceedings of Conference on Concrete Ships and Floating Structures, University of California 1975.
7. Leeuwen J Van and A J M Siemens: Miner's Rule with respect to Plain Concrete. Boss 79, 2nd International Conference on Behaviour of Offshore Structures, London 1979.
8. Waagard K: Fatigue Strength Evaluation of Offshore Structures. Proceedings of American Concrete Institute Convention, Dallas, February 1981.

TABLE 2 SUMMARY OF FATIGUE DAMAGE CALCULATIONS

Structure	Material	Location	Stress Conc. Factor	Fatigue Damage n/N								
				Period Years	Concrete		Reinforcement				Tendon $\frac{S_r}{S_c}$ MN/m ²	
					f_k MN/m ²	C1	C2	R1	R1a	R2		R3
Tower Platform	Prestressed Concrete	Base of Tower	1.0	100	45	0.00	0.01					125
		Base of Tower	2.0	100	45	5.3	6.2					
	Reinforced Concrete	Base of Tower (Tower Flooded)	1.0	100	45	0.00	0.01					
		Base of Tower	1.0	100				0.00		0.56	0.00	
Column Platform Articulated	Prestressed Concrete	Mid-height	1.0	100	45	0.00	2.7					
Pontoon Hull	Prestressed Concrete	Base-Longitudinal Compression	1.0	100	40	0.00	6.0					
		Base-Transverse Bending	1.0	100	40	0.00	0.03	0.00		3.2	0.16	
		Side Wall-Shear	1.0	100	40	V1 0.00	V2 15.0					
Wave Energy Converter - Raft Hull	Reinforced Concrete	Side Wall	1.0	25	60	0.06	0.10					
		Side Wall - Fore/Aft	1.0	25				0.40	3.4			
		Side Wall-Midship	1.0	25				3.6	9.6			
		Side Wall-Shear	0.6	25		V1 0.00	V2 0.20					
Wave Energy Converter - Spine Hull	Prestressed Concrete	Midship-Bending	1.0	25	80	0.00	0.02					76
		1/4 Point-Shear	0.6	25		V1 0.00	V2 0.20					
	Reinforced Concrete	Midship-Bending	1.0	25				0.41	1.58			
		1/4 Point-Shear	1.0	25		V1 0.00	V2 0.20					